The influence of the imine bond direction on the phase behaviour of symmetric and non-symmetric liquid crystal dimers.

CRUICKSHANK, E., WALKER, R., STRACHAN, G.J. GOODE, C.H.F., MAJEWSKA, M.M., POCIECHA, D., GORECKO, E., STOREY, J.M.D. and IMRIE, C.T.

2023

Journal of Molecular Liquids 391 (2023) 123226

Contents lists available at ScienceDirect

Journal of Molecular Liquids

journal homepage: www.elsevier.com/locate/molliq

The influence of the imine bond direction on the phase behaviour of symmetric and non-symmetric liquid crystal dimers

Ewan Cruickshank [a,1,*], Rebecca Walker [a], Grant J. Strachan [a], Charlotte H.F. Goode [a], Magdalena M. Majewska [b], Damian Pociecha [b], Ewa Gorecka [b], John M.D. Storey [a], Corrie T. Imrie [a]

[a] Department of Chemistry, University of Aberdeen, Old Aberdeen, AB24 3UE, UK
[b] Faculty of Chemistry, University of Warsaw, ul. Zwirki i Wigury 101, 02-089 Warsaw, Poland

ARTICLE INFO

Keywords:
Liquid crystal dimers
Symmetric
Non-symmetric
Structure–property relationships
Imine bond

ABSTRACT

The synthesis and characterisation of two series of liquid crystal dimers are reported: the symmetric 1,5-bis(4′-oxyanilinebenzylidene-4-alkane)pentanes (*m*-O5O-*m*), and the non-symmetric 1-(4-cyanobiphenyl-4′-yloxy)-5-(4′-oxyanilinebenzylidene-4-alkane)pentanes (CBO5O-*m*). In the acronyms for each series *m* refers to the terminal chain length. The *m*-O5O-*m* series showed monotropic nematic phases for $m = 1$-7. Smectic behaviour emerged at $m = 7$ and nematic behaviour extinguished at $m = 8$. For the CBO5O-*m* series, an enantiotropic nematic phase is seen for $m = 1$-10. In addition, $m = 1$ shows a twist-bend nematic phase, and $m = 9$ and 10 an interdigitated smectic A phase. These series are compared to the corresponding dimers in which the imine link in the benzylideneaniline fragments is reversed, the *m*.O5O.*m* and CBO5O.*m* series. For the symmetric dimers, reversing the imine link has a small effect on the nematic-isotropic transition temperatures, T_{NI}, but a much larger effect on the smectic-isotropic transition temperatures, T_{SmI}. In both cases, the *m*.O*n*O.*m* series shows the higher values. The values of T_{NI} are also slightly higher for the CBO5O.*m* series than the CBO5O-*m* series. Surprisingly, the values of T_{SmI} are higher for the CBO5O-*m* than for the CBO5O.*m* series. These differences are discussed in terms of the changes in shape and electronic distributions arising from reversing the imine link.

1. Introduction

Liquid crystal dimers consist of molecules containing two mesogenic units linked through a flexible spacer, most commonly an alkyl chain, and are termed symmetric if the mesogenic units are the same and non-symmetric if they differ [1–3]. The length and parity of the spacer play a key role in determining the transitional properties of the dimer, and within a homologous series in which the number of methylene units in the spacer is increased, pronounced alternations in, for example, the liquid crystal-isotropic transition temperatures are observed. To a first approximation, this behaviour may be attributed to the role of the spacer in controlling the average molecular shape. Thus, for an even-membered spacer, there is an even number of atoms connecting the two mesogenic groups, the two units are more or less parallel, and the molecule is linear. By comparison, for an odd-membered dimer the units are inclined at some angle with respect to each other and the molecule is bent [4]. The intense research interest focussed on liquid crystal dimers in recent years has arisen due the observation of twist-bend nematic [4–12] and twist-bend smectic phases [13–17] for bent, odd-membered dimers.

The dimeric molecular architecture represents an inversion of that of conventional low molar mass liquid crystals which consist of molecules containing a single semi-rigid core attached to one or two flexible alkyl chains. The interactions between the cores give rise to liquid crystalline behaviour whereas the roles of the terminal chain are to reduce the melting point and modify phase behaviour. Specifically, increasing the length of a terminal chain in a homologous series of conventional low molar mass mesogens sees a change from nematic to smectic behaviour and this is attributed to an increasing tendency towards space segregation of chemical incompatible molecular fragments. It was initially suggested that the inherent flexibility of liquid crystal dimers would inhibit the formation of smectic phases [18] but this was shown not to be the case by Date *et al.*[19] who reported the extensive smectic

* Corresponding author.
E-mail address: ewan.cruickshank2@abdn.ac.uk (E. Cruickshank).
[1] Present Address: School of Pharmacy and Life Sciences, Robert Gordon University, Aberdeen, AB10 7GJ, U.K.

https://doi.org/10.1016/j.molliq.2023.123226
Received 20 July 2023; Received in revised form 21 September 2023; Accepted 2 October 2023
Available online 9 October 2023

polymorphism exhibited by the α,ω-bis(4-alkylanilinebenzylidine-4′-oxy)alkanes, Fig. 1. The materials reported by Date *et al* [19] are referred to as the *m*.O*n*O.*m* series in which *n* refers to the number of methylene units in the flexible spacer, and *m* the number of carbon atoms on the terminal chains. This acronym reflects the structural relationship to the *N*-(4-alkyloxybenzylidine)-4′-alkylanilines, Fig. 2. These compounds are referred to using the acronym *n*O.*m* in which *n* and *m* refer to the number of carbon atoms in the alkyloxy and alkyl chains, respectively.

The *n*O.*m* series are a rich source of smectic phases, and their study played a key role in establishing the structures of smectic phases and their relationships to molecular structure [20–24]. All the smectic phases seen for the *m*.O*n*O.*m* series were observed when the length of the terminal chains was greater than half the length of the spacer and all showed monolayer structures. This relationship was accounted for in terms of microphase separation into three distinct regions; the aromatic moieties, the terminal chains and the spacers [19]. This is now established as rather general behaviour for symmetric liquid crystal dimers [14,25–29].

Non-symmetric dimers showed very different smectic behaviour and the study of the α-(4-cyanobiphenyl-4′-yloxy)-ω-(4-alkylanilinebenzylidene-4′-oxy)alkanes, Fig. 3, led to the discovery of the intercalated smectic phases [30–32].

These dimers are referred to as the CBO*n*O.*m* series in which *n* and *m* refer to the number of carbon atoms in the spacer and terminal chain, respectively [30–32]. Their design was again based on the strong smectic tendencies of the *n*O.*m* series referred to earlier, and that binary mixtures of a member of the *n*O.*m* series with a member of the 4-alkoxy-4′-cyanobiphenyls were known to show induced or enhanced smectic phases [20,33]. The smectic behaviour observed for the CBO*n*O.*m* series was without precedent; for example, for the CBO6O.*m* series a smectic A, SmA, phase was seen for both short and long terminal chains but intermediate chain lengths only showed nematic, N, behaviour. This behaviour was in stark contrast to that observed for conventional low molar mass liquid crystals for which increasing a terminal chain length simply increases the smectic tendencies of the material. The remarkable behaviour of the CBO6O.*m* series was accounted for in terms of the structure of the smectic phases observed [32]. Specifically, for short terminal chains an intercalated smectic A phase was seen in which differing parts of the molecules overlap. The mesogenic units form one microdomain and the alkyl chains another. This arrangement is thought to be stabilised by a favourable interaction between the unlike mesogenic units and suggested to be an electrostatic quadrupolar interaction between groups having quadrupole moments of opposite signs [34]. For long terminal chains lengths, an interdigitated smectic A phase was observed, driven by the anti-parallel association of the cyanobiphenyl units to minimise dipolar energy and resulting from the molecular inhomogeneity arising from the long terminal alkyl chain. For intermediate chain lengths, presumably there is a competition between these incompatible structures in which neither is preferred and hence, only nematic behaviour is observed.

The question arises, what happens if we reverse the imine (–CH=N-) link in the benzylideneaniline moieties in the symmetric *m*.O*n*O.*m* and non-symmetric CBO*n*O.*m* dimers? If we first consider the conventional low molar mass mesogens upon which the dimers were based, the *n*O.*m* series, then reversing the link gives the *m*.O*n* series in which the *period* represents –CH=N- such that 2O.3 on reversing the link becomes 3.O2. The *n*O.*m* series has attracted the greater research focus due to their more straightforward synthesis, but where comparisons are possible

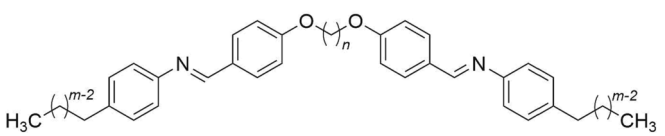

Fig. 1. Molecular structure of the *m*.O*n*O.*m* series.

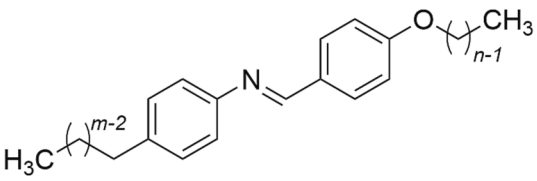

Fig. 2. Molecular structure of the *n*O.*m* series.

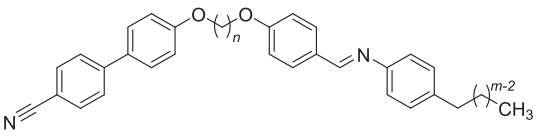

Fig. 3. Molecular structure of the CBO*n*O.*m* series.

reversing the imine link appears to have little effect. For example, 2O.6 and 6.O2 both show only nematic phases and their nematic-isotropic transition temperatures, T_{NI}, are 80 C and 82 C, respectively [35,36]. This similarity in behaviour is perhaps unsurprising. If we consider the dimeric architecture, however, then by tethering one benzylideneaniline unit *via* the spacer to another mesogenic moiety fixes, at least to some extent, their relative orientations, and given that the behaviour of the non-symmetric dimers, in particular, appears to be predicated upon specific interactions between the unlike mesogenic units, the effects of reversing the imine link are far less predictable than for the conventional low molar mass systems.

Surprisingly, this important question appears not to have not been investigated, and to rectify this, here we report the synthesis and characterisation of the 1,5-bis(4′-oxyanilinebenzylidene-4-alkane)pentanes, Fig. 4, and refer to these dimers using the acronym *m*-O5O-*m* in which the hyphen indicates the reversal of the imine linkages compared to the *m*.O5O.*m* series.

We also report the behaviour of the 1-(4-cyanobiphenyl-4′-yloxy)-5-(4′-oxyanilinebenzylidene-4-alkane)pentanes, Fig. 5, and use the acronym CBO5O-*m* to describe these. In order to evaluate the effects of reversing the imine linkage, we also revisit the behaviour of the CBO5O.*m* series.

We choose odd-membered dimers to be the focus of this study reflecting the very high level of interest in these bent molecules and their ability to exhibit the new twist-bend phases [4,13–17,37–40].

2. Experimental

2.1. Synthesis

The synthetic route used to prepare the *m*-O5O-*m* series is shown in Scheme 1, and for the CBO5O-*m* series in Scheme 2. A detailed description of the preparation of all members of these series, including the structural characterisation data for all intermediates and final products, is provided in the Supplementary Information.

2.2. Optical studies

Phase characterisation was performed by polarised light microscopy, using an Olympus BH2 polarising light microscope equipped with a

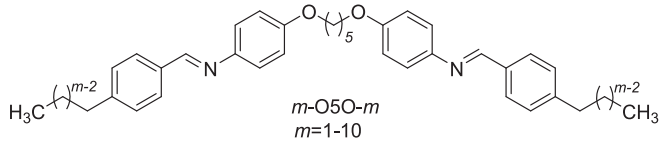

Fig. 4. Molecular structure of the *m*-O5O-*m* series.

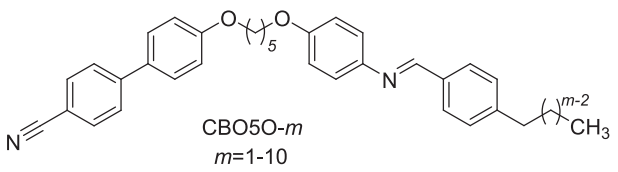

Fig. 5. Molecular structure of the CBO5O-*m* series.

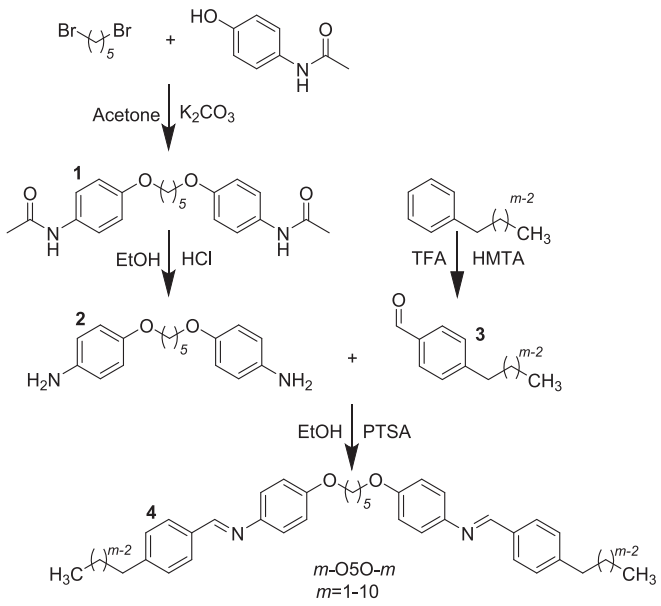

Scheme 1. Synthesis of the *m*-O5O-*m* series.

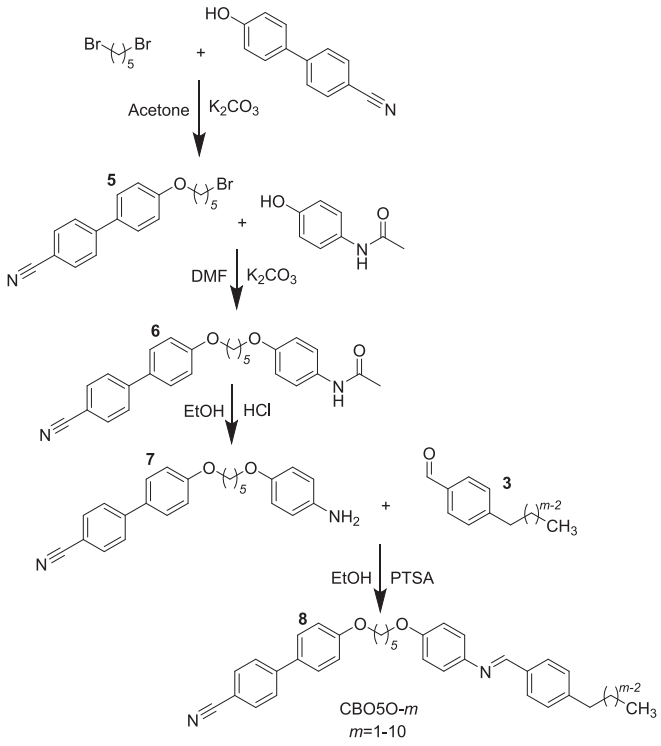

Scheme 2. Synthesis of the CBO5O-*m* series.

Linkam TMS 92 hot stage. The untreated glass microscope slides used were 0.17 mm thick.

2.3. Differential scanning calorimetry

The phase behaviour of the materials was studied by differential scanning calorimetry performed using a Mettler Toledo DSC1 or DSC3 differential scanning calorimeter equipped with TSO 801RO sample robots and calibrated using indium and zinc standards. Heating and cooling rates were 10 °C min^{-1}, with a 3-min isotherm between either heating or cooling, and all samples were measured under a nitrogen atmosphere. Transition temperatures and associated enthalpy changes were extracted from the heating traces unless otherwise noted.

2.4. Molecular modelling

The geometric parameters of the *m*-O*n*O-*m*, and CBO5O-*m* series were obtained using quantum mechanical DFT calculations with Gaussian09 software [41]. Optimisation of the molecular structures was carried out at the B3LYP/6-31G(d) level of theory. Visualisations of electronic surfaces and ball-and-stick models were generated from the optimised geometries using the GaussView 5 software, and visualisations of the space-filling models were produced post-optimisation using the QuteMol package [42].

2.5. X-ray diffraction measurements

The wide-angle X-ray diffraction measurements were obtained with a Bruker D8 GADDS system (CuKα line, Goebel mirror, point beam collimator, Vantec2000 area detector). Samples were prepared as droplets on a heated surface. The small angle X-ray diffraction (SAXS) patterns were obtained with a Bruker Nanostar system using CuKα radiation and patterns were collected with a Vantec2000 area detector. Samples were prepared as droplets on a heated surface. The temperature dependence of the layer thickness was determined from the small-angle X-ray diffraction experiments performed with a Bruker D8 Discover system (CuKα line, Goebel mirror, Anton Paar DCS350 heating stage, scintillation counter) working in the reflection mode. Homeotropically aligned samples were used, prepared as a thin film on a silicon reflectionless wafer.

2.6. Birefringence measurements

The birefringence was calculated from the optical retardation measured with a setup based on a photoelastic modulator (PEM-90, Hinds) working at a modulation frequency $f = 50$ kHz; as a light source, a halogen lamp (Hamamatsu LC8) was used equipped with a narrow band pass filter (532 nm). The signal from a photodiode (FLC Electronics PIN-20) was deconvoluted by a lock-in amplifier (EG&G 7265) into 1*f* and 2*f* components to yield the retardation induced by the sample. Knowing the sample thickness, the retardation was recalculated into optical birefringence. For measurements 3-μm-thick cells were used with a planar alignment layer.

3. Results and discussion

The transitional properties for the *m*-O5O-*m* series are listed in Table 1. For $m \leq 7$, a conventional monotropic nematic phase, N, was observed, and assigned by the observation of a characteristic schlieren texture containing both two- and four-point brush defects, and which flashed when subjected to mechanical stress, Fig. 6 **(a)**. This assignment is supported by the values of $\Delta S_{NI}/R$ which are typical for odd-membered dimers [19,43,44]. On cooling the N phase of 7-O5O-7 a

Table 1
Transition temperatures for the *m*-O5O-*m* series with the associated scaled entropy changes, ΔS/R, given in brackets.

m	T_{Cr-}/ °C (ΔS/R)	T_{SmYSmC}/ °C (ΔS/R)	T_{SmCSmA}/ °C (ΔS/R)	T_{SmAN}/ °C (ΔS/R)	T_{NI}/ °C (ΔS/R) ‡T_{SmAI}/ °C (ΔS/R) *T_{SmCI}/ °C (ΔS/R)
1	164 (14.5)	–	–	–	[b]140
2	150 (15.0)	–	–	–	[b]119
3	146 (15.7)	–	–	–	[a]139 (0.43)
4	133 (16.7)	–	–	–	[a]123 (0.27)
5	133 (16.9)	–	–	–	[a]132 (0.48)
6	130 (17.4)	–	–	–	[a]123 (0.34)
7	128 (17.6)	[b]112	[b]115	[a,c]126 (2.04)	[a,c]127 (2.04)
8	126 (17.8)	[b]115	[c]*127 (2.91)	–	[c]‡129 (2.91)
9	123 (13.7)	[a]116 (3.12)	–	–	*132 (3.39)
10	120 (14.3)	[a]117 (4.56)	–	–	*131 (3.92)

[a] Values extracted from DSC cooling traces.
[b] Measured using the polarised light microscope.
[c] Combined ΔS/R value of those associated with both phase transitions due to peak overlap in the DSC trace.

focal conic fan texture developed which could be sheared to give homeotropic regions, characteristics of a smectic A, SmA, phase, Fig. 6 **(b)**. For 8-O5O-8, a focal conic fan texture was observed directly from the isotropic phase in co-existence with homeotropic regions indicative of a SmA phase. Cooling the sample further saw the emergence of a birefringent schlieren texture from the previously homeotropic regions, Fig. 6 **(c)**, characteristic of a smectic C, SmC, phase. For $m = 9$ and 10, a focal conic fan texture in co-existence with regions of schlieren texture was observed directly from the isotropic phase indicating a SmC-I transition. This assignment was consistent with the values of $\Delta S_{SmCI}/R$ which are typical for odd-membered dimers [19,43,45]. On cooling the smectic C phase shown by $m = 7$-10, the focal conic fans became broken with banding and the regions of schlieren texture became poorly defined, Fig. 6 **(d)**. This texture does not allow for an unambiguous phase assignment and instead the phase is termed the smectic Y phase. The values of $\Delta S_{SmYSmC}/R$ suggest that the smectic Y phase is either a hexatic or soft crystal phase. Further examples of the textures observed for these materials are shown in **Figure S1**.

X-ray diffraction was used to characterise the smectic phases of 9-O5O-9 and 10-O5O-10. The diffraction patterns of the smectic C phases contained a sharp peak in the small angle region, Fig. 7 **(a)**, corresponding to distances of 46.6 Å and 47.0 Å for 9-O5O-9 and 10-O5O-10, and these values are comparable to their molecular lengths, 49.1 Å and 50.6 Å respectively, suggesting a monolayer packing arrangement. The signal in the wide-angle region was diffuse indicating liquid-like ordering within the layers. The layer spacing in the SmC phase decreased with decreasing temperature as would be expected, Fig. 8. In

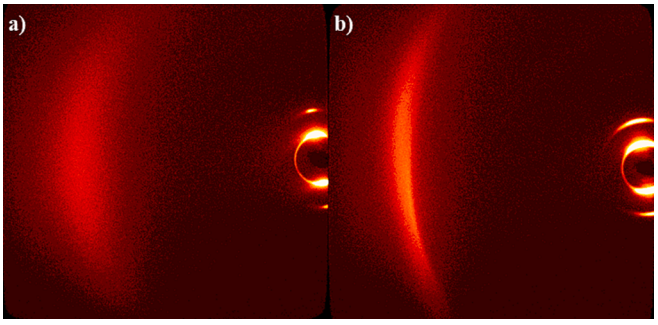

Fig. 7. X-ray diffraction pattern for 10-O5O-10 in the (a) smectic C phase (T = 128 °C) and (b) smectic Y phase (T = 117 °C).

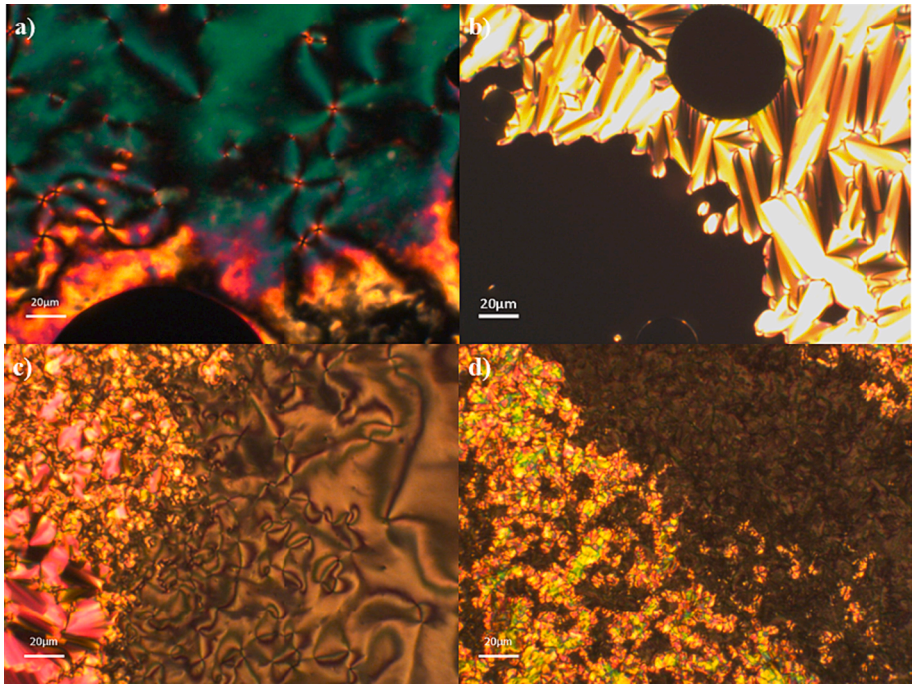

Fig. 6. Optical textures observed for the *m*-O5O-*m* series: (a) the schlieren texture of the nematic phase (T = 127 °C) for 7-O5O-7; (b) the focal conic fan texture in coexistence with homeotropic regions of the smectic A phase (T = 126 °C) for 7-O5O-7; (c) the focal conic fan texture in coexistence with regions of schlieren texture of the smectic C phase (T = 130 °C) for 10-O5O-10; (d) representative texture of the smectic Y phase (T = 117 °C) for 10-O5O-10.

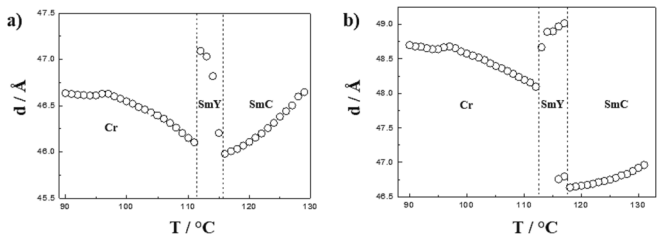

Fig. 8. The dependence of the layer spacing, *d*, on temperature for (a) 9-O5O-9 and (b) 10-O5O-10 measured on cooling.

the SmY phase, additional low angle signals appeared in the scattering pattern, **Figure S2**, suggesting that it has a modulated structure built of layer fragments. There is a narrowing of the wide-angle signal at the SmC-SmY transition indicating an increase in the ordering within the layers, Fig. 7 **(b)**. These observations suggest that the SmY phase is a hexatic smectic phase. At the transition to the SmY phase, the layer spacing increases, Fig. 8, presumably associated with the increase in order. The SmY phase also has a monolayer structure.

The dependence of the transition temperatures on the length of the terminal alkyl chain, *m*, for the *m*-O5O-*m* series is shown in Fig. 9. The melting points decrease on increasing *m,* and this may be attributed to the longer terminal chains disrupting the packing in the crystalline phase, and the increased component of the melting entropy change associated with the increasing number of conformations of the terminal chain in the fluid phase. The values of T_{NI} alternate on increasing *m* with the odd members showing the higher values. The alternation is associated with the change in molecular shape on varying the parity of *m* and this has been discussed in detail elsewhere [32,37,44]. Smectic phase behaviour emerges at $m = 7$, and the nematic phase is extinguished at $m = 8$. The emergence of smectic behaviour at this chain length is consistent with the empirical rule proposed by Date *et al* [19] that for smectic behaviour to be observed in symmetric dimers the length of the terminal chains must be greater than half the length of the spacer.

For comparative purposes, Fig. 10 shows the dependence of the transition temperatures on *m* for the *m*.O5O.*m* series [19]. It is immediately apparent that the melting points of the *m*-O5O-*m* series tend to be higher than those of the corresponding members of the *m*.O5O.*m* series, such that the former series is largely monotropic in nature whereas the latter tends to be enantiotropic. Smectic behaviour emerges earlier in the *m*.O5O.*m* series, for 4.O5O.4, and the nematic phase is extinguished earlier, at 6.O5O.6. Both series show the SmA and SmC phases, and a hexatic phase, all of which have monolayer structures. The relative stability of the SmC phase is greater for the *m*-O5O-*m* series. Fig. 11 compares the clearing temperatures of the *m*-O5O-*m* and *m*.O5O.*m*

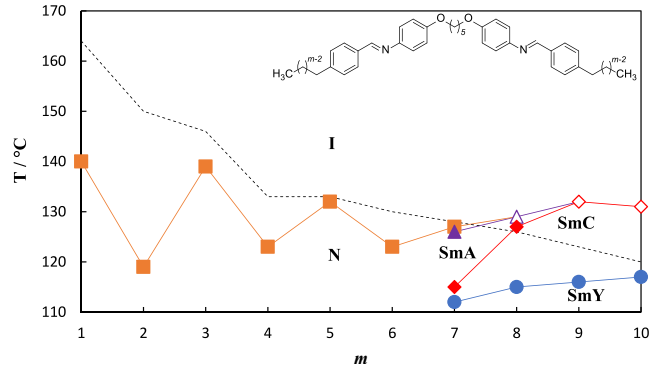

Fig. 9. Dependence of the transition temperatures on the length of the terminal alkyl chain, *m*, for the *m*-O5O-*m* series. The filled squares denote T_{NI}, the filled triangle T_{SmAN}, the open triangle T_{SmAI}, the filled diamonds T_{SmCSmA}, the open diamonds T_{SmCI}, the circles T_{SmYSmC} and the dotted line indicates the melting points.

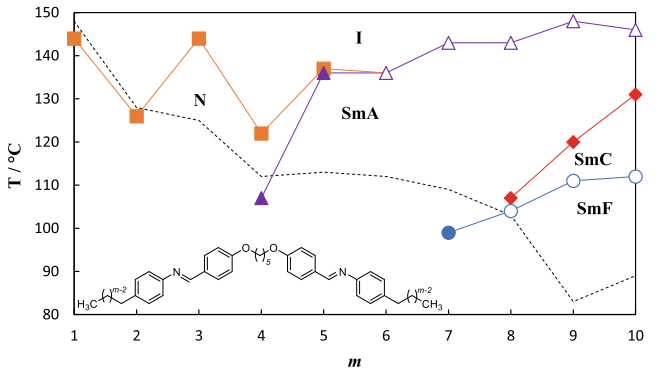

Fig. 10. Dependence of the transition temperatures on the length of the terminal alkyl chain, *m*, for the *m*.O5O.*m* series. The filled squares denote T_{NI}, the filled triangles T_{SmAN}, the open triangles T_{SmAI}, the filled diamonds T_{SmCSmA}, the open diamonds T_{SmCI}, the circles T_{SmYSmC} and the dotted line indicates the melting points.

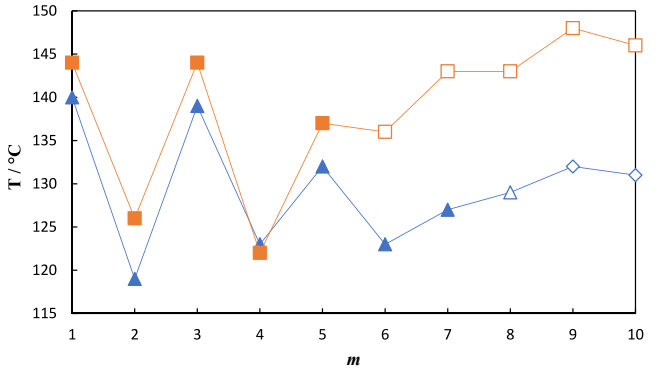

Fig. 11. A comparison of the clearing temperatures of the *m*.O5O.*m* series, represented by squares, and *m*-O5O-*m* series, represented by triangles and diamonds. Filled symbols represent N-I transitions, open symbols SmA-I transitions and the open diamonds SmC-I transitions.

series [19]. We revisited the behaviour of 5.O5O.5 and found a short nematic phase ($T_{SmAN} = 136$ °C and $T_{NI} = 137$ °C) not reported by Date *et al.* [19]. For short terminal chains, $m \leq 5$, both series show nematic-isotropic transitions, and on average the values of T_{NI} for the *m*.O5O.*m* series are around 4 °C higher than that of the corresponding member of the *m*-O5O-*m* series. It is unsurprising that there are only small differences in these values and this is consistent with the behaviour reported for similar symmetric dimers [25,37,44]. Quite different behaviour is observed, however, when comparing the smectic-isotropic transition temperatures shown by the two series for which those of the *m*.O5O.*m* series are, on average, over 19 °C higher than that of the corresponding member of the *m*-O5O-*m* series. We note that this comparison is between the unlike transitions, i.e. SmA-I transitions for the *m*.O5O.*m* series and SmC-I transitions for the *m*-O5O-*m* series with the sole exception being $m = 8$, for which T_{SmAI} of 8.O5O.8 is 26 °C higher than that of 8-O5O-8. It is clear that reversing the imine link in these dimers has a considerably more pronounced effect on the stability of the smectic phases than the nematic phase.

Fig. 12 compares the molecular shapes and electrostatic potential surfaces for 4-O5O-4 with 4.O5O.4. Reversing the direction of the imine link has little effect on molecular shape and this presumably accounts, at least in part, for the rather similar values of T_{NI} shown by these materials. By contrast, the electrostatic potential surfaces reveal more significant differences between the two dimers. It is clear for 4-O5O-4 that the electron distribution is more evenly spread across the benzylideneaniline fragment than it is for 4.O5O.4 in which greater electron density is located on the aniline ring. In addition, there is a significant

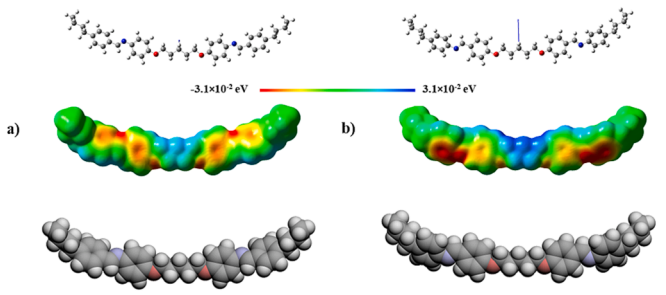

Fig. 12. (top) Ball-and-stick models, (middle) electrostatic potential surfaces and (bottom) space-filling models of (a) 4-O5O-4 and (b) 4.O5O.4. The arrows denote the positive direction of the dipole moment of the molecule: for 4-O5O-4, μ = 1.44 D into the plane and for 4.O5O.4, μ = 3.59 D parallel to the plane.

Table 2
Transition temperatures for the CBO5O-*m* series with the associated scaled entropy changes, ΔS/R, given in brackets.

m	T_{Cr-}/ °C (ΔS/R)	T_{SmXSmA}/ °C (ΔS/R)	T_{SmAN}/ °C (ΔS/R)	T_{NTBN}/ °C (ΔS/R)	T_{NI}/ °C (ΔS/R)
1	140 (9.11)	–	–	[b]85	166 (0.26)
2	143 (6.83)	–	–	–	158 (0.24)
3	118 (8.95)	–	–	[c]84	160 (0.26)
4	114 (9.84)	–	–	–	151 (0.26)
5	107 (8.80)	–	–	–	150 (0.33)
6	108 (9.45)	–	–	–	142 (0.28)
7	109 (9.16)	–	–	–	143 (0.34)
8	107 (11.3)	–	–	–	137 (0.26)
9	110 (9.18)	–	[b]103	–	136 (0.34)
10	108 (10.7)	[a]92 (≈ 0)	123 (0.027)	–	132 (0.28)

[a] Values extracted from DSC cooling traces.
[b] Measured using the polarised light microscope.
[c] Virtual transition temperature estimated from a binary phase diagram with CB7CB.

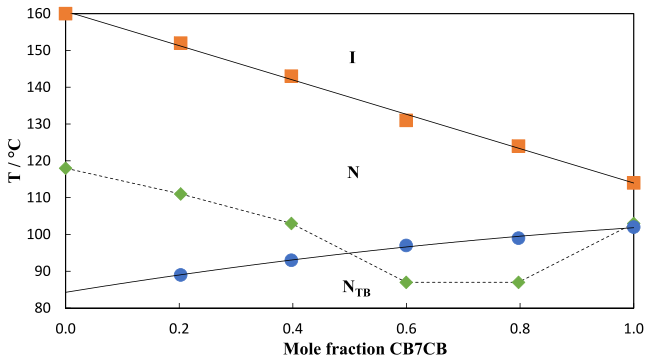

Fig. 14. Phase diagram constructed for binary mixtures of CBO5O-3 and CB7CB. Squares denote T_{NI}, circles T_{NTBN} and diamonds the melting points. The solid lines indicate trend lines drawn for both T_{NI} and T_{NTBN}. The dotted line connects the melting points.

difference in the magnitude and orientation of the dipole moments of the two dimers, and that of 4.O5O.4 is larger by over 2 D. Similar differences have been reported for conventional low molar mass mesogens on reversing the direction of an imine linkage [46]. These changes presumably have a more significant effect on the interactions between the mesogenic units which drive the formation of smectic phases. We will return to this theme later.

We now turn our attention to the effects of reversing the direction of the imine bond in a non-symmetric dimeric series, and the transitional properties for the CBO5O-*m* series are listed in Table 2. All ten members of the series exhibited a conventional, enantiotropic nematic phase, N, assigned by the observation of a characteristic schlieren texture containing both two- and four-point brush defects and which flashed when subjected to mechanical stress, Fig. 13 **(a)**. The measured values of $\Delta S_{NI}/R$ are consistent with those found for bent dimers [19,43,45]. On cooling

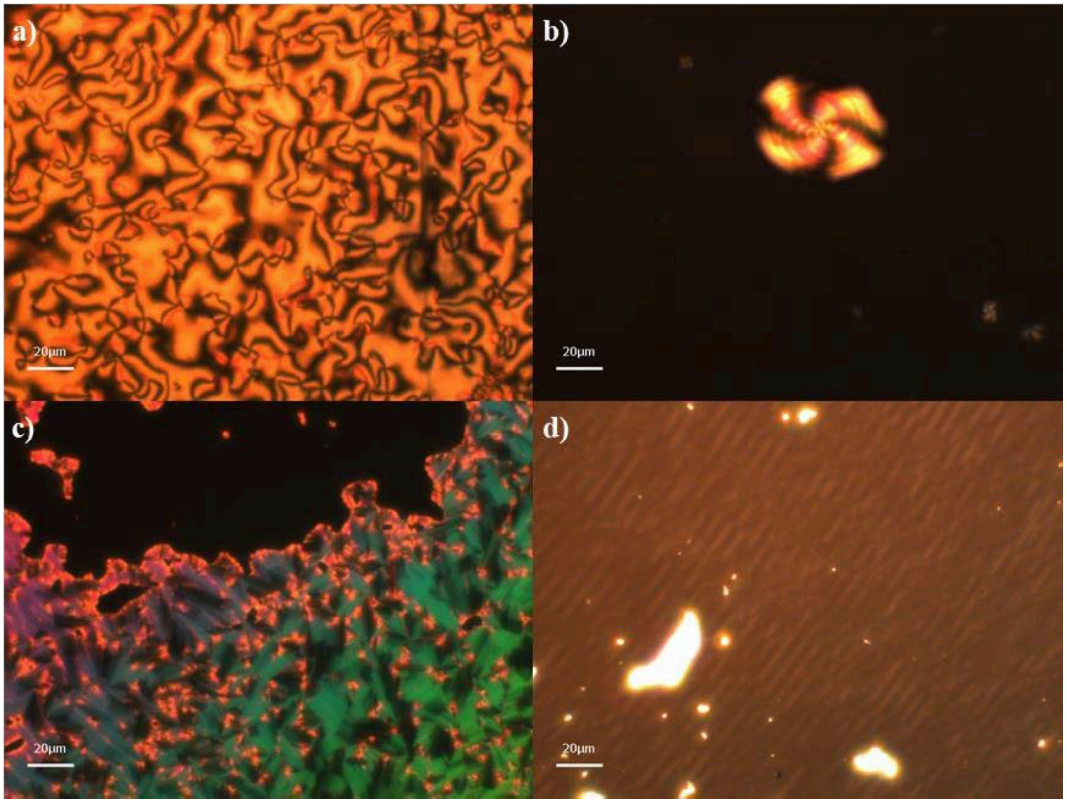

Fig. 13. Textures observed for the CBO5O-*m* series: (a) schlieren texture of the nematic phase (T = 136 °C) for CBO5O-9; (b) blocky schlieren texture in isolated droplets of the twist–bend nematic phase (T = 84 °C) for CBO5O-1; (c) focal conic fan texture with extinct regions of the smectic A phase (T = 121 °C) for CBO5O-10; (d) region of moving stripes of opposing birefringence of the smectic X phase (T = 91 °C) for CBO5O-10.

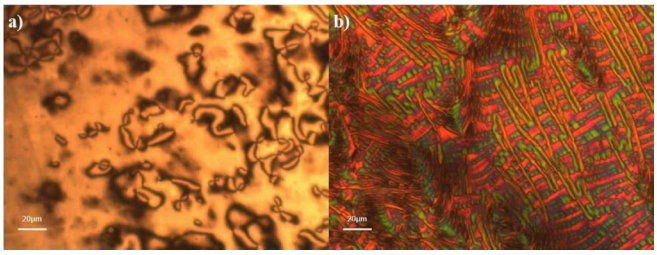

Fig. 15. Textures observed for the 40:60 mol % mixture of CB7CB:CBO5O-3: (a) schlieren texture of the nematic phase (T = 141 °C) and (b) rope-like and parabolic texture of the twist-bend nematic phase (T = 80 °C).

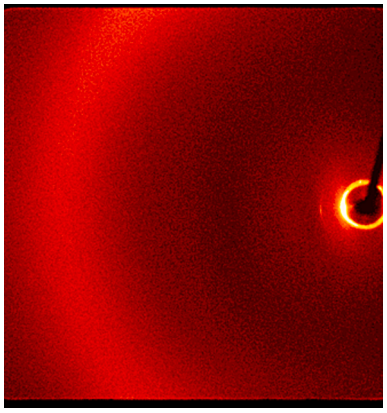

Fig. 16. 2D X-ray diffraction pattern for CBO5O-10 in the smectic A phase (T = 128 °C).

the nematic phase for $m = 1$, in isolated droplets a cessation of the optical flickering associated with director fluctuations was observed and a blocky schlieren texture emerged, characteristic of the twist-bend nematic phase, Fig. 13 **(b)**. For the other homologues with $m \leq 8$, the rapid onset of crystallisation precluded the observation of additional liquid crystalline behaviour. For the homologues with $m \geq 9$, on cooling the nematic phase, a focal conic fan texture developed, which could be sheared to give optically extinct regions characteristic of the uniaxial

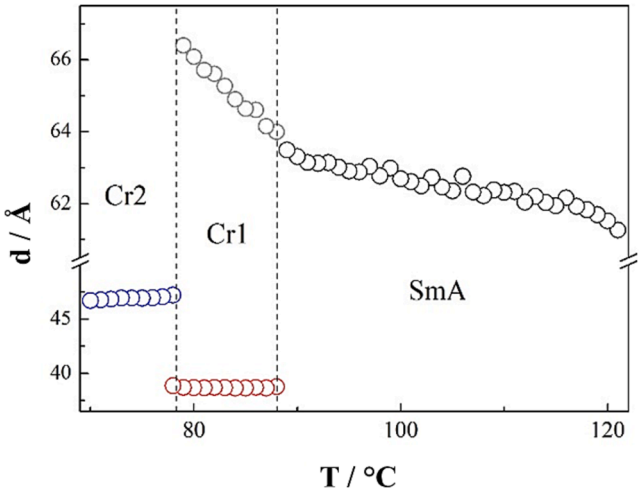

Fig. 17. The dependence of the layer spacing (*d*) on temperature for CBO5O-10 measured on cooling (black circles). The red and blue circles represent the longest periodicities measured in the two crystalline phases observed on cooling the sample. Note that in the temperature range of Cr1, the sample was not fully crystalized and the SmA phase co-existed with the Cr1 phase. (For interpretation of the references to colour in this figure legend, the reader is referred to the web version of this article.)

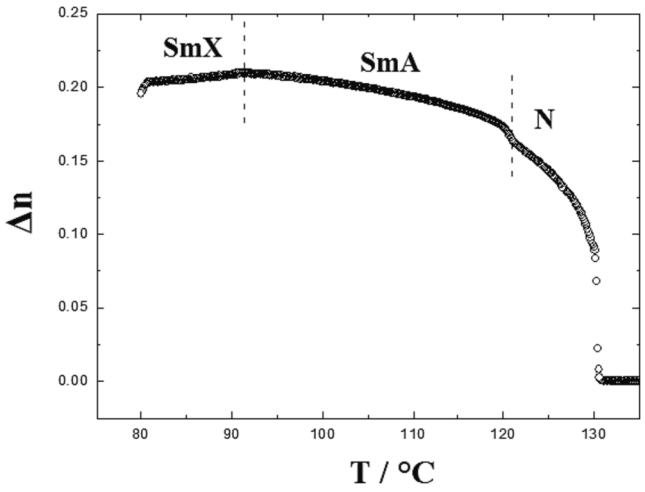

Fig. 18. Temperature dependence of the optical birefringence for green light (λ = 532 nm) for CBO5O-10.

smectic A phase, Fig. 13 **(c)**. For $m = 10$, on cooling the smectic A phase, a weakly birefringent schlieren texture emerged from the extinct regions containing moving stripes of opposing birefringence, Fig. 13 **(d)**. We have reported the observation of similar schlieren textures for the $SmC_{TB\text{-}SH}$ phase, [16,17,47] but this texture cannot be used to provide an unambiguous phase assignment and so the phase was labelled smectic X.

To investigate potential twist-bend nematic phase behaviour in the longer homologues, a binary phase diagram was constructed using mixtures of CBO5O-3 and CB7CB, Fig. 14. Complete miscibility between the two compounds was observed over the whole composition range. The melting points of the mixtures show eutectic behaviour. The higher temperature phase seen for all the mixtures was a conventional nematic phase, see Fig. 15 **(a)**. On cooling the nematic phase, regions of rope-like textures coexisting with a parabolic texture formed, characteristic of the twist-bend nematic phase, Fig. 15 **(b)**. In addition, the transition was accompanied by the cessation of the optical flickering associated with director fluctuations. The values of T_{NI} increase in essentially a linear manner as the concentration of CBO5O-3 increases, Fig. 14. The T_{NTBN} trendline shows a small upwards curvature and the virtual transition temperature for the N_{TB}-N phase transition was estimated to be 84 °C. This is similar to the value observed for CBO5O-1 of 85 °C and suggests that the stability of the N_{TB} phase does not fall dramatically on increasing *m*, but instead it is the tendency of the materials to crystallise that precludes the observation of the N_{TB} phase.

The X-ray diffraction pattern of the smectic A phase shown by CBO5O-10 consists of a sharp reflection in the small angle region arising

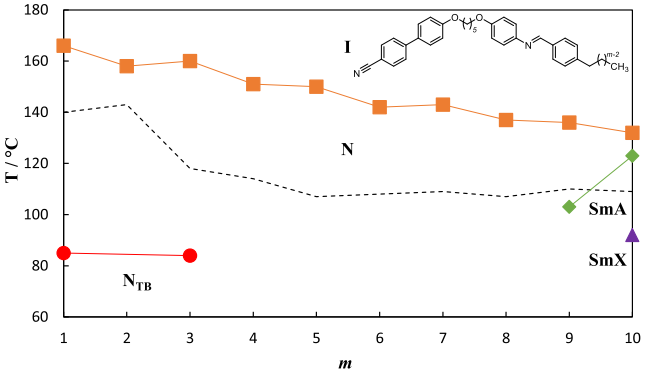

Fig. 19. Dependence of the transition temperatures on the length of the terminal alkyl chain, *m*, for the CBO5O-*m* series represented by squares for T_{NI}, circles for T_{NTBN}, diamonds for T_{SmAN} and the triangle for T_{SmXSmA}. The dotted line indicates the melting points.

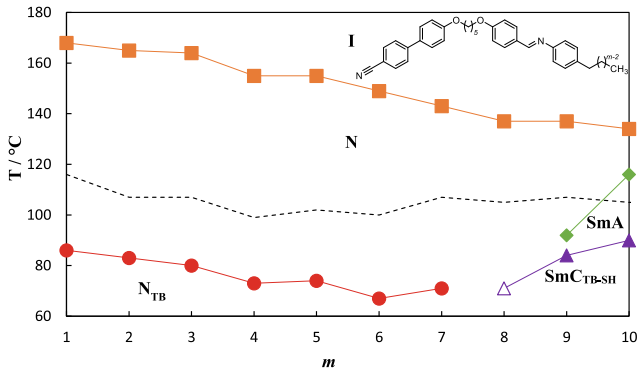

Fig. 20. Dependence of the transition temperatures on the length of the terminal alkyl chain, *m*, for the CBO5O.*m* series represented by squares for T_{NI}, circles for T_{NTBN}, diamonds for T_{SmAN}, the open triangle for $T_{SmCTB-SHN}$ and the filled triangles for $T_{SmCTB-SHSmA}$. The dotted line indicates the melting points.

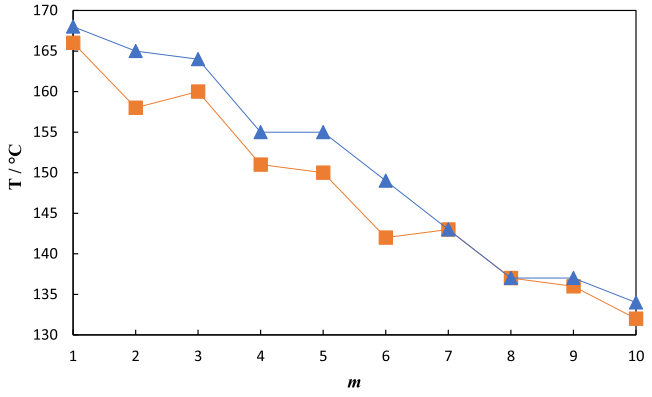

Fig. 21. The dependence of T_{NI} on *m* for the CBO5O-*m* series represented by squares and the CBO5O.*m* series represented by triangles.

from the layered structure and a diffuse peak in the wide angle indicating the liquid-like arrangement of the molecules within the layers, see Fig. 16. The layer periodicity is 61 Å, around 1.7 times the molecular length, implying an interdigitated packing arrangement. The layer spacing increases slightly on decreasing temperature as expected for an orthogonal phase when the order parameter increases, Fig. 17. Crystallisation precluded the study of the SmX phase using X-ray diffraction.

Fig. 18 shows the temperature dependence of the optical birefringence, Δ*n*, for CBO5O-10. On cooling from isotropic phase, a rapid increase is seen in Δ*n* at the I-N transition which followed a power law temperature dependence. At the SmA-N transition, the birefringence increased in a stepwise manner due to the increase in the order parameter and continued to increase throughout the SmA phase as expected for an orthogonal phase. In the smectic X phase, Δ*n* is smaller than expected from the extrapolation of the dependence seen in the smectic A phase. This suggests that the increase in the order parameter is compensated for by a secondary factor such as the molecules tilting within the phase supporting the suggestion made on the basis of optical textures that this is the SmC_{TB-SH} phase.

The dependence of the transition temperatures on the length of the terminal alkyl chain, *m*, for the CBO5O-*m* series is shown in Fig. 19. The values of T_{NI} decrease as *m* increases, and superimposed on this decrease is an alternation in which the odd members show the higher values. This may be attributed to the change in shape associated with the parity of *m* as described in detail in the literature [19,30]. The stability of the N_{TB} phase appears not to be strongly dependent on *m*. Smectic behaviour appears for $m = 9$ and the value of T_{SmAN} shows a strong increase moving from $m = 9$ to 10.

The dependence of the transition temperatures on the length of the terminal alkyl chain, *m*, for the CBO5O.*m* series is shown in Fig. 20 [14,30,48]. The transitional properties are listed in **Table SI5**. For $m =$ 1-7, an enantiotropic conventional nematic phase and monotropic N_{TB} phase are observed. The N_{TB} phase is extinguished for $m = 8$ and is replaced by the SmC_{TB-SH} phase. The remaining members, $m = 9$ and 10, exhibit an enantiotropic nematic phase and SmA phase and SmC_{TB-SH} phases. The phase behaviour of the CBO5O-*m* and CBO5O.*m* series is rather similar unlike the contrasting behaviour seen between the *m*-O5O-*m* and *m*.O5O.*m* series, and we will return to this later.

Fig. 21 compares the values of T_{NI} for the CBO5O-*m* series and CBO5O.*m* series [14,30,48]. The values of T_{NI} for the CBO5O.*m* series tend to be higher, but by only around 3 °C on average. This implies that changing the direction of the imine linkage within the benzylideneaniline unit of these dimers has only a small impact on how the molecules interact within the nematic phase. This presumably reflects, at least to some extent, the very similar shapes of the CBO5O-*m* and CBO5O.*m* series, see Fig. 22. This also accounts for the very similar T_{NTBN} values seen for CBO5O.1 and CBO5O-1. It is surprising, however, that reversing

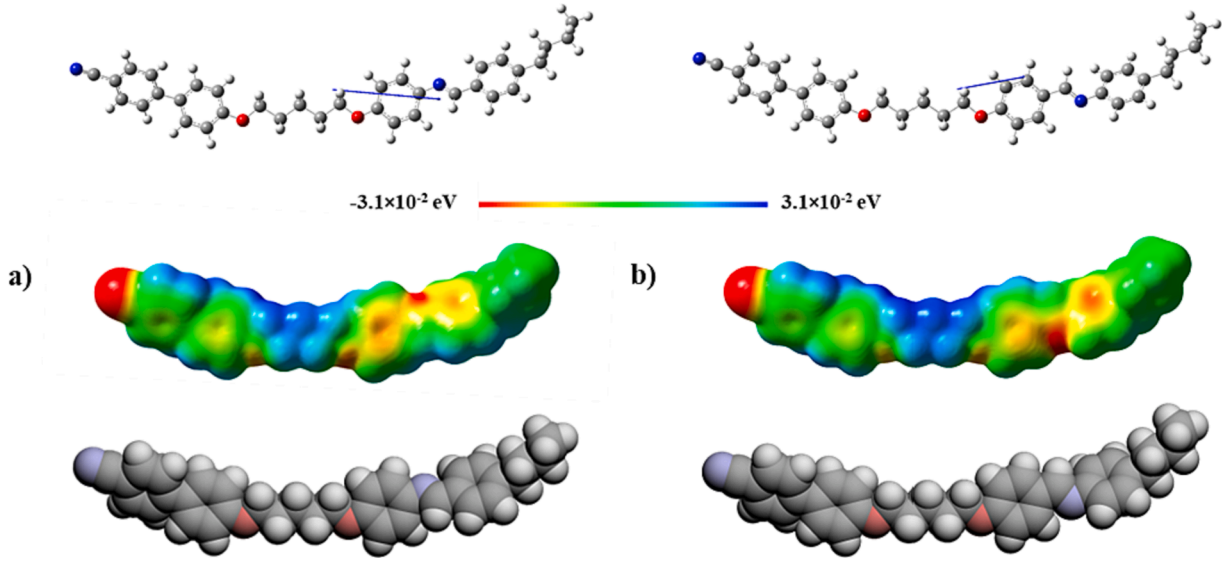

Fig. 22. (top) Ball-and-stick models, (middle) electrostatic potential surfaces and (bottom) space-filling models of (a) CBO5O-4 and (b) CBO5O.4. The arrows denote the positive direction of the dipole moment of the molecule: for CBO5O-4, μ = 6.94 D parallel to the plane and for CBO5O.4, μ = 4.42 D parallel to the plane.

the direction of the imine linkage has not significantly changed the specific interaction between the unlike mesogenic units that is thought to be important in determining the transition temperatures of these dimers [30]. Unlike the behaviour seen for the symmetric dimers earlier, the values of T_{SmAN} for the CBO5O-*m* series are in fact higher than those for the CBO5O.*m* series by some 9 °C [14]. The overall molecular dipole of CBO5O-4 is 6.94 D, Fig. 22 **(a)**, compared 4.42 D for CBO5O.4, Fig. 22 **(b)**. As we saw earlier for the symmetric dimers, reversing the imine link changes the electrostatic potential surface of the benzylideneaniline fragment and for CBO5O-4, Fig. 22 **(a)**, the electron density appears more evenly spread between the two rings whereas for CBO5O.4, Fig. 22 **(b)**, this distribution is shifted to the aniline ring. Both dimers show an interdigitated smectic A phase in which the relative orientation of the benzylideneaniline fragments are the same as in a monolayer smectic A phase. It is not clear, therefore, why reversing the imine link in the symmetric *m*.O*n*O.*m* series reduces the tendency to show smectic behaviour but for the CBO*n*O.*m* series instead increases the smectic tendency.

4. Conclusions

Reversing the direction of the imine link in the benzylideneaniline fragments in the symmetric *m*.O5O.*m* dimers to give the *m*-O5O-*m* series has little effect on the values of T_{NI}. Specifically, members of the *m*.O5O.*m* series show slightly higher values. By contrast, members of the *m*.O5O.*m* series show considerably higher values of the smectic-isotropic transition temperature than the corresponding member of the *m*-O5O-*m series*. The values of T_{NI} are also similar for the non-symmetric CBO5O.*m* and CBO5O.*m* dimers, with those of the CBO5O.*m* series marginally higher. Unlike the behaviour seen for the symmetric dimers, however, the values of T_{SmAN} are higher for the CBO5O-*m* than the CBO5O.*m* dimers. The similarity in the values of T_{NI} between the corresponding dimers with inverted imine linkages is attributed, at least in part, to the similarity in shapes between the respective series. The contrasting trends in the values of T_{SmI} between the symmetric and nonsymmetric dimers is surprising given that the relative orientations of the benzylideneaniline units are the same in the monolayer phases seen for the symmetric dimers and interdigitated smectic phases seen in the nonsymmetric materials. Furthermore, the phase behaviour of the CBO5O.*m* series is thought to be governed, to some extent, by the mixed interaction between the unlike mesogenic groups and it would be expected that inverting the imine link would affect this interaction to a greater extent than it appears to have done given the associated change to the fragment's electrostatic potential surface. It is clear that we have much to learn about how chemically linking the mesogenic units in a dimer, as well as in higher oligomers, constrains their ability to interact, and that this important aspect of the behaviour of dimers has been rather neglected.

CRediT authorship contribution statement

Ewan Cruickshank: Conceptualization, Investigation, Visualization, Writing – original draft, Writing – review & editing, Validation. **Rebecca Walker:** Investigation, Visualization, Validation, Writing – review & editing. **Grant J. Strachan:** Investigation, Visualization, Writing – review & editing. **Charlotte H.F. Goode:** Investigation. **Magdalena M. Majewska:** Investigation, Visualization. **Damian Pociecha:** Investigation, Visualization, Resources, Writing – original draft, Writing – review & editing. **Ewa Gorecka:** Investigation, Resources, Writing – original draft, Writing – review & editing. **John M.D. Storey:** Resources, Supervision. **Corrie T. Imrie:** Conceptualization, Resources, Writing – original draft, Writing – review & editing, Supervision.

Declaration of Competing Interest

The authors declare that they have no known competing financial interests or personal relationships that could have appeared to influence the work reported in this paper.

Data availability

Data will be made available on request.

Acknowledgements

D. P. gratefully thanks the National Science Centre (Poland) under the grant no. 2021/43/B/ST5/00240.

Appendix A. Supplementary data

Supplementary data to this article can be found online at https://doi.org/10.1016/j.molliq.2023.123226.

References

[1] C.T. Imrie, P.A. Henderson, Liquid crystal dimers and higher oligomers: Between monomers and polymers, Chem. Soc. Rev. 36 (2007) 2096–2124.
[2] C.T. Imrie, P.A. Henderson, Liquid crystal dimers and oligomers, Curr. Opin. Colloid Interface Sci. 7 (2002) 298–311.
[3] C.T. Imrie, P.A. Henderson, G.Y. Yeap, Liquid crystal oligomers: Going beyond dimers, Liq. Cryst. 36 (2009) 755–777.
[4] E. Cruickshank, M. Salamończyk, D. Pociecha, G.J. Strachan, J.M.D. Storey, C. Wang, J. Feng, C. Zhu, E. Gorecka, C.T. Imrie, Sulfur-linked cyanobiphenyl-based liquid crystal dimers and the twist-bend nematic phase, Liq. Cryst. 46 (2019) 1595–1609.
[5] M. Cestari, S. Diez-Berart, D.A. Dunmur, A. Ferrarini, M.R. De La Fuente, D.J. B. Jackson, D.O. Lopez, G.R. Luckhurst, M.A. Perez-Jubindo, R.M. Richardson, J. Salud, B.A. Timimi, H. Zimmermann, Phase behavior and properties of the liquid-crystal dimer 1″,7″-bis(4-cyanobiphenyl-4′-yl) heptane: A twist-bend nematic liquid crystal, Phys. Rev. E 84 (2011) 031704.
[6] R.J. Mandle, A ten-year perspective on twist-bend nematic materials, Mol. 27 (2022) 2689.
[7] V. Borshch, Y.K. Kim, J. Xiang, M. Gao, A. Jákli, V.P. Panov, J.K. Vij, C.T. Imrie, M. G. Tamba, G.H. Mehl, O.D. Lavrentovich, Nematic twist-bend phase with nanoscale modulation of molecular orientation, Nat. Commun. 4 (2013) 2635.
[8] D. Chen, J.H. Porada, J.B. Hooper, A. Klittnick, Y. Shen, M.R. Tuchband, E. Korbloèa, D. Bedrov, D.M. Walba, M.A. Glaser, J.E. Maclennan, N.A. Clark, Chiral heliconical ground state of nanoscale pitch in a nematic liquid crystal of achiral molecular dimers, PNAS 110 (2013) 15931–15936.
[9] R. Walker, The twist-bend phases : Structure – property relationships, chirality and hydrogen-bonding, Liq. Cryst. Today 29 (2020) 2–14.
[10] D.A. Paterson, J.P. Abberley, W.T.A. Harrison, J.M.D. Storey, C.T. Imrie, Cyanobiphenyl-based liquid crystal dimers and the twist-bend nematic phase, Liq. Cryst. 44 (2017) 127–146.
[11] Y. Arakawa, Y. Ishida, K. Komatsu, Y. Arai, H. Tsuji, Thioether-linked benzylideneaniline-based twist-bend nematic liquid crystal dimers: Insights into spacer lengths, mesogenic arm structures, and linkage types, Tetrahedron 95 (2021) 132351.
[12] Y. Arakawa, K. Komatsu, S. Inui, H. Tsuji, Thioether-linked liquid crystal dimers and trimers: The twist-bend nematic phase, J. Mol. Struct. 1199 (2020) 126913.
[13] J.P. Abberley, R. Killah, R. Walker, J.M.D. Storey, C.T. Imrie, M. Salamończyk, C. Zhu, E. Gorecka, D. Pociecha, Heliconical smectic phases formed by achiral molecules, Nat. Commun. 9 (2018) 228.
[14] C.T. Imrie, R. Walker, J.M.D. Storey, E. Gorecka, D. Pociecha, Liquid crystal dimers and smectic phases from the intercalated to the twist-bend, Crystals 12 (2022) 1245.
[15] M. Salamończyk, N. Vaupotič, D. Pociecha, R. Walker, J.M.D. Storey, C.T. Imrie, C. Wang, C. Zhu, E. Gorecka, Multi-level chirality in liquid crystals formed by achiral molecules, Nat. Commun. 10 (2019) 1922.
[16] A.F. Alshammari, D. Pociecha, R. Walker, J.M.D. Storey, E. Gorecka, C.T. Imrie, New patterns of twist-bend liquid crystal phase behaviour: the synthesis and characterisation of the 1-(4-cyanobiphenyl-4′-yl)-10-(4-alkylaniline-benzylidene-4′-oxy)decanes (CB10O·m), Soft Matter 18 (2022) 4679–4688.
[17] E. Cruickshank, K. Anderson, J.M.D. Storey, C.T. Imrie, E. Gorecka, D. Pociecha, A. Makal, M.M. Majewska, Helical phases assembled from achiral molecules: Twist-bend nematic and helical filamentary B4 phases formed by mesogenic dimers, J. Mol. Liq. 346 (2022) 118180.
[18] A.C. Griffin, T.R. Britt, Effect of molecular structure on mesomorphism. 12. Flexible-center siamese-twin liquid crystalline diesters-A "Prepolymer" model, J. Am. Chem. Soc. 103 (1981) 4957–4959.

[19] R.W. Date, C.T. Imrie, G.R. Luckhurst, J.M. Seddon, Smectogenic dimeric liquid crystals: The preparation and properties of the α, ω-bis(4-n-alkylanilinebenzylidine-4′-oxy)alkanes, Liq. Cryst. 12 (1992) 203–238.
[20] J.W. Park, C.S. Bak, M.M. Labes, Effects of molecular complexing on the properties of binary nematic liquid crystal mixtures, J. Am. Chem. Soc. 97 (1975) 4398–4400.
[21] V.G.K.M. Pisipati, Polymesomorphism in N-(p-n-Alkoxybenzylidene)-p-n-Alkylanilines (nO.m) compounds, Zeitschrift Fur Naturforsch. a. 58 (2003) 661–663.
[22] V.G.K.M. Pisipati, P.V.D. Prasad, Orientational order parameter in homogeneous binary mixtures of 6O.4 + 4O.6 of N-(p-n-Alkoxybenzylidene)-p-n-Alkyl Anilines, (nO.m) Series – A birefringence method, Mol. Cryst. Liq. Cryst. 506 (2009) 13–21.
[23] J.W. Goodby, G.W. Gray, A.J. Leadbetter, M.A. Mazid, The unclassified smectic phase of N-(4-n-pentyloxybenzylidene)-4-n-hexylaniline (50.6), J. Phys. 41 (1980) 591–595.
[24] A.J. Leadbetter, M.A. Mazid, B.A. Kelly, J.W. Goodby, G.W. Gray, Structure of the smectic-B phase and the nature of the smectic-H transition in the N-(4-n-Alkoxybenzylidene-4'-Alkylanilines, Phys. Rev. Lett. 43 (1979) 630.
[25] E. Cruickshank, G.J. Strachan, M.M. Majewska, D. Pociecha, E. Górecka, J.M. D. Storey, C.T. Imrie, The effects of alkylthio chains on the properties of symmetric liquid crystal dimers, New J. Chem. 47 (2023) 7356–7368.
[26] M. Šepelj, A. Lesac, U. Baumeister, S. Diele, H.L. Nguyen, D.W. Bruce, Intercalated liquid-crystalline phases formed by symmetric dimers with an α, ω-diiminoalkylene spacer, J. Mater. Chem. 17 (2007) 1154–1165.
[27] P.A. Henderson, J.M. Seddon, C.T. Imrie, Methylene- and ether-linked liquid crystal dimers II. Effects of mesogenic linking unit and terminal chain length, Liq. Cryst. 32 (2005) 1499–1513.
[28] R. Achten, A.T.M. Marcelis, A. Koudijs, E.J.R. Sudhölter, Symmetrical dimer liquid crystals with tilted smectic phases, Mol. Cryst. Liq. Cryst. 411 (2010) 177–184.
[29] R.W. Date, G.R. Luckhurst, M. Shuman, J.M. Seddon, Novel modulated hexatic phases in symmetric liquid crystal dimers, J. Phys. II (5) (1995) 587–605.
[30] G.S. Attard, R.W. Date, C.T. Imrie, G.R. Luckhurst, S.J. Roskilly, J.M. Seddon, L. Taylor, Non-symmetric dimeric liquid crystals The preparation and properties of the α-(4-cyanobiphenyl-4′-yloxy)-ω-(4-n-alkylanilinebenzylidene-4′-oxy)alkanes, Liq. Cryst. 16 (1994) 529–581.
[31] C.T. Imrie, Non-symmetric liquid crystal dimers: How to make molecules intercalate, Liq. Cryst. 33 (2011) 1449–1485.
[32] J.L. Hogan, C.T. Imrie, G.R. Luckhurst, Asymmetric dimeric liquid crystals The preparation and properties of the α-(4-cyanobiphenyl-4′-oxy)-ω-(4-n-alkylanilinebenzylidene-4′-oxy)hexanes, Liq. Cryst. 3 (1988) 645–650.
[33] P.E. Cladis, The Re-entrant nematic, enhanced smectic A phases and molecular composition, Mol. Cryst. Liq. Cryst. 67 (1981) 177–191.
[34] A.E. Blatch, I.D. Fletcher, G.R. Luckhurst, The intercalated smectic A phase. The liquid crystal properties of the α-(4-cyanobiphenyl-4′-yloxy)-ω)-(4-alkyloxycinnamoate)alkanes, Liq. Cryst. 18 (1995) 801–809.
[35] D. Demus, H. Demus, H. Zaschke, Flüssige kristalle in tabellen, Zeitschrift Für Chemie. 14 (1974) 295.
[36] D. Demus, H. Zaschke, Flüssige kristalle in tabellen II, Zeitschrift Für Chemie. 24 (1984) 235.
[37] E. Forsyth, D.A. Paterson, E. Cruickshank, G.J. Strachan, E. Gorecka, R. Walker, J. M.D. Storey, C.T. Imrie, Liquid crystal dimers and the twist-bend nematic phase: On the role of spacers and terminal alkyl chains, J. Mol. Liq. 320 (2020) 114391.
[38] P.A. Henderson, C.T. Imrie, Methylene-linked liquid crystal dimers and the twist-bend nematic phase, Liq. Cryst. 38 (2011) 1407–1414.
[39] A.A. Dawood, M.C. Grossel, G.R. Luckhurst, R.M. Richardson, B.A. Timimi, N. J. Wells, Y.Z. Yousif, Twist-bend nematics, liquid crystal dimers, structure–property relations, Liq. Cryst. 44 (2017) 106–126.
[40] R.J. Mandle, J.W. Goodby, Progression from nano to macro science in soft matter systems: dimers to trimers and oligomers in twist-bend liquid crystals, RSC Adv. 6 (2016) 34885–34893.
[41] M.J. Frisch G.W. Trucks H.B. Schlegel G.E. Scuseria M.A. Robb J.R. Cheeseman G. Scalmani V. Barone B. Mennucci G.A. Petersson H. Nakatsuji M. Caricato X. Li H.P. Hratchian A.F. Izmaylov J. Bloino G. Zheng J.L. Sonnenberg M. Hada M. Ehara K. Toyota R. Fukuda J. Hasegawa M. Ishida T. Nakajima Y. Honda O. Kitao H. Nakai T. Vreven J.A. Montgomery J.E. Peralta F. Ogliaro M. Bearpark J.J. Heyd E. Brothers K.N. Kudin V.N. Staroverov R. Kobayashi J. Normand K. Raghavachari A. Rendell J.C Burant S.S. Iyengar J. Tomasi M. Cossi N. Rega J.M. Millam M. Klene J. E. Knox J.B. Cross V. Bakken C. Adamo J. Jaramillo R. Gomperts R.E. Stratmann O. Yazyev A.J. Austin R. Cammi C. Pomelli J.W. Ochterski R.L. Martin K. Morokuma V.G. Zakrzewski G.A. Voth P. Salvador J.J. Dannenberg S. Dapprich A.D. Daniels J. B. Farkas, Foresman J.V. Ortiz J. Cioslowski D.J. Fox Gaussian 09, Revision B.01. *Gaussian 09, Revision B.01, Gaussian, Inc., Wallingford CT*. (2010).
[42] M. Tarini, P. Cignoni, C. Montani, Ambient occlusion and edge cueing to enhance real time molecular visualization, IEEE Trans. Vis. Comput. Graph. 12 (2006) 1237–1244.
[43] P.J. Barnes, S.K. Heeks, S.K. Heeks, G.R. Luckhurst, An enhanced odd-even effect of liquid crystal dimers Orientational order in the α, ω-bis(4′-cyanobiphenyl-4-yl) alkanes, Liq. Cryst. 13 (2006) 603–613.
[44] P.A. Henderson, O. Niemeyer, C.T. Imrie, Methylene-linked liquid crystal dimers, Liq. Cryst. 28 (2001) 463–472.
[45] K.L. Sandhya, D.S. Shankar Rao, S. Krishna Prasad, U.S. Hiremath, C. V. Yelamaggad, Effect of pressure on liquid crystal dimers, Liq. Cryst. 30 (2010) 1351–1355.
[46] S. Nada, M. Hagar, O. Farahat, A.A. Hasanein, A.H. Emwas, A.A. Sharfalddin, M. Jaremko, M.A. Zakaria, Three rings schiff base ester liquid crystals: Experimental and computational approaches of mesogenic core orientation effect, Heterocycle Impact. *Molecules*. 27 (2022) 2304.
[47] D. Pociecha, N. Vaupotič, M. Majewska, E. Cruickshank, R. Walker, J.M.D. Storey, C.T. Imrie, C. Wang, E. Gorecka, Photonic bandgap in achiral liquid crystals—A twist on a twist, Adv. Mater. 33 (2021) 2103288.
[48] R. Walker, D. Pociecha, G.J. Strachan, J.M.D. Storey, E. Gorecka, C.T. Imrie, Molecular curvature, specific intermolecular interactions and the twist-bend nematic phase: the synthesis and characterisation of the 1-(4-cyanobiphenyl-4′-yl)-6-(4-alkylanilinebenzylidene-4′-oxy)hexanes (CB6O.m), Soft Matter 15 (2019) 3188–3197.

The Role of Imine Bond Direction and Spacer Linking Group on the Phase Behaviour of Liquid Crystal Dimers

[1]Ewan Cruickshank[‡,*], [1]Rebecca Walker, [1]Grant J. Strachan, [1]Charlotte H. F. Goode, [2]Magdalena M. Majewska, [2]Damian Pociecha, [2]Ewa Gorecka, [1]John M.D. Storey & [1]Corrie T. Imrie

[1]Department of Chemistry, University of Aberdeen, Old Aberdeen, AB24 3UE, U.K.

‡Present Address: School of Pharmacy and Life Sciences, Robert Gordon University, Aberdeen, AB10 7GJ, U.K.

[2]Faculty of Chemistry, University of Warsaw, ul. Zwirki i Wigury 101, 02-089 Warsaw, Poland

*Author for correspondence: ewan.cruickshank2@abdn.ac.uk

Materials and Methods

Reagents

All reagents and solvents that were available commercially were purchased from Sigma Aldrich, Fisher Scientific or Fluorochem and were used without further purification unless otherwise stated.

Thin Layer Chromatography

Reactions were monitored using thin layer chromatography, and the appropriate solvent system, using aluminium-backed plates with a coating of Merck Kieselgel 60 F254 silica which were purchased from Merck KGaA. The spots on the plate were visualised by UV light (254 nm).

Column Chromatography

For normal phase column chromatography, the separations were carried out using silica gel grade 60 Å, 40-63 µm particle size, purchased from Fluorochem and using an appropriate solvent system or using a Biotage Selekt system with Biotage Sfar Silica High Capacity Duo Columns of 50 g or 100 g load capacity. The desired spots were identified using a UV detector which was set to 254 nm and the instrument collected the spots when a threshold of 250 mAU was surpassed.

Structure Characterisation

All final products and intermediates that were synthesised were characterised using ^{1}H NMR, ^{13}C NMR and infrared spectroscopies. The NMR spectra were recorded on a 400 MHz Bruker Avance III HD NMR spectrometer. The infrared spectra were recorded on a Perkin Elmer Spectrum Two FTIR with an ATR diamond cell.

Purity Analysis

In order to determine the purity of the final products, elemental analysis or high-resolution mass spectrometry was used. C, H, N, S microanalysis were carried out by the Sheffield Analytical and Scientific Services Elemental Microanalysis Service at the University of Sheffield using an Elementar Vario MICRO Cube or by the Elemental Analysis Service at OEA Laboratories Limited using a CE Instruments EA1110 CHNS-O Elemental Analyser. The instruments were calibrated using series of different masses of sulphanilamide and acetanilide.

Phase Diagrams

In order to construct phase diagrams to confirm phase assignments or to determine virtual transition temperatures, binary mixtures were prepared by co-dissolving pre-weighed masses in chloroform or dichloromethane and allowing the solvent to evaporate slowly at room temperature. Each mixture was further dried in a vacuum oven at 50 °C overnight.

Synthesis and Analytical Data

m-O5O-*m* Series

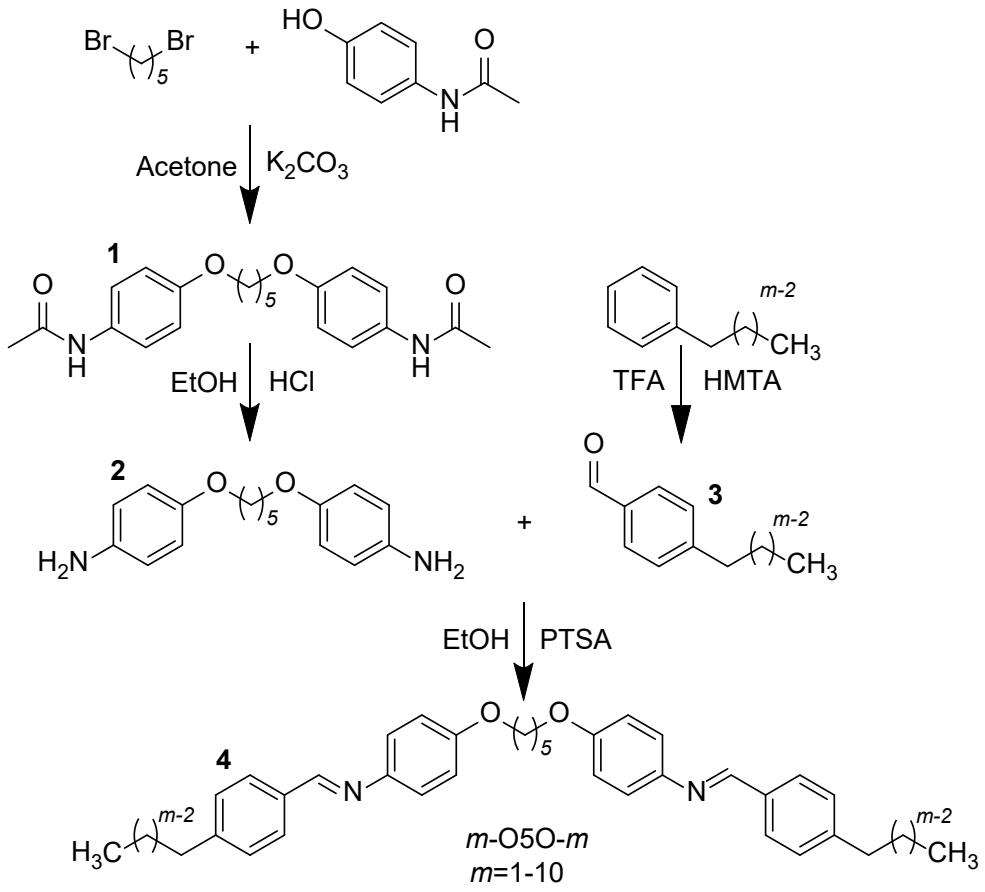

Scheme 1. Synthesis of the *m*-O5O-*m* series.

(1) N,N'-[Pentane-1,5-diylbis(oxy-4,1-phenylene)]diacetamide

To a pre-dried flask flushed with argon and fitted with a condenser, 4-acetamidophenol (13.0 g, 0.086 mol) and potassium carbonate (22.7 g, 0.164 mol) were added. Acetone (150 mL) was added with 1,5-dibromopentane (5.59 mL, 9.43 g, 0.041 mol) and stirred. The reaction was heated at reflux overnight and the extent of the reaction monitored by TLC using 80 % dichloromethane and 20 % ethyl acetate as the solvent system (RF value quoted in the product data). The reaction mixture was cooled to room temperature and poured into water (500 mL). The resulting white precipitate was vacuum filtered and recrystallised from hot ethanol (300 mL).

Yield: 11.1 g, 73.1 %. RF: 0.56. MP: 207 °C

ν_{max}/cm^{-1}: 3292, 2914, 2867, 1657, 1596, 1532, 1512, 1473, 1412, 1393, 1365, 1298, 1241, 1172, 1114, 1036, 1019, 970, 824, 800, 742, 716, 704, 655, 605, 537, 521

δ_H/ppm (400 MHz, DMSO-d_6): 9.75 (2 H, s, NH), 7.45 (4 H, d, J 8.6 Hz, Ar-H), 6.85 (4 H, d, J 8.6 Hz, Ar-H), 3.92 (4 H, t, J 6.5 Hz, O-$\underline{CH_2}$-CH_2-), 1.99 (6 H, s, (C=O)-$\underline{CH_3}$), 1.74 (4 H, tt, J 7.0 Hz, 6.5 Hz, O-CH_2-$\underline{CH_2}$-CH_2-), 1.54 (2 H, m, O-CH_2-CH_2-$\underline{CH_2}$-CH_2-)

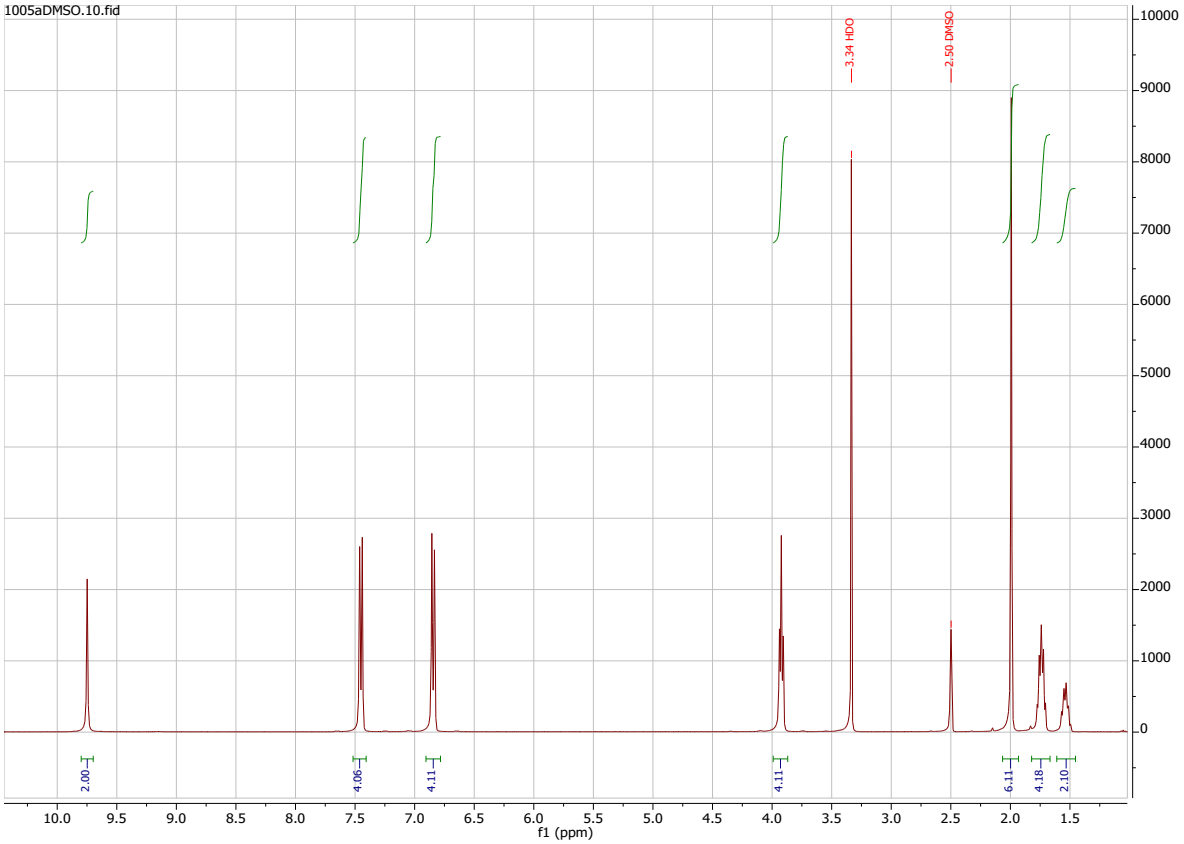

δ_C/ppm (100 MHz, DMSO-d_6): 168.13, 154.87, 132.91, 120.95, 114.83, 67.93, 28.97, 24.26, 22.74

Data consistent with reported values.[1]

(2) 4,4'-[Pentane-1,5-diylbis(oxy)]dianiline

To a pre-dried flask flushed with argon and fitted with a condenser, compound **(1)** (11.0 g, 0.0297 mol) was added. Ethanol (175 mL) was added along with 32 % hydrochloric acid (40 mL, 46.4 g, 1.27 mol) and stirred. The reaction was heated at reflux overnight and the extent of the reaction monitored by TLC using 80 % dichloromethane and 20 % ethyl acetate as the solvent system (RF value quoted in the product data). The reaction mixture was cooled to room temperature, poured into ice (160 g), and made alkaline using 15 M sodium

hydroxide solution. The resulting brown solid was vacuum filtered and was recrystallised from hot toluene (200 mL).

Yield: 5.02 g, 59.0 %. RF: 0.21. MP: 84 °C

ν_{max}/cm^{-1}: 3433, 3352, 2949, 2867, 1630, 1508, 1472, 1455, 1396, 1272, 1225, 1179, 1129, 1059, 1029, 1002, 910, 823, 769, 605, 516

δ_H/ppm (400 MHz, $CDCl_3$): 6.74 (4 H, d, J 8.0 Hz, Ar-H), 6.63 (4 H, d, J 8.0 Hz, Ar-H), 3.91 (4 H, t, J 6.4 Hz, O-$\underline{CH_2}$-CH_2-), 1.82 (4 H, tt, J 7.3 Hz, 6.4 Hz, O-CH_2-$\underline{CH_2}$-CH_2-), 1.61 (2 H, m, O-CH_2-CH_2-$\underline{CH_2}$-CH_2-)

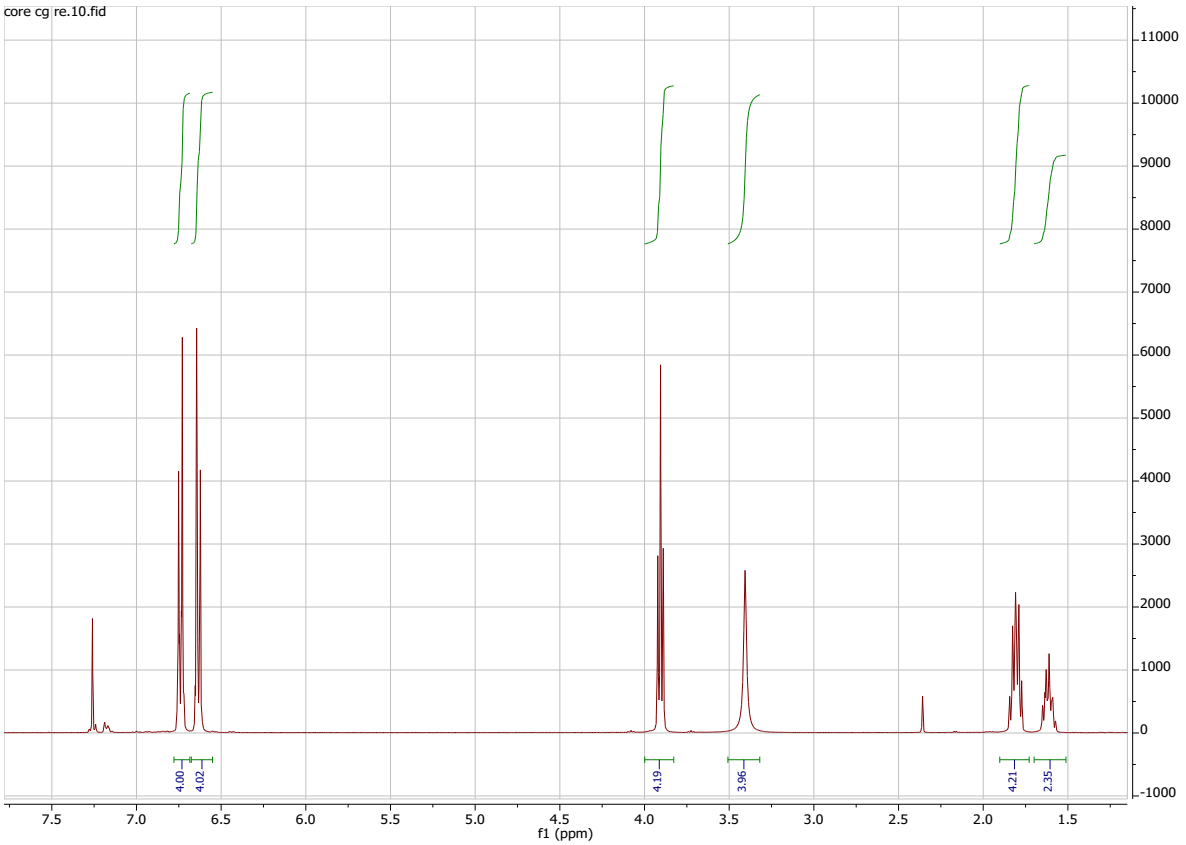

δ_C/ppm (100 MHz, $CDCl_3$): 152.27, 139.79, 116.40, 115.69, 68.50, 29.22, 22.74

Data consistent with reported values.[1]

(3) 4-Alkylbenzaldehydes

To a pre-dried flask flushed with argon and fitted with a condenser, hexamethylenetetramine (1.1 eq, 2.24 g, 0.0160 mol) and trifluoroacetic acid (18 eq, 20.0 mL 29.8 g, 0.261 mol) were added. The appropriate alkylbenzene (1 eq) was added and the reaction mixture was stirred. The quantities of alkylbenzenes used in each reaction are listed in **Table SI1**. The reaction mixture was heated at reflux overnight. The reaction was cooled to room temperature and

the solvent removed under vacuum. The oil remaining was made alkaline by the addition of 6 M sodium hydroxide and extracted by diethyl ether (3 × 50 mL). The diethyl ether was removed under vacuum to leave an orange/brown oil. The crude product was purified using a silica gel column with 90 % 40:60 petroleum ether and 10 % ethyl acetate as eluent (RF values quoted in product data). The eluent fractions of interest were evaporated under vacuum to leave a pale-yellow oil. The column did not remove all impurities, but the product was carried forwards without any further purification.

Table SI1. Quantities of alkylbenzenes used in the syntheses of 4-alkylbenzaldehydes (**3**).

m	Alkylbenzene
6	2.73 mL, 2.35 g, 0.0145 mol
7	2.97 mL, 2.56 g, 0.0145 mol
8	3.22 mL, 2.76 g, 0.0145 mol
9	3.45 mL, 2.96 g, 0.0145 mol
10	3.70 mL, 3.17 g, 0.0145 mol

4-Methylbenzaldehyde **-** Was purchased commercially from Sigma Aldrich and used without further purification.

4-Ethylbenzaldehyde **-** Was purchased commercially from Sigma Aldrich and used without further purification.

4-Propylbenzaldehyde **-** Was purchased commercially from Sigma Aldrich and used without further purification.

4-Butylbenzaldehyde **-** Was purchased commercially from Fisher Scientific and used without further purification.

4-Pentylbenzaldehyde **-** Was purchased commercially from Fisher Scientific and used without further purification.

(3.1) 4-Hexylbenzaldehyde

Yield: 2.43 g, 88.1 %. RF: 0.47

ν_{max}/cm^{-1}: 2927, 2856, 1699, 1606, 1576, 1466, 1305, 1212, 1167, 824, 778, 724, 698, 622, 532

δ_H/ppm (400 MHz, $CDCl_3$): 9.98 (1 H, s, (C=O)-H), 7.80 (2 H, d, J 7.9 Hz, Ar-H), 7.33 (2 H, d, J 7.9 Hz, Ar-H), 2.68 (2 H, t, J 7.5 Hz, Ar-$\underline{CH_2}$-CH_2-), 1.64 (2 H, m, Ar-CH_2-$\underline{CH_2}$-CH_2-), 1.31 (9 H, m, Ar-CH_2-CH_2-$\underline{CH_2}$-$\underline{CH_2}$-$\underline{CH_2}$-CH_3), 0.88 (8 H, m, Ar-CH_2-CH_2-CH_2-CH_2-CH_2-$\underline{CH_3}$)

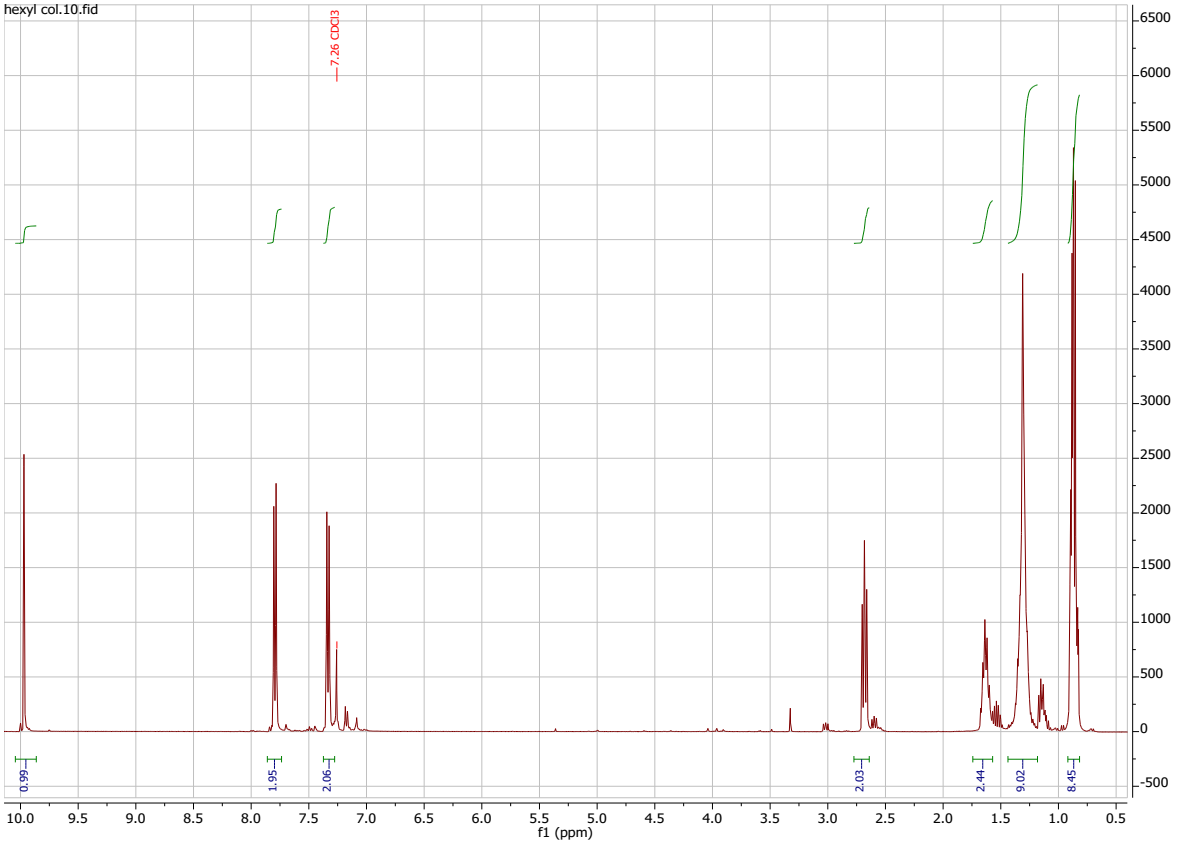

δ_C/ppm (100 MHz, $CDCl_3$): 191.98, 150.48, 134.40, 129.88, 129.07, 36.23, 31.65, 31.06, 28.93, 22.63, 14.06

Data consistent with reported values.[2]

(3.2) 4-Heptylbenzaldehyde

Yield: 2.36 g, 78.0 %. RF: 0.59

ν_{max}/cm^{-1}: 2925, 2855, 1701, 1605, 1575, 1466, 1305, 1212, 1167, 823, 780, 749, 723, 698, 622, 532

δ_H/ppm (400 MHz, $CDCl_3$): 9.95 (1 H, s, (C=O)-H), 7.78 (2 H, d, J 8.2 Hz, Ar-H), 7.33 (2 H, d, J 8.2 Hz, Ar-H), 2.68 (2 H, t, J 7.8 Hz, Ar-$\underline{CH_2}$-CH_2-), 1.62 (2 H, m, Ar-CH_2-$\underline{CH_2}$-CH_2-), 1.29 (12 H, m, Ar-CH_2-CH_2-$\underline{CH_2}$-$\underline{CH_2}$-$\underline{CH_2}$-$\underline{CH_2}$-CH_3), 0.88 (11 H, m, Ar-CH_2-CH_2-CH_2-CH_2-CH_2-CH_2--CH_2-$\underline{CH_3}$)

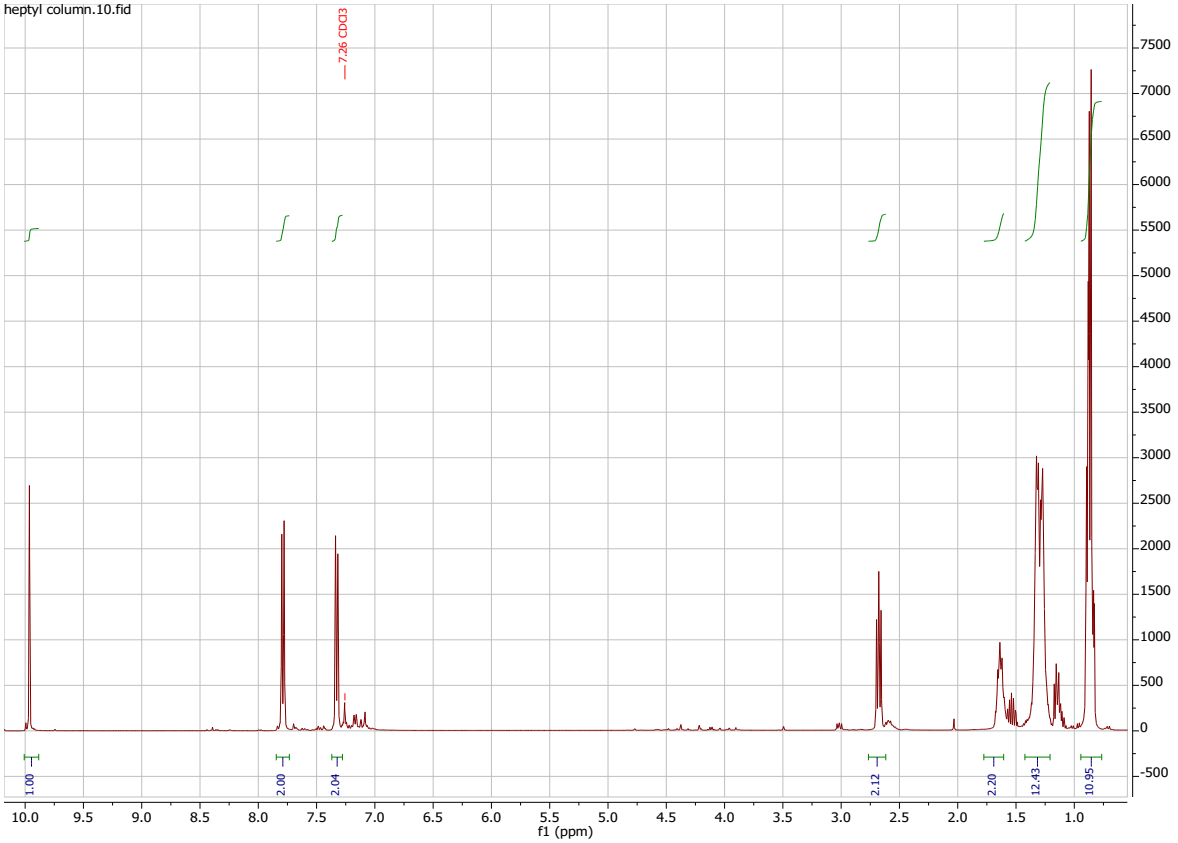

δ_C/ppm (100 MHz, $CDCl_3$): 191.88, 150.44, 134.42, 129.86, 129.05, 36.23, 31.78, 31.10, 29.24, 29.13, 22.65, 14.07

Data consistent with reported values.[3]

(3.3) 4-Octylbenzaldehyde

Yield: 2.17 g, 68.5 %. RF: 0.57

ν_{max}/cm^{-1}: 2924, 2854, 1701, 1606, 1575, 1465, 1305, 1212, 1167, 824, 778, 722, 698, 622, 534

δ_H/ppm (400 MHz, $CDCl_3$): 9.95 (1 H, s, (C=O)-H), 7.78 (2 H, d, J 8.2 Hz, Ar-H), 7.33 (2 H, d, J 8.2 Hz, Ar-H), 2.68 (2 H, t, J 7.8 Hz, Ar-$\underline{CH_2}$-CH_2-), 1.62 (2 H, m, Ar-CH_2-$\underline{CH_2}$-CH_2-), 1.29 (10 H, m, Ar-CH_2-CH_2-$\underline{CH_2\text{-}CH_2\text{-}CH_2\text{-}CH_2\text{-}CH_2}$-$CH_3$), 0.88 (3 H, t, J 7.0 Hz, Ar-CH_2-CH_2-CH_2-CH_2-CH_2-CH_2--CH_2-$\underline{CH_3}$)

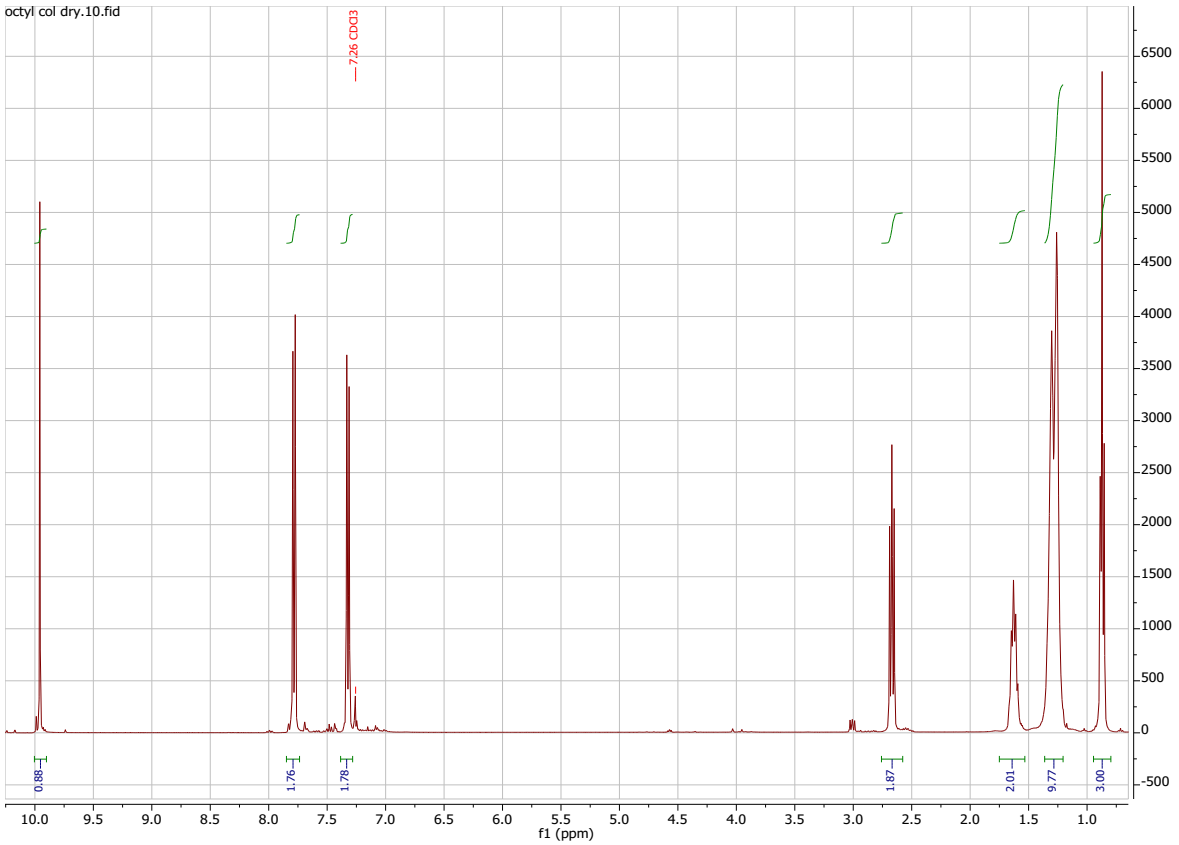

δ_C/ppm (100 MHz, $CDCl_3$): 191.94, 150.46, 134.40, 129.86, 129.06, 36.22, 31.86, 31.09, 29.41, 29.27, 29.22, 22.66, 14.10

Data consistent with reported values.[4]

(3.4) 4-Nonylbenzaldehyde

Yield: 2.61 g, 77.4 %. RF: 0.51

ν_{max}/cm^{-1}: 2924, 2853, 1702, 1606, 1576, 1466, 1305, 1212, 1167, 824, 779, 747, 722, 698, 622, 533

δ_H/ppm (400 MHz, $CDCl_3$): 9.95 (1 H, s, (C=O)-H), 7.78 (2 H, d, J 8.2 Hz, Ar-H), 7.33 (2 H, d, J 8.2 Hz, Ar-H), 2.68 (2 H, t, J 7.8 Hz, Ar-$\underline{CH_2}$-CH_2-), 1.62 (2 H, m, Ar-CH_2-$\underline{CH_2}$-CH_2-), 1.29 (17 H, m, Ar-CH_2-CH_2-$\underline{CH_2\text{-}CH_2\text{-}CH_2\text{-}CH_2\text{-}CH_2\text{-}CH_2}$-$CH_3$), 0.88 (5 H, m, Ar-$CH_2$-$CH_2$-$CH_2$-$CH_2$-$CH_2$-$CH_2$-$CH_2$-$CH_2$-$\underline{CH_3}$)

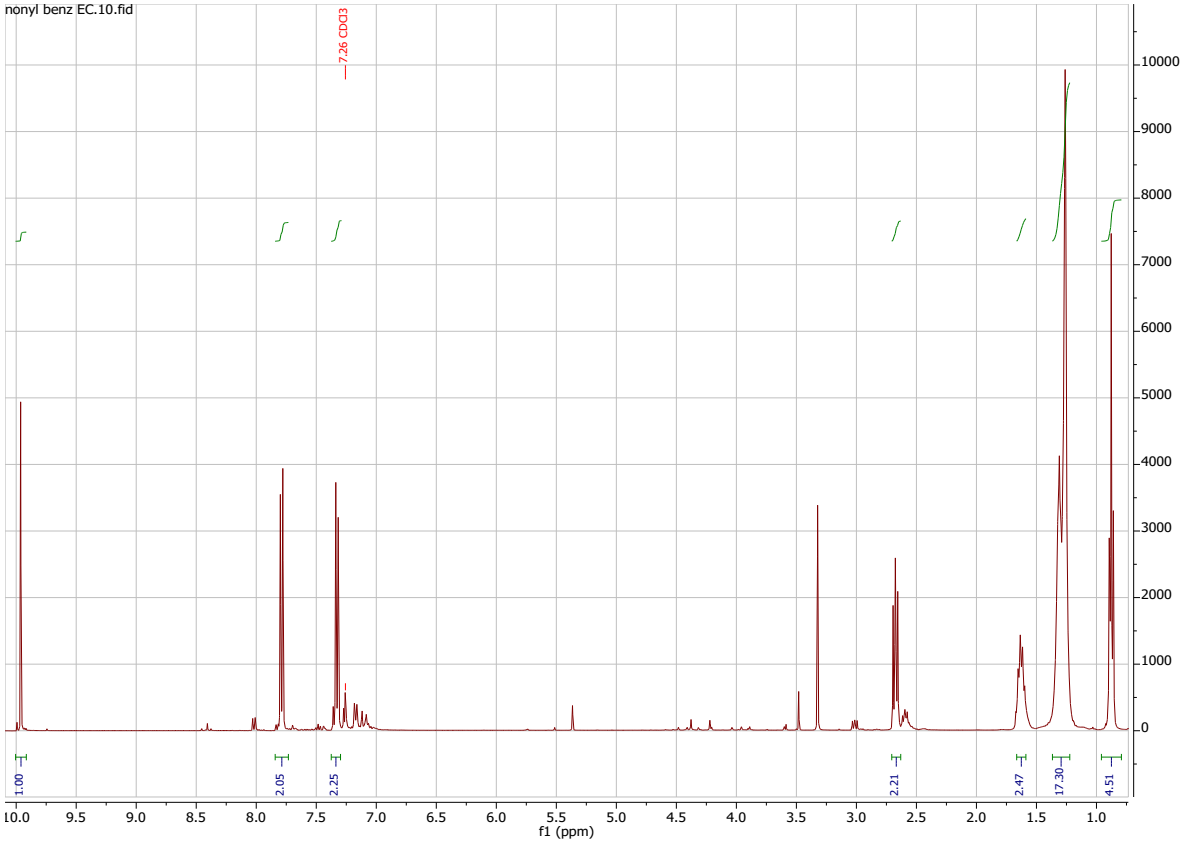

δ_C/ppm (100 MHz, $CDCl_3$): 191.90, 150.45, 134.40, 129.90, 129.08, 36.21, 31.92, 31.09, 29.58, 29.45, 29.38, 29.23, 22.68, 14.12

Data consistent with reported values.[3]

(3.5) 4-Decylbenzaldehyde

Yield: 3.06 g, 85.7 %. RF: 0.58

ν_{max}/cm^{-1}: 2923, 2853, 1702, 1606, 1576, 1466, 1305, 1212, 1167, 824, 779, 748, 721, 698, 622. 534

δ_H/ppm (400 MHz, $CDCl_3$): 9.95 (1 H, s, (C=O)-H), 7.78 (2 H, d, J 8.2 Hz, Ar-H), 7.33 (2 H, d, J 8.2 Hz, Ar-H), 2.68 (2 H, t, J 7.8 Hz, Ar-$\underline{CH_2}$-CH_2-), 1.62 (2 H, m, Ar-CH_2-$\underline{CH_2}$-CH_2-), 1.29 (18 H, m, Ar-CH_2-CH_2-$\underline{CH_2\text{-}CH_2\text{-}CH_2\text{-}CH_2\text{-}CH_2\text{-}CH_2\text{-}CH_2}$-$CH_3$), 0.88 (11 H, m, J 7.0 Hz, Ar-CH_2-CH_2-CH_2-CH_2-CH_2-CH_2-CH_2-CH_2-$\underline{CH_3}$)

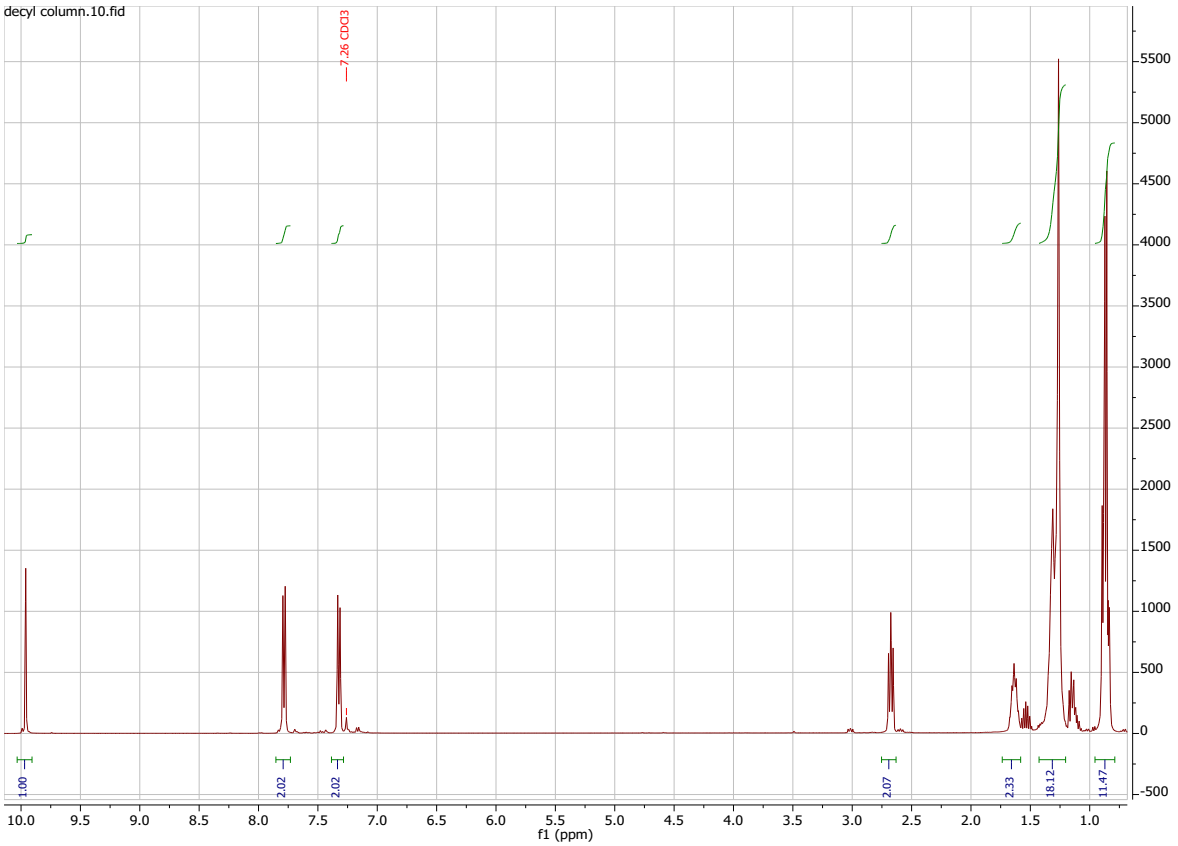

δ_C/ppm (100 MHz, $CDCl_3$): 191.95, 150.47, 134.40, 129.87, 129.06, 36.23, 31.91, 31.09, 29.61, 29.56, 29.46, 29.34, 29.28, 22.70, 14.13

Data consistent with reported values.[5]

(4) (E,E)-N,N'-[Pentane-1,5-diylbis(oxy-4,1-phenylene)]bis[1-(4-alkylphenyl)methanimine]s (*m*-O5O-*m*)

To a pre-dried flask flushed with argon and fitted with a condenser, compound **(2)** (1 eq, 0.200 g, 6.98×10^{-4} mol) and compound **(3)** (3 eq) of the appropriate chain length were added along with ethanol (20 mL) and the mixture was stirred. The quantities of 4-alkylbenzaldehydes used in each reaction are listed in **Table SI2**. The reaction was heated to reflux, *p*-toluenesulfonic acid (catalytic amount) was added, and left overnight. The reaction mixture was cooled to room temperature and a brown precipitate formed which was collected by vacuum filtration. The brown solid was recrystallised from hot toluene (10 mL).

Table SI2. Quantities of 4-alkylbenzaldehydes (**3**) used in the syntheses of (E,E)-N,N'-[pentane-1,5-diylbis(oxy-4,1-phenylene)]bis[1-(4-alkylphenyl)methanimine]s (**4**).

m	4-Alkylbenzaldehyde (**3**)
1	0.247 mL, 0.252 g, 2.10×10^{-3} mol
2	0.288 mL, 0.282 g, 2.10×10^{-3} mol
3	0.310 mL, 0.311 g, 2.10×10^{-3} mol
4	0.352 mL, 0.341 g, 2.10×10^{-3} mol
5	0.386 mL, 0.370 g, 2.10×10^{-3} mol
6	0.400 g, 2.10×10^{-3} mol
7	0.429 g, 2.10×10^{-3} mol
8	0.459 g, 2.10×10^{-3} mol
9	0.488 g, 2.10×10^{-3} mol
10	0.517 g, 2.10×10^{-3} mol

(4.1) (E,E)-N,N'-[Pentane-1,5-diylbis(oxy-4,1-phenylene)]bis[1-(4-methylphenyl)methanimine] (1-O5O-1)

Yield: 0.250 g, 73.0 %

T_{CrI} 164 °C T_{NI} (140 °C)

ν_{max}/cm^{-1}: 2930, 2862, 1623, 1608, 1574, 1509, 1470, 1393, 1284, 1241, 1191, 1174, 1114, 1064, 1033, 946, 836, 814, 772, 744, 724, 605, 553, 519, 498, 404

δ_H/ppm (400 MHz, $CDCl_3$): 8.44 (2 H, s, (C=N)-H), 7.78 (4 H, d, J 8.1 Hz, Ar-H), 7.27 (4 H, d, J 8.1 Hz, Ar-H), 7.21 (4 H, d, J 8.8 Hz, Ar-H), 6.92 (4 H, d, J 8.8 Hz, Ar-H), 4.02 (4 H, t, J 6.4 Hz, O-$\underline{CH_2}$-CH_2-), 2.41 (6 H, s, Ar-$\underline{CH_3}$), 1.89 (4 H, tt, J 7.1 Hz, 6.4 Hz, O-CH_2-$\underline{CH_2}$-CH_2-), 1.69 (2 H, m, O-CH_2-CH_2-$\underline{CH_2}$-CH_2-)

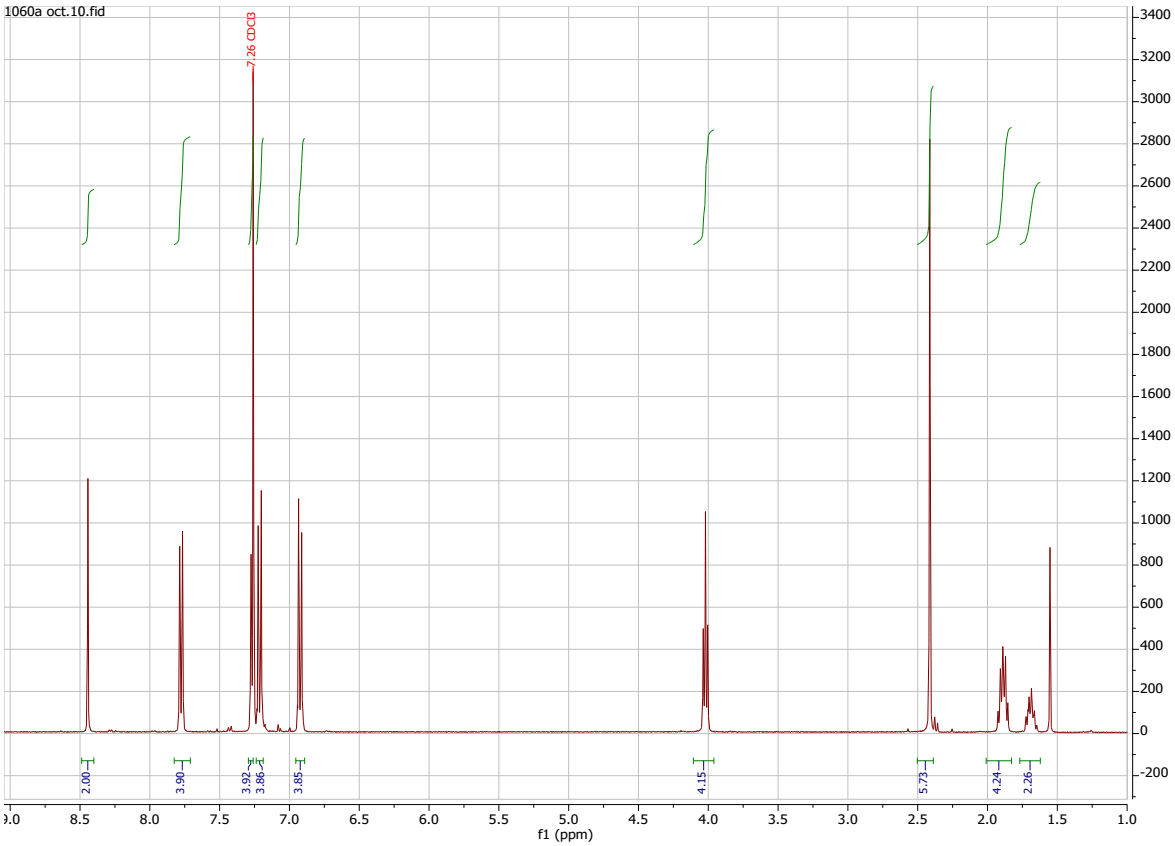

δ_C/ppm (100 MHz, $CDCl_3$): 158.49, 157.74, 145.17, 141.56, 134.05, 129.60, 128.70, 122.27, 115.11, 77.48, 77.16, 76.84, 68.17, 29.23, 22.90, 21.75

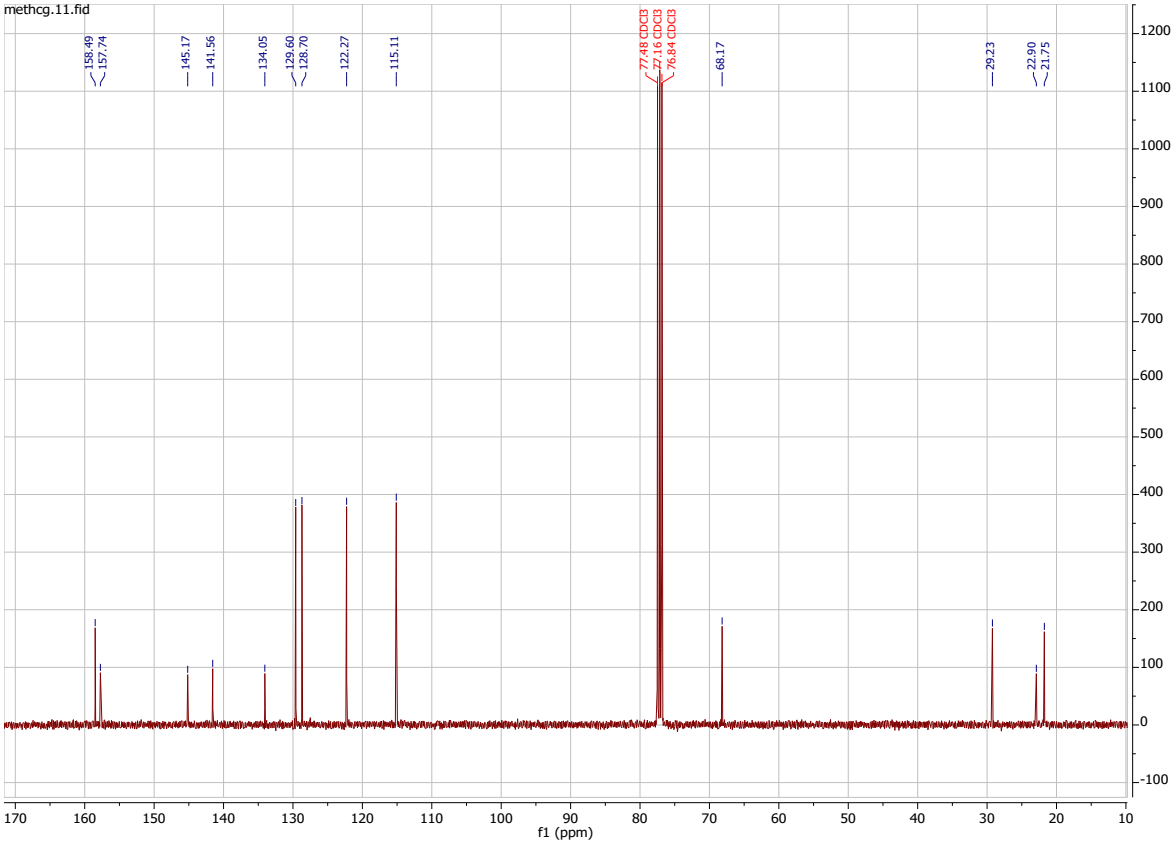

EA: Calculated for $C_{33}H_{34}N_2O_2$: C = 80.78 %, H = 6.99 %, N = 5.71 %; Found: C = 80.85 %, H = 6.99 %, N = 5.60 %

(4.2) (E,E)-N,N'-[Pentane-1,5-diylbis(oxy-4,1-phenylene)]bis[1-(4-ethylphenyl)methanimine] (2-O5O-2)

Yield: 0.210 g, 58.0 %

T_{CrI} 150 °C T_{NI} (119 °C)

ν_{max}/cm^{-1}: 2929, 2873, 1622, 1608, 1574, 1501, 1470, 1393, 1284, 1240, 1191, 1173, 1113, 1064, 1033, 945, 836, 554, 500

δ_H/ppm (400 MHz, $CDCl_3$): 8.45 (2 H, s, (C=N)-H), 7.81 (4 H, d, J 7.9 Hz, Ar-H), 7.29 (4 H, d, J 7.9 Hz, Ar-H), 7.21 (4 H, d, J 8.6 Hz, Ar-H), 6.92 (4 H, d, J 8.6 Hz, Ar-H), 4.02 (4 H, t, J 6.5 Hz, O-$\underline{CH_2}$-CH_2-), 2.71 (4 H, quart, J 7.6 Hz, Ar-$\underline{CH_2}$-CH_3) 1.89 (4 H, tt, J 7.2 Hz, 6.5 Hz, O-CH_2-$\underline{CH_2}$-CH_2-), 1.68 (2 H, m, O-CH_2-CH_2-$\underline{CH_2}$-CH_2-), 1.27 (6 H, t, J 7.6 Hz, Ar-CH_2-$\underline{CH_3}$)

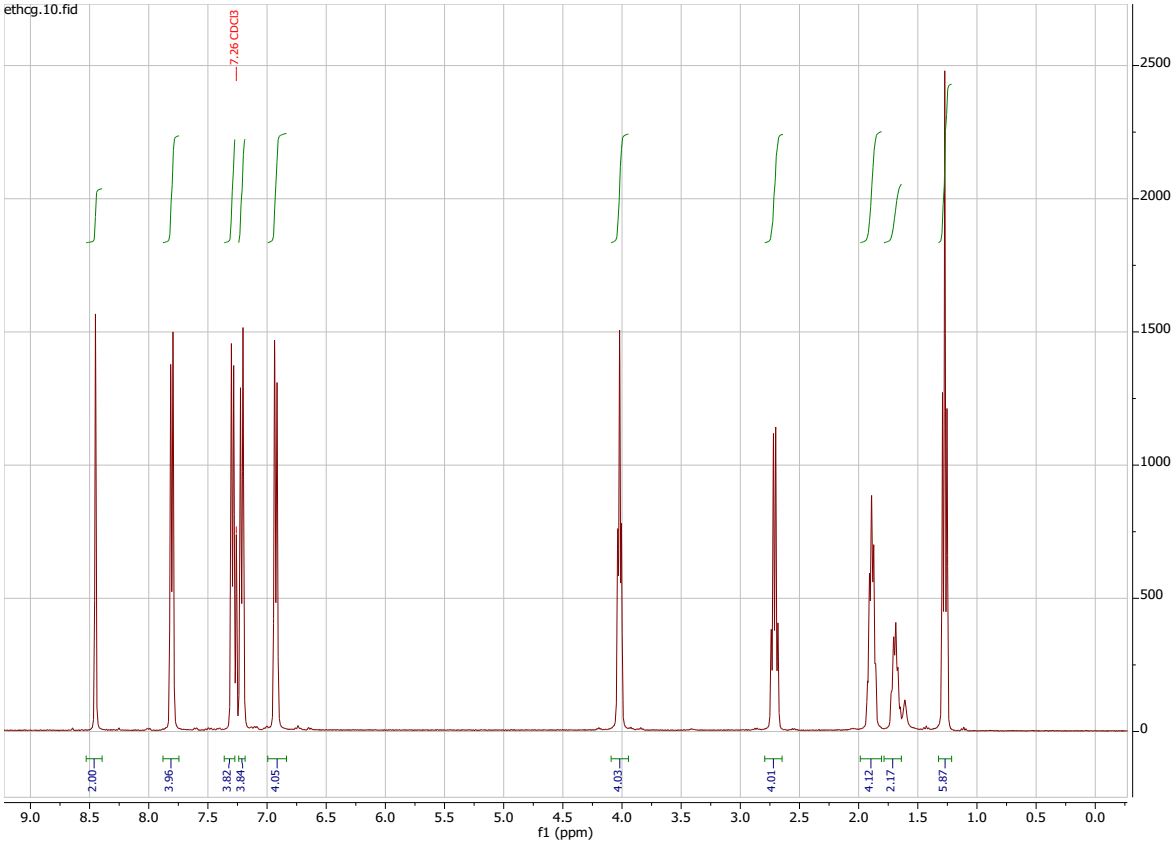

δ_C/ppm (100 MHz, $CDCl_3$): 158.40, 157. 60, 147.74, 145.09, 134.15, 128.67, 128.29, 122.14, 114.98, 68.04, 29.10, 28.95, 22.77, 15.40

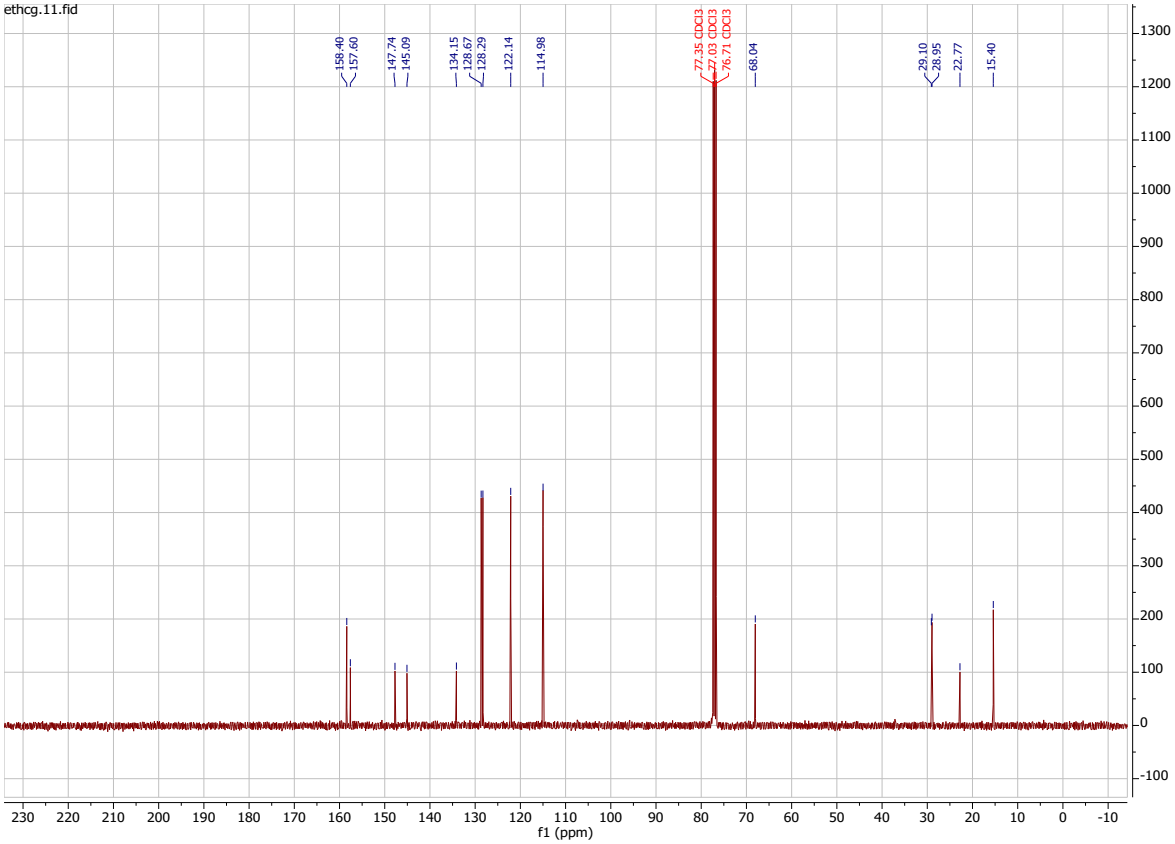

EA: Calculated for $C_{35}H_{38}N_2O_2$: C = 81.05 %, H = 7.38 %, N = 5.40 %; Found: C = 80.63 %, H = 7.36 %, N = 5.27 %

(4.3) (E,E)-N,N'-[Pentane-1,5-diylbis(oxy-4,1-phenylene)]bis[1-(4-propylphenyl)methanimine] (3-O5O-3)

Yield: 0.242 g, 63.4 %

T_{CrI} 146 °C T_{NI} (139 °C)

ν_{max}/cm^{-1}: 2953, 2930, 2870, 1622, 1608, 1574, 1501, 1469, 1393, 1284, 1241, 1190, 1173, 1113, 1063, 1030, 976, 946, 835, 554, 500

δ_H/ppm (400 MHz, $CDCl_3$): 8.45 (2 H, s, (C=N)-H), 7.80 (4 H, d, J 7.8 Hz, Ar-H), 7.27 (4 H, d, J 7.8 Hz, Ar-H), 7.21 (4 H, d, J 8.2 Hz, Ar-H), 6.93 (4 H, d, J 8.2 Hz, Ar-H), 4.02 (4 H, t, J 6.4 Hz, O-$\underline{CH_2}$-CH_2-), 2.64 (4 H, t, J 7.3 Hz, Ar-$\underline{CH_2}$-CH_2-), 1.89 (4 H, tt, J 6.9 Hz, 6.4 Hz, O-CH_2-$\underline{CH_2}$-CH_2-), 1.68 (6 H, m, O-CH_2-CH_2-$\underline{CH_2}$-CH_2-, Ar-CH_2-$\underline{CH_2}$-CH_3), 0.96 (6 H, t, J 7.3 Hz, Ar-CH_2-CH_2-$\underline{CH_3}$)

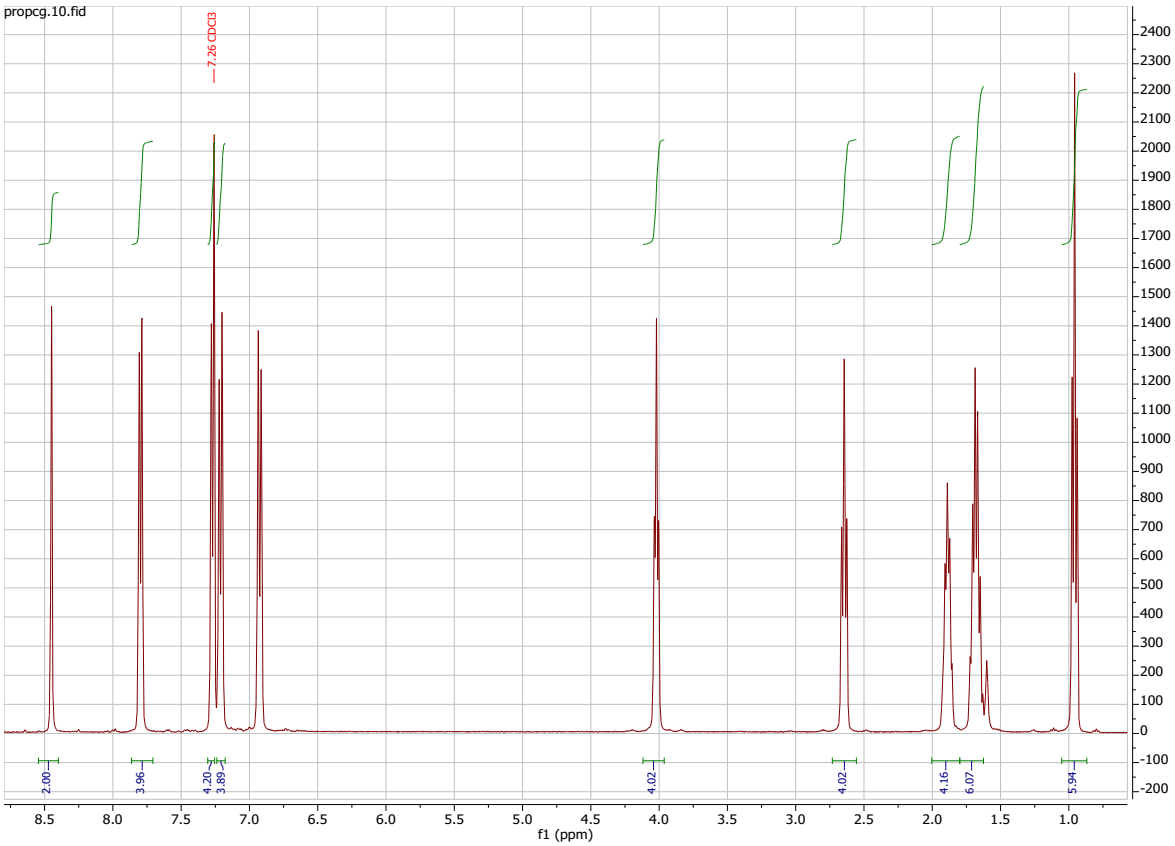

δ_C/ppm (100 MHz, $CDCl_3$): 158.43, 157.60, 146.21, 145.10, 134.16, 128.90, 128.57, 122.13, 114.98, 68.04, 38.06, 29.10, 24.39, 22.77, 13.79

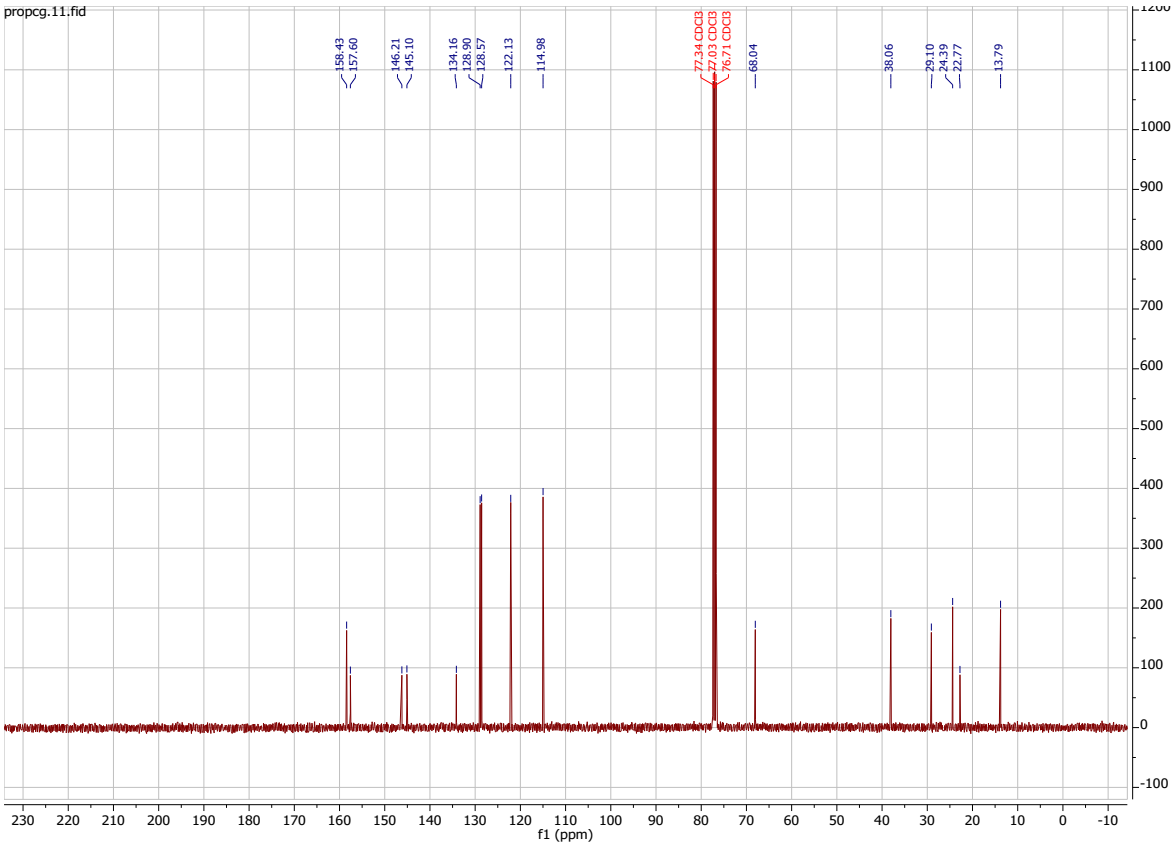

EA: Calculated for $C_{37}H_{42}N_2O_2$: C = 81.28 %, H = 7.74 %, N = 5.12 %; Found: C = 81.17 %, H = 7.62 %, N = 5.01 %

(4.4) (E,E)-N,N'-[Pentane-1,5-diylbis(oxy-4,1-phenylene)]bis[1-(4-butylphenyl)methanimine] (4-O5O-4)

Yield: 0.255 g, 63.6 %

T_{Crl} 133 °C T_{NI} (123 °C)

ν_{max}/cm^{-1}: 2959, 2928, 2873, 1623, 1608, 1574, 1501, 1470, 1393, 1284, 1241, 1191, 1174, 1114, 1064, 1033, 946, 836, 750, 552, 502

δ_H/ppm (400 MHz, $CDCl_3$): 8.44 (2 H, s, (C=N)-H), 7.79 (4 H, d, J 7.8 Hz, Ar-H), 7.27 (4 H, d, J 7.8 Hz, Ar-H), 7.21 (4 H, d, J 8.1 Hz, Ar-H), 6.92 (4 H, d, J 8.1 Hz, Ar-H), 4.02 (4 H, t, J 6.3 Hz, O-$\underline{CH_2}$-CH_2-), 2.67 (4 H, t, J 7.6 Hz, Ar-$\underline{CH_2}$-CH_2-), 1.89 (4 H, tt, J 7.3 Hz, 6.3 Hz, O-CH_2-$\underline{CH_2}$-CH_2-), 1.64 (6 H, m, O-CH_2-CH_2-$\underline{CH_2}$-CH_2-, Ar-CH_2-$\underline{CH_2}$-CH_2-), 1.37 (4 H, sext, J 7.3 Hz, Ar-CH_2-CH_2-$\underline{CH_2}$-CH_3), 0.94 (6 H, t, J 7.3 Hz, Ar-CH_2-CH_2-CH_2-$\underline{CH_3}$)

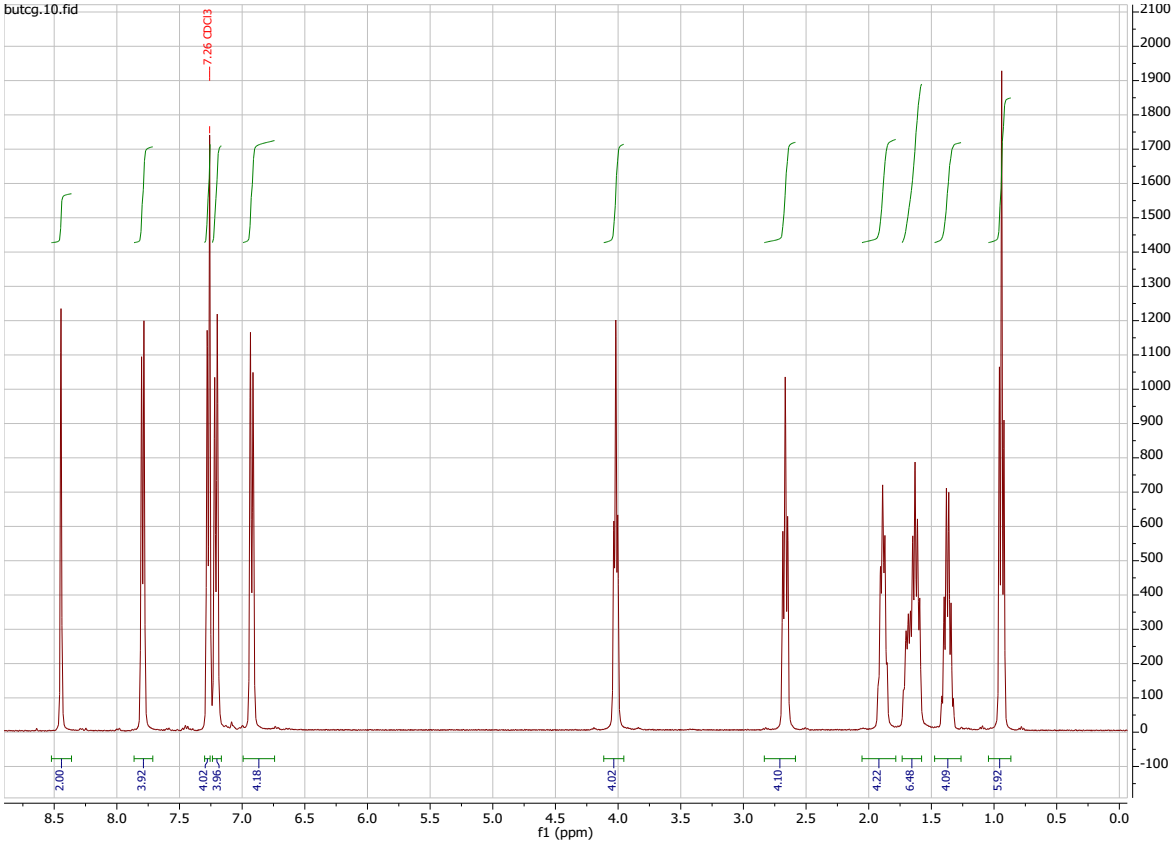

δ_C/ppm (100 MHz, $CDCl_3$): 158.43, 157.59, 146.45, 145.10, 134.11, 128.84, 128.58, 122.13, 114.98, 68.04, 35.70, 33.43, 29.10, 22.77, 22.35, 13.95

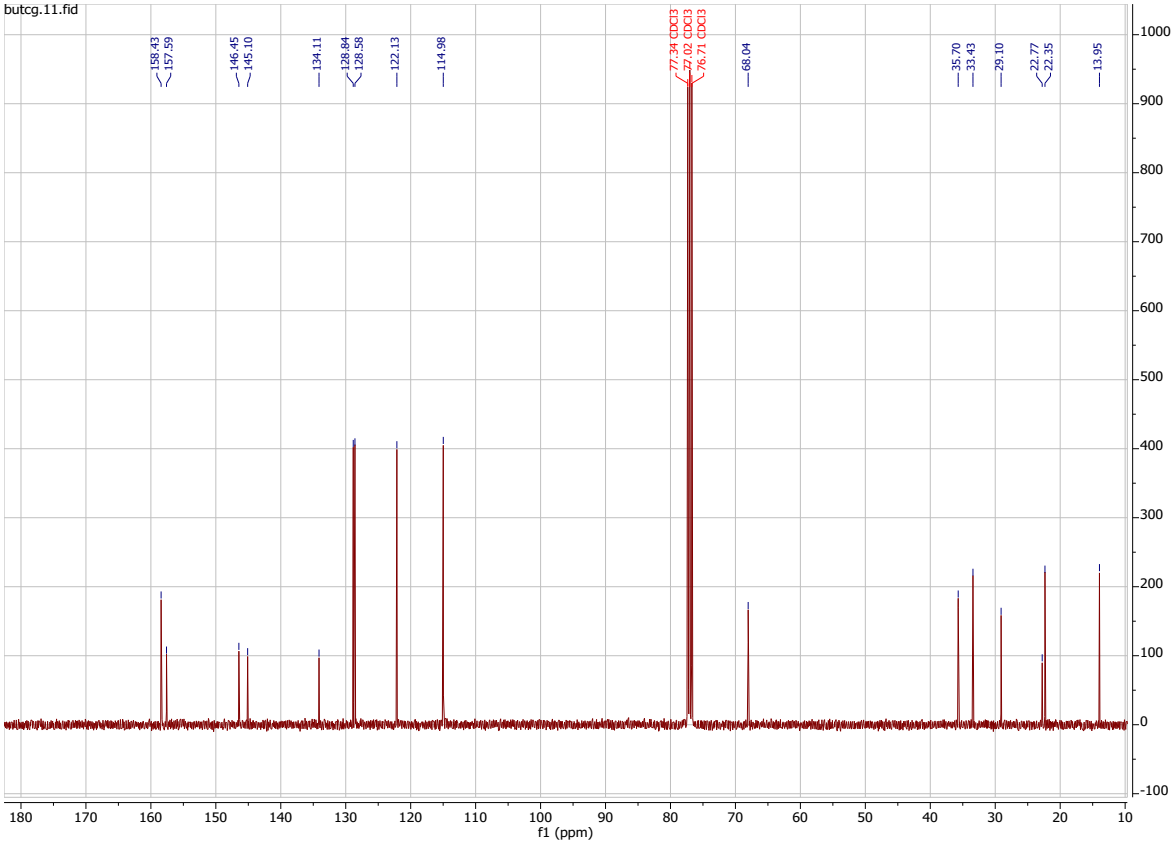

EA: Calculated for $C_{39}H_{46}N_2O_2$: C = 81.49 %, H = 8.07 %, N = 4.87 %; Found: C =81.12 %, H = 8.23 %, N = 4.80 %

(4.5) (E,E)-N,N'-[Pentane-1,5-diylbis(oxy-4,1-phenylene)]bis[1-(4-pentylphenyl)methanimine] (5-O5O-5)

Yield: 0.261 g, 62.0 %

T_{CrI} 133 °C T_{NI} (132 °C)

ν_{max}/cm^{-1}: 2953, 2926, 2871, 1623, 1608, 1573, 1501, 1470, 1392, 1242, 1242, 1191, 1174, 1163, 1113, 1063, 1033, 946, 836, 750, 727, 546, 504

δ_H/ppm (400 MHz, $CDCl_3$): 8.45 (2 H, s, (C=N)-H), 7.79 (4 H, d, J 7.8 Hz, Ar-H), 7.27 (4 H, d, J 7.8 Hz, Ar-H), 7.21 (4 H, d, J 8.2 Hz, Ar-H), 6.92 (4 H, d, J 8.2 Hz, Ar-H), 4.02 (4 H, t, J 6.5 Hz, O-$\underline{CH_2}$-CH_2-), 2.66 (4 H, t, J 7.6 Hz, Ar-$\underline{CH_2}$-CH_2-), 1.89 (4 H, tt, J 7.1 Hz, 6.5 Hz, O-CH_2-$\underline{CH_2}$-CH_2-), 1.67 (6 H, m, O-CH_2-CH_2-$\underline{CH_2}$-CH_2-, Ar-CH_2-$\underline{CH_2}$-CH_2-), 1.34 (8 H, m, Ar-CH_2-CH_2-$\underline{CH_2}$-$\underline{CH_2}$-CH_3), 0.90 (6 H, t, J 6.9 Hz, Ar-CH_2-CH_2-CH_2-$\underline{CH_3}$)

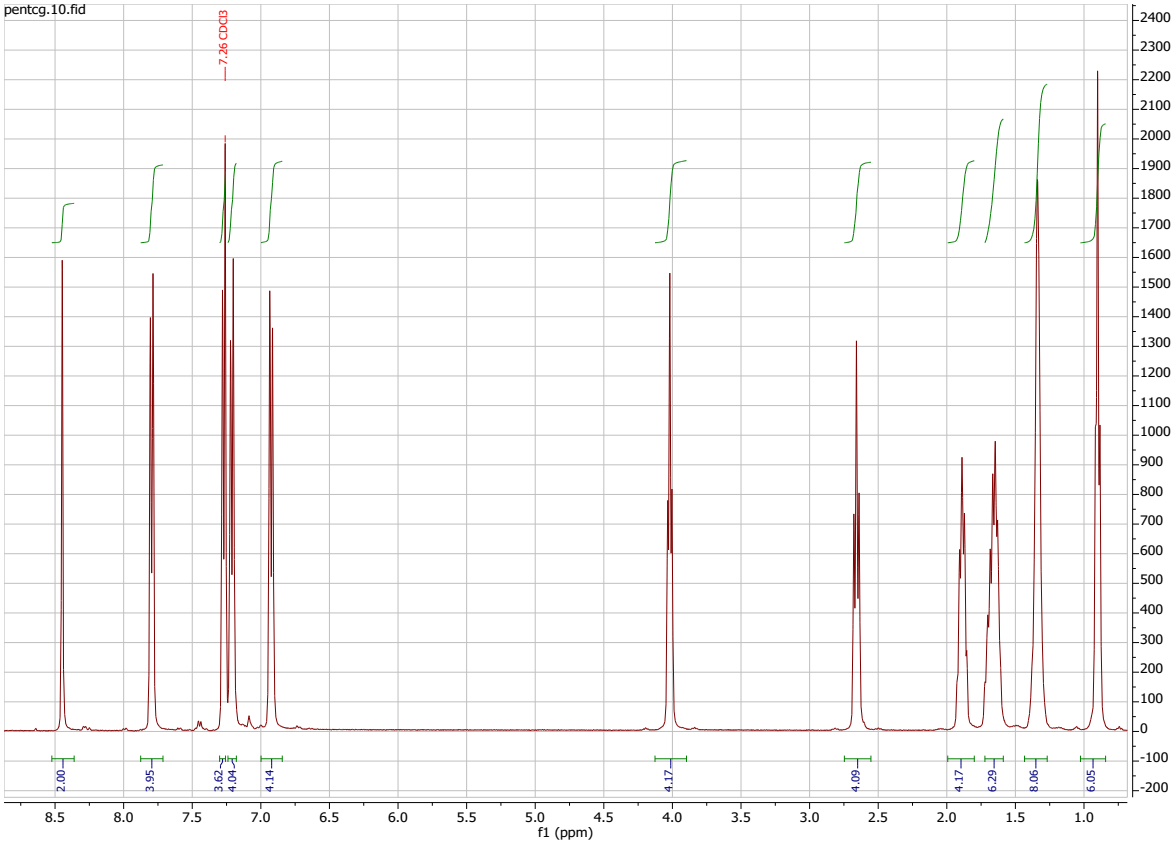

δ_C/ppm (100 MHz, $CDCl_3$): 158.43, 157.60, 146.49, 145.10, 134.12, 128.84, 128.58, 122.13, 114.98, 68.04, 35.98, 31.47, 30.97, 29.10, 22.77, 22.54, 14.04

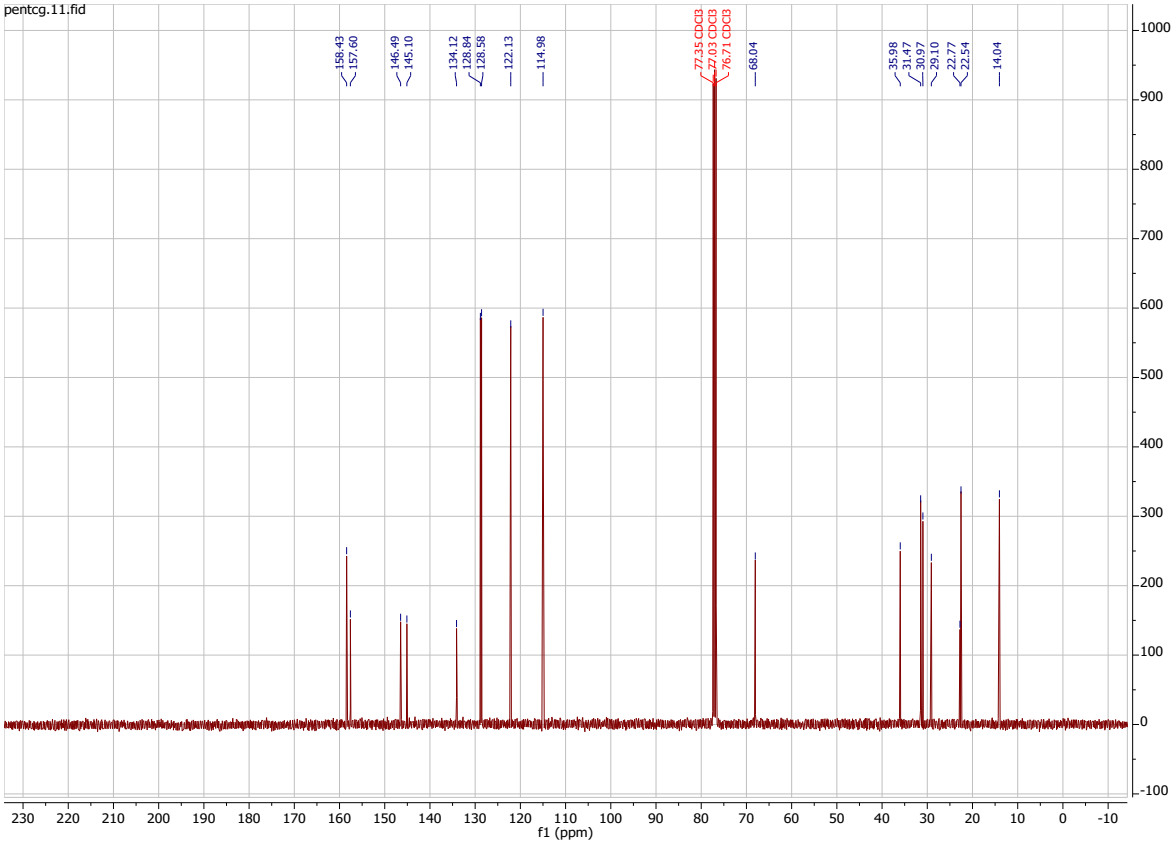

EA: Calculated for $C_{41}H_{50}N_2O_2$: C = 81.69 %, H = 8.36 %, N = 4.65 %; Found: C = 81.27 %, H = 8.39 %, N = 4.54 %

(4.6) (E,E)-N,N'-[Pentane-1,5-diylbis(oxy-4,1-phenylene)]bis[1-(4-hexylphenyl)methanimine] (6-O5O-6)

Yield: 0.313 g, 71.1 %

T_{Crl} 130 °C T_{Nl} (123 °C)

ν_{max}/cm^{-1}: 2957, 2923, 2851, 1623, 1609, 1574, 1502, 1469, 1393, 1284, 1244, 1192, 1174, 1164, 1114, 1064, 1033, 946, 836, 750, 725, 546, 505

δ_H/ppm (400 MHz, $CDCl_3$): 8.45 (2 H, s, (C=N)-H), 7.79 (4 H, d, J 7.7 Hz, Ar-H), 7.27 (4 H, d, J 7.7 Hz, Ar-H), 7.21 (4 H, d, J 8.0 Hz, Ar-H), 6.92 (4 H, d, J 8.0 Hz, Ar-H), 4.02 (4 H, t, J 6.4 Hz, O-$\underline{CH_2}$-CH_2-), 2.66 (4 H, t, J 7.8 Hz, Ar-$\underline{CH_2}$-CH_2-), 1.89 (4 H, tt, J 7.1 Hz, 6.4 Hz, O-CH_2-$\underline{CH_2}$-CH_2-), 1.67 (6 H, m, O-CH_2-CH_2-$\underline{CH_2}$-CH_2-, Ar-CH_2-$\underline{CH_2}$-CH_2-), 1.33 (12 H, m, Ar-CH_2-CH_2-$\underline{CH_2}$-$\underline{CH_2}$-$\underline{CH_2}$-CH_3), 0.89 (6 H, t, J 7.0 Hz, Ar-CH_2-CH_2-CH_2-CH_2-CH_2-$\underline{CH_3}$)

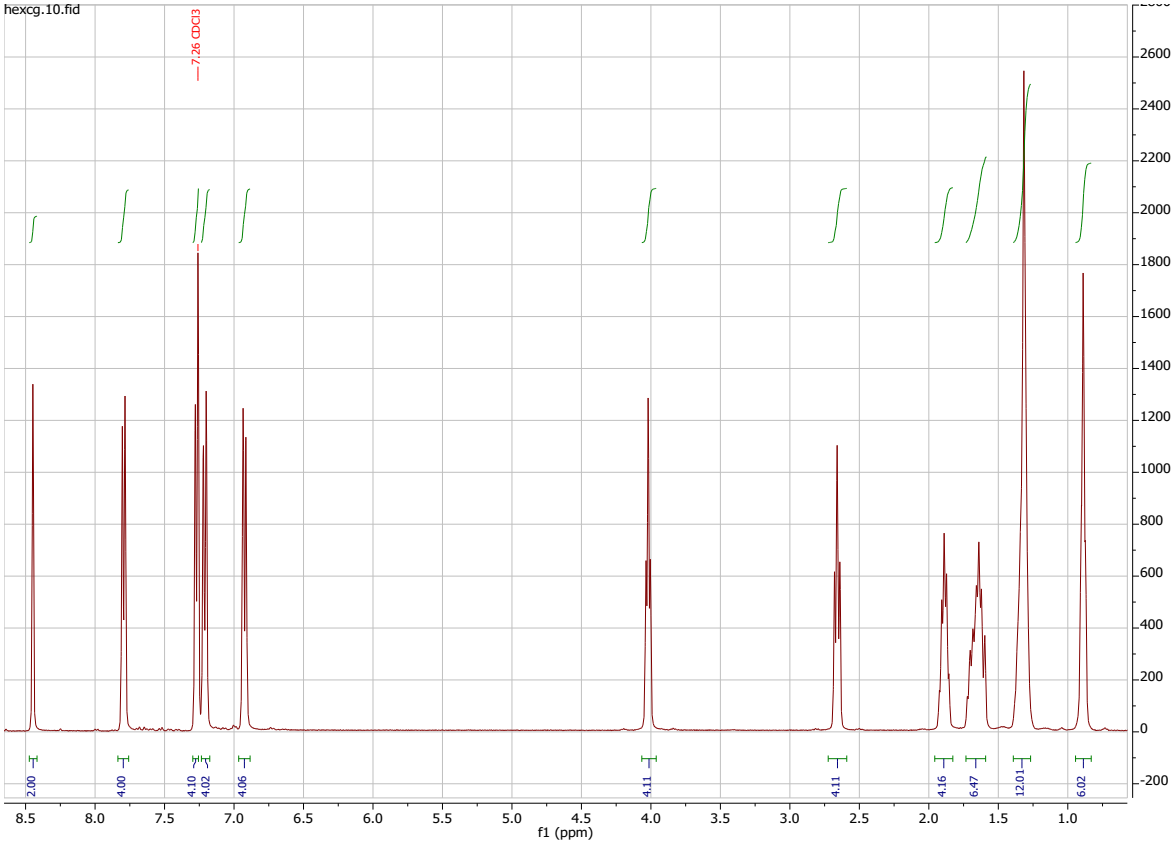

δ_C/ppm (100 MHz, $CDCl_3$): 158.43, 157.60, 146.49, 145.10, 134.11, 128.84, 128.58, 122.13, 114.98, 68.04, 36.01, 31.71, 31.25, 29.10, 28.95, 22.77, 22.61, 14.11

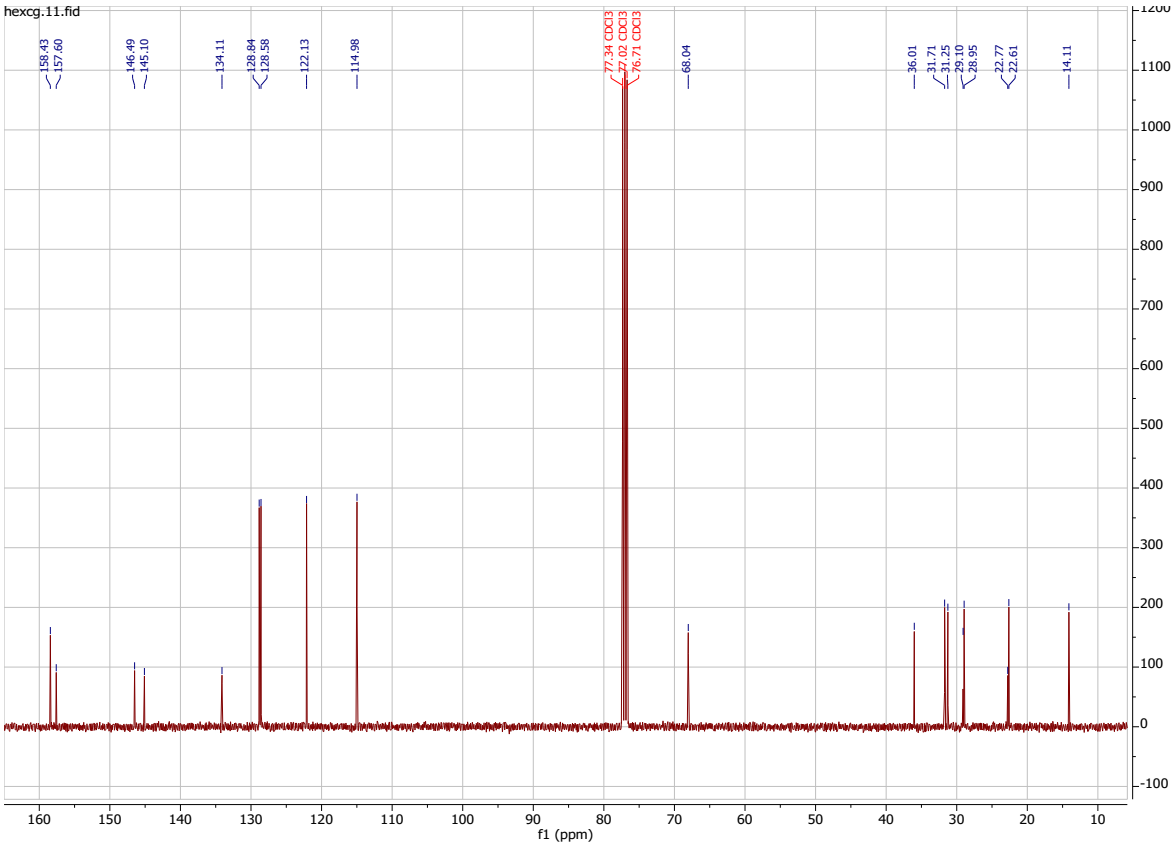

EA: Calculated for $C_{43}H_{54}N_2O_2$: C = 81.86 %, H = 8.63 %, N = 4.44 %; Found: C = 81.65 %, H = 8.70 %, N = 4.36 %

(4.7) (E,E)-N,N'-[Pentane-1,5-diylbis(oxy-4,1-phenylene)]bis[1-(4-heptylphenyl)methanimine] (7-O5O-7)

Yield: 0.272 g, 59.1 %

T_{CrI} 128 °C T_{SmYSmC} (112 °C) T_{SmCSmA} (115 °C) T_{SmAN} (126 °C) T_{NI} (127 °C)

ν_{max}/cm^{-1}: 2955, 2921, 2849, 1623, 1609, 1574, 1502, 1469, 1394, 1284, 1246, 1192, 1174, 1114, 1064, 1033, 946, 837, 750, 723, 546, 508

δ_H/ppm (400 MHz, $CDCl_3$): 8.45 (2 H, s, (C=N)-H), 7.79 (4 H, d, J 7.8 Hz, Ar-H), 7.27 (4 H, d, J 7.8 Hz, Ar-H), 7.21 (4 H, d, J 8.3 Hz, Ar-H), 6.93 (4 H, d, J 8.3 Hz, Ar-H), 4.02 (4 H, t, J 6.5 Hz, O-$\underline{CH_2}$-CH_2-), 2.66 (4 H, t, J 7.7 Hz, Ar-$\underline{CH_2}$-CH_2-), 1.89 (4 H, tt, J 7.3 Hz, 6.5 Hz, O-CH_2-$\underline{CH_2}$-CH_2-), 1.65 (6 H, m, O-CH_2-CH_2-$\underline{CH_2}$-CH_2-, Ar-CH_2-$\underline{CH_2}$-CH_2-), 1.32 (16 H, m, Ar-CH_2-CH_2-$\underline{CH_2}$-$\underline{CH_2}$-$\underline{CH_2}$-$\underline{CH_2}$-CH_3), 0.89 (6 H, t, J 6.8 Hz, Ar-CH_2-CH_2-CH_2-CH_2-CH_2-CH_2-$\underline{CH_3}$)

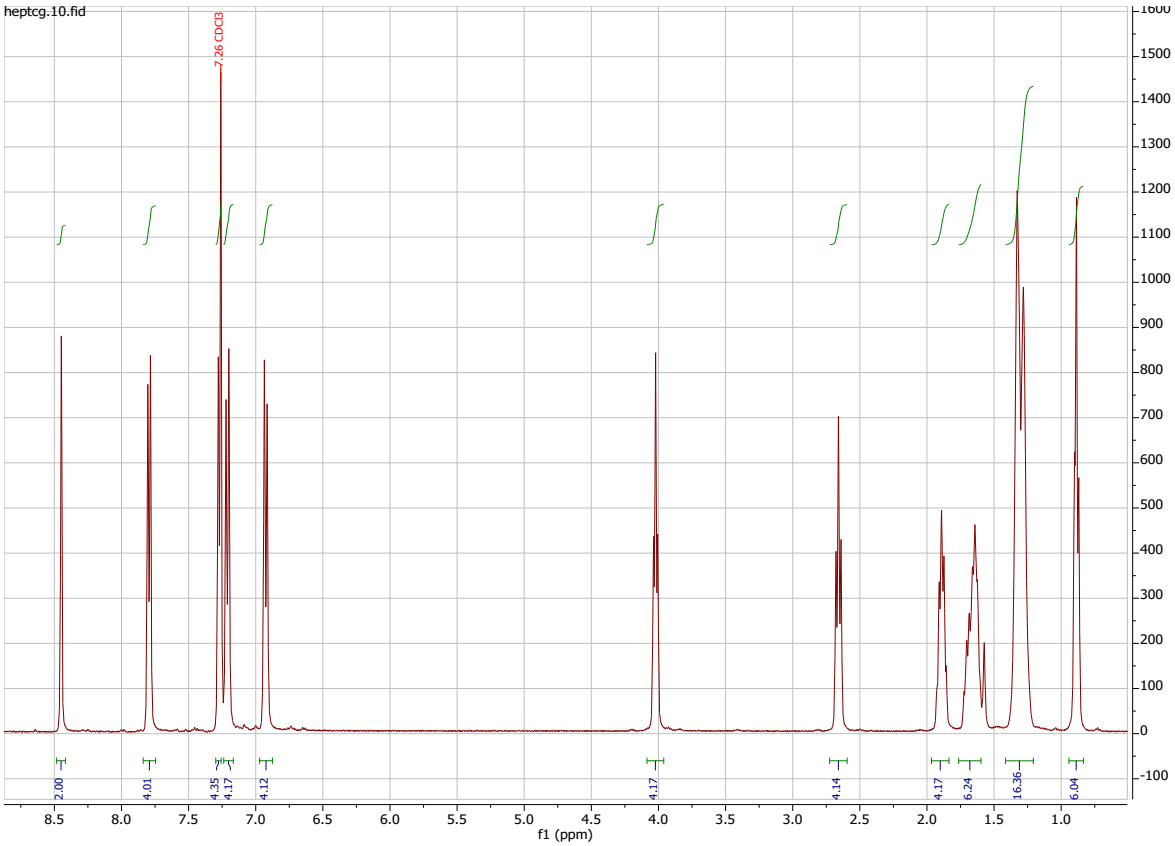

δ_C/ppm (100 MHz, $CDCl_3$): 158.43, 157.59, 146.50, 145.10, 134.11, 128.84, 128.58, 122.12, 114.98, 68.04, 36.01, 31.81, 31.30, 29.24, 29.17, 29.10, 22.77, 22.67, 14.11

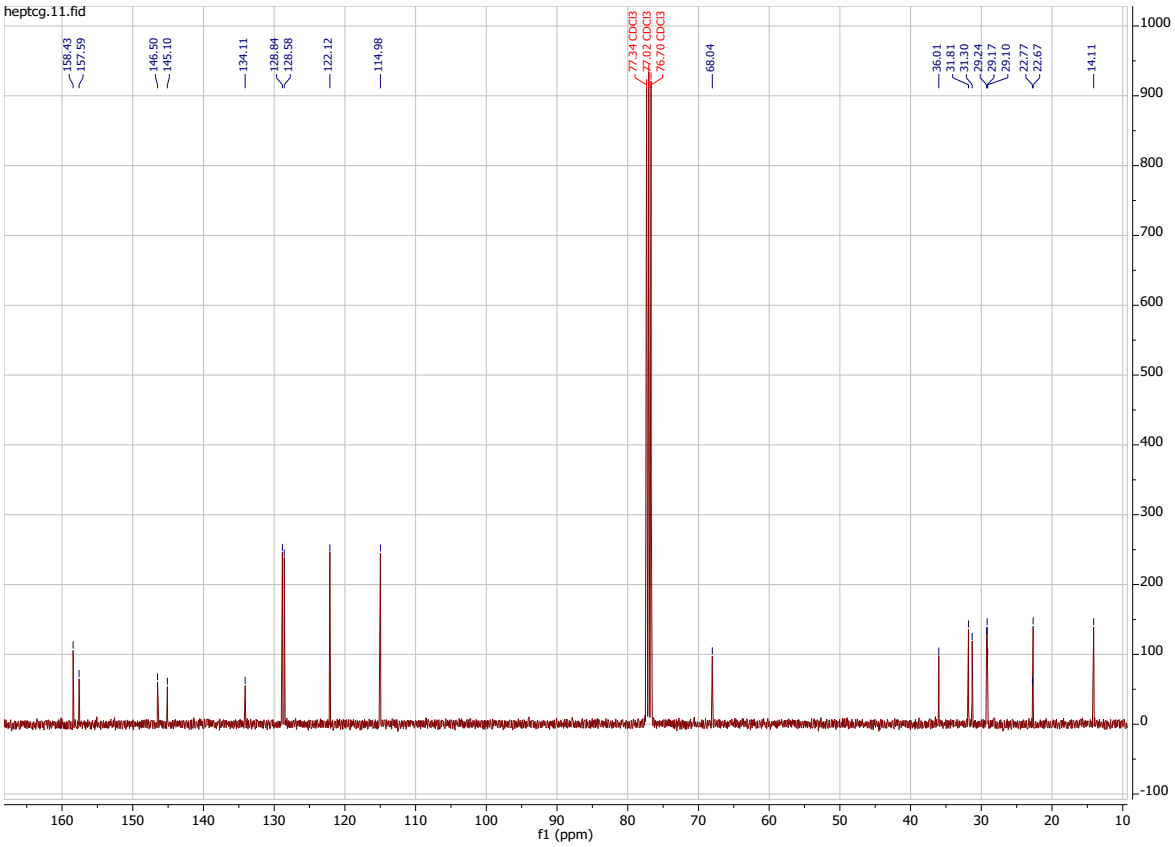

EA: Calculated for $C_{45}H_{58}N_2O_2$: C = 82.02 %, H = 8.87 %, N = 4.25 %; Found: C = 81.83 %, H = 9.04 %, N = 4.18 %

(4.8) (E,E)-N,N'-[Pentane-1,5-diylbis(oxy-4,1-phenylene)]bis[1-(4-octylphenyl)methanimine] (8-O5O-8)

Yield: 0.289 g, 60.3 %

T_{CrSmC} 126 °C T_{SmYSmC} (115 °C) T_{SmCSmA} 127 °C T_{SmAI} 129 °C

ν_{max}/cm^{-1}: 2956, 2920, 2849, 1623, 1609, 1574, 1502, 1469, 1394, 1284, 1246, 1191, 1174, 1114, 1064, 1033, 946, 837, 750, 722, 552, 509

δ_H/ppm (400 MHz, $CDCl_3$): 8.45 (2 H, s, (C=N)-H), 7.80 (4 H, d, J 7.7 Hz, Ar-H), 7.28 (4 H, d, J 7.7 Hz, Ar-H), 7.21 (4 H, d, J 8.2 Hz, Ar-H), 6.92 (4 H, d, J 8.2 Hz, Ar-H), 4.02 (4 H, t, J 6.4 Hz, O-$\underline{CH_2}$-CH_2-), 2.66 (4 H, t, J 7.6 Hz, Ar-$\underline{CH_2}$-CH_2-), 1.89 (4 H, tt, J 7.2 Hz, 6.4 Hz, O-CH_2-$\underline{CH_2}$-CH_2-), 1.65 (6 H, m, O-CH_2-CH_2-$\underline{CH_2}$-CH_2-, Ar-CH_2-$\underline{CH_2}$-CH_2-), 1.30 (20 H, m, Ar-CH_2-CH_2-$\underline{CH_2}$-$\underline{CH_2}$-$\underline{CH_2}$-CH_2-CH_2-CH_2-CH_3), 0.89 (6 H, t, J 7.2 Hz, Ar-CH_2-CH_2-CH_2-CH_2-CH_2-CH_2-CH_2-$\underline{CH_3}$)

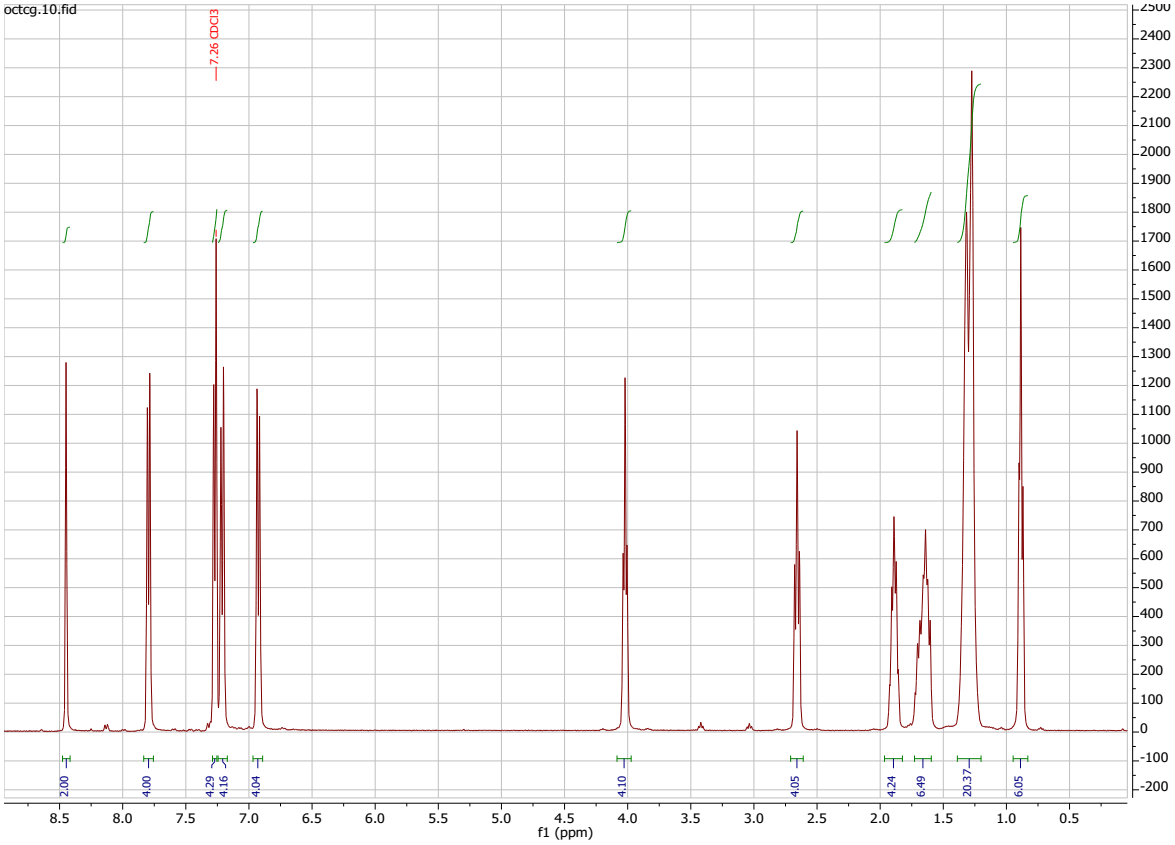

δ_C/ppm (100 MHz, $CDCl_3$): 158.43, 157.60, 146.50, 145.11, 134.11, 128.84, 128.58, 122.13, 114.98, 68.04, 36.02, 31.89, 31.30, 29.47, 29.30, 29.27, 29.10, 22.77, 22.68, 14.12

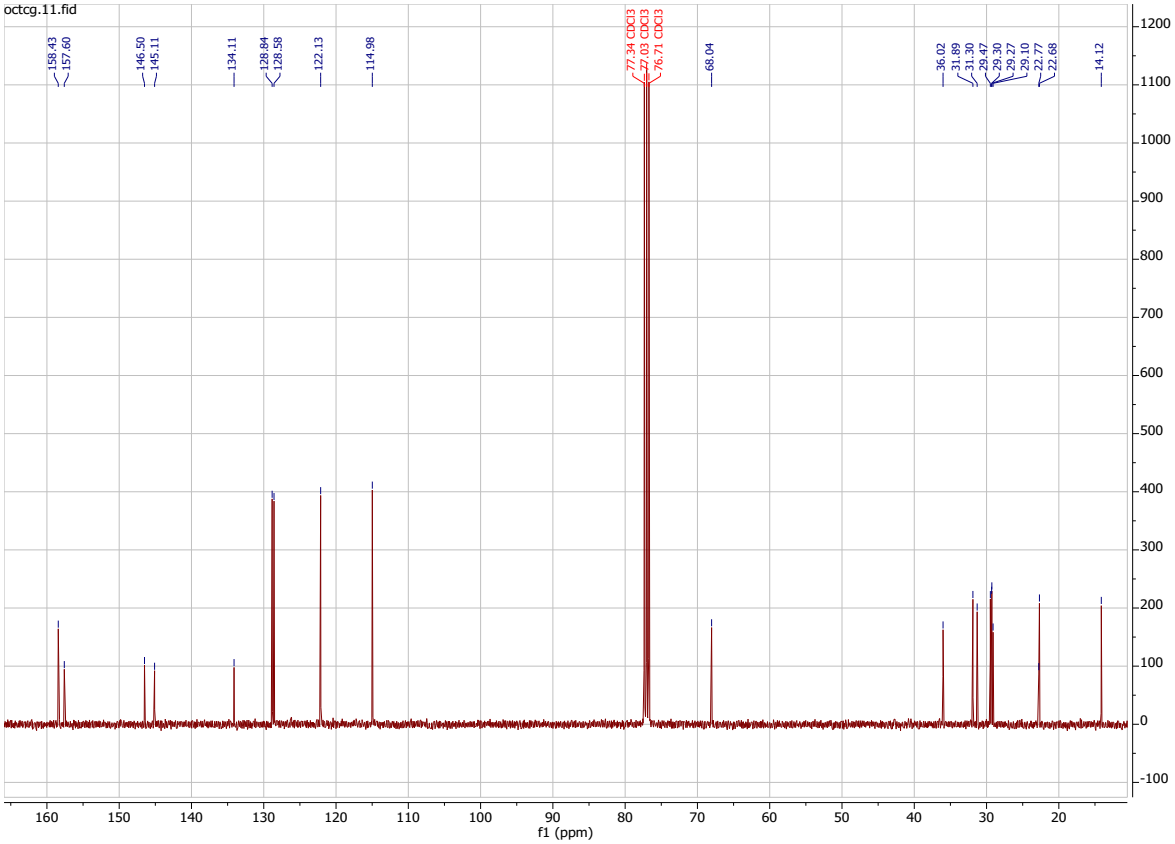

EA: Calculated for $C_{47}H_{62}N_2O_2$: C = 82.17 %, H = 9.10 %, N = 4.08 %; Found: C = 81.74 %, H = 9.22 %, N = 4.02 %

(4.9) (E,E)-N,N'-[Pentane-1,5-diylbis(oxy-4,1-phenylene)]bis[1-(4-nonylphenyl)methanimine] (9-O5O-9)

Yield: 0.208 g, 41.7 %

T_{CrSmC} 123 °C T_{SmYSmC} (116 °C) T_{SmCI} 132 °C

ν_{max}/cm^{-1}: 2953, 2918, 2849, 1623, 1608, 1574, 1501, 1469, 1394, 1284, 1244, 1192, 1174, 1114, 1065, 1031, 946, 837, 751, 721, 547

δ_H/ppm (400 MHz, $CDCl_3$): 8.45 (2 H, s, (C=N)-H), 7.80 (4 H, d, J 7.9 Hz, Ar-H), 7.28 (4 H, d, J 7.9 Hz, Ar-H), 7.21 (4 H, d, J 8.4 Hz, Ar-H), 6.93 (4 H, d, J 8.4 Hz, Ar-H), 4.02 (4 H, t, J 6.5 Hz, O-$\underline{CH_2}$-CH_2-), 2.66 (4 H, t, J 7.6 Hz, Ar-$\underline{CH_2}$-CH_2-), 1.89 (4 H, tt, J 7.1 Hz, 6.5 Hz, O-CH_2-$\underline{CH_2}$-CH_2-), 1.66 (6 H, m, O-CH_2-CH_2-$\underline{CH_2}$-CH_2-, Ar-CH_2-$\underline{CH_2}$-CH_2-), 1.30 (24 H, m, Ar-CH_2-CH_2-$\underline{CH_2\text{-}CH_2\text{-}CH_2\text{-}CH_2\text{-}CH_2\text{-}CH_2}$-$CH_3$), 0.88 (6 H, t, J 7.0 Hz, Ar-CH_2-CH_2-CH_2-CH_2-CH_2-CH_2-CH_2-$\underline{CH_3}$)

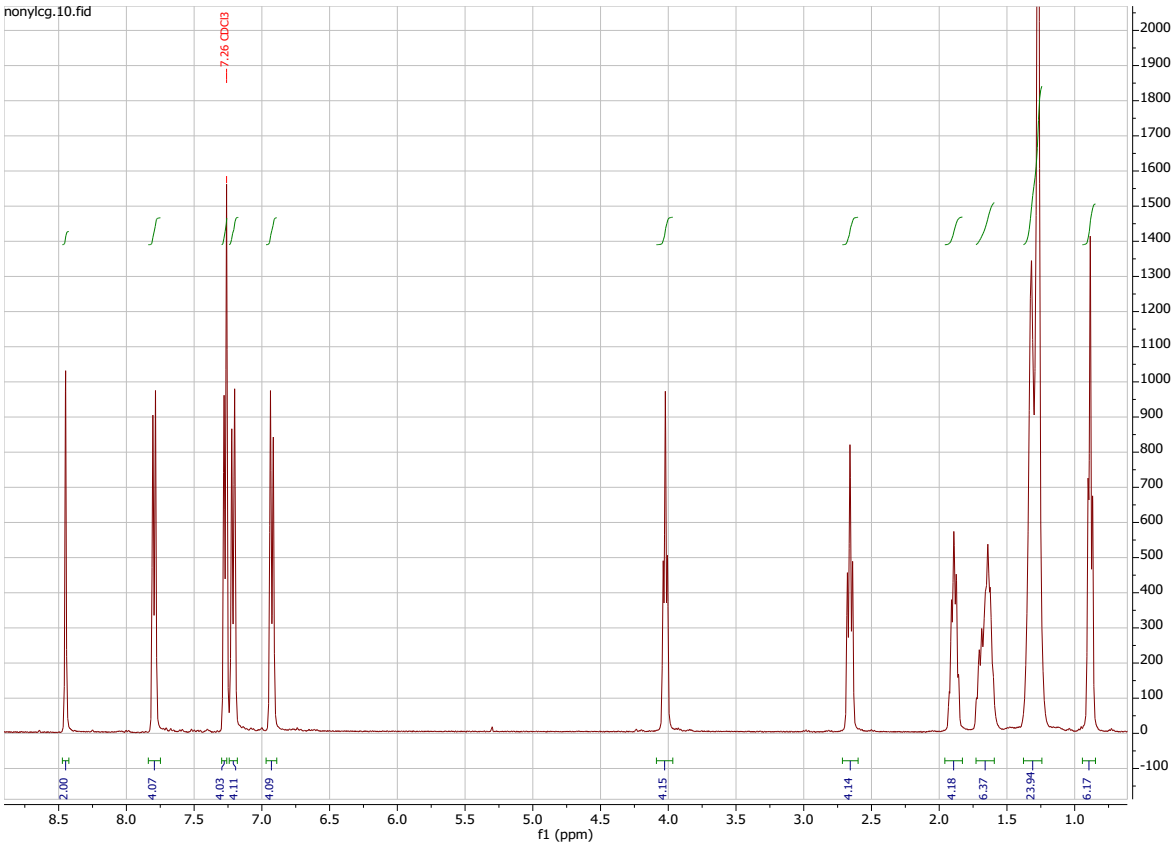

δ_C/ppm (100 MHz, $CDCl_3$): 158.43, 157.60, 146.50, 145.10, 134.11, 128.84, 128.59, 122.13, 114.98, 68.04, 36.02, 31.91, 31.30, 29.56, 29.52, 29.34, 29.30, 29.10, 22.77, 22.70, 14.14

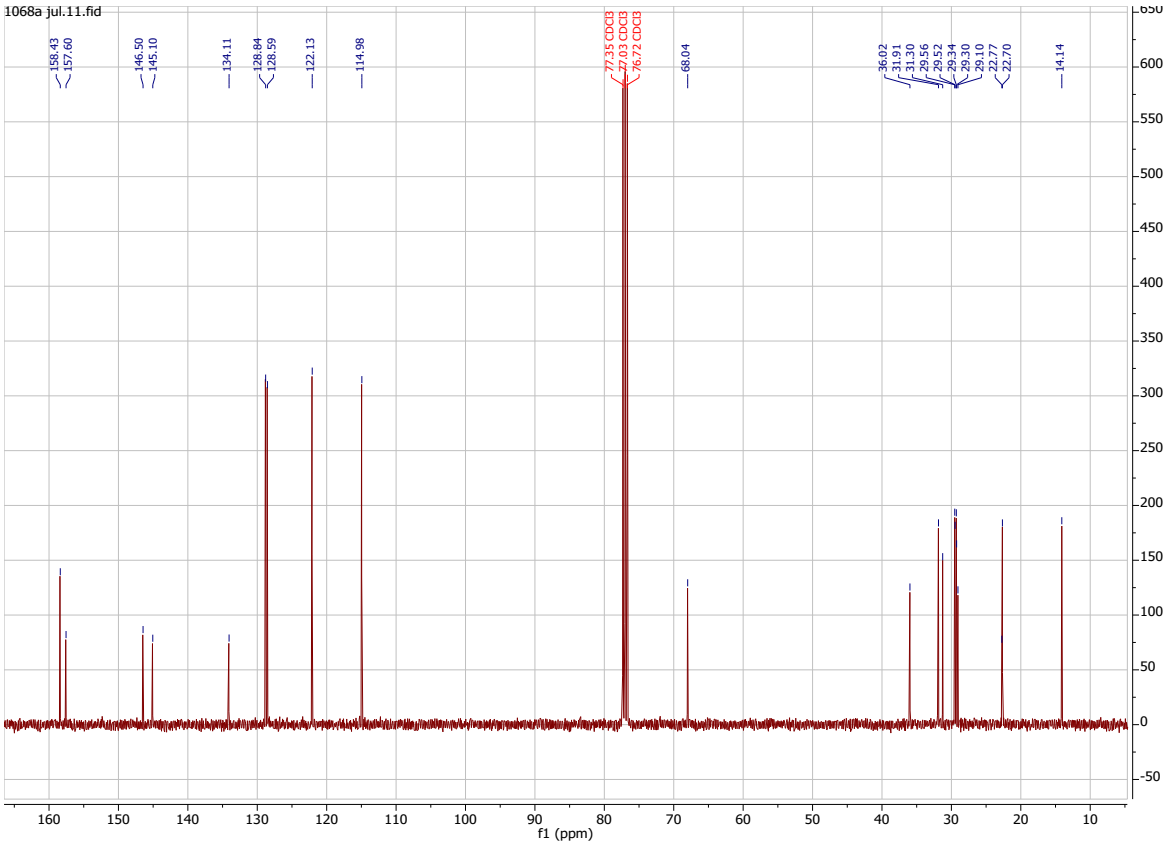

EA: Calculated for $C_{49}H_{66}N_2O_2$: C = 82.30 %, H = 9.30 %, N = 3.92 %; Found: C = 81.98 %, H = 9.46 %, N = 3.74 %

(4.10) (E,E)-N,N'-[Pentane-1,5-diylbis(oxy-4,1-phenylene)]bis[1-(4-decylphenyl)methanimine] (10-O5O-10)

Yield: 0.109 g, 21.0 %

T_{CrSmC} 120 °C T_{SmYSmC} (117 °C) T_{SmCI} 131 °C

ν_{max}/cm^{-1}: 2918, 2849, 1623, 1609, 1574, 1502, 1469, 1394, 1284, 1245, 1192, 1174, 1114, 1032, 1015, 946, 837, 751, 721, 546

δ_H/ppm (400 MHz, $CDCl_3$): 8.45 (2 H, s, (C=N)-H), 7.79 (4 H, d, J 7.8 Hz, Ar-H), 7.27 (4 H, d, J 7.8 Hz, Ar-H), 7.21 (4 H, d, J 8.3 Hz, Ar-H), 6.92 (4 H, d, J 8.3 Hz, Ar-H), 4.02 (4 H, t, J 6.4 Hz, O-$\underline{CH_2}$-CH_2-), 2.65 (4 H, t, J 7.7 Hz, Ar-$\underline{CH_2}$-CH_2-), 1.88 (4 H, m, O-CH_2-$\underline{CH_2}$-CH_2-), 1.66 (6 H, m, O-CH_2-CH_2-$\underline{CH_2}$-CH_2-, Ar-CH_2-$\underline{CH_2}$-CH_2-), 1.29 (28 H, m, Ar-CH_2-CH_2-$\underline{CH_2}$-$\underline{CH_2}$-$\underline{CH_2}$-$\underline{CH_2}$-$\underline{CH_2}$-$\underline{CH_2}$-$\underline{CH_2}$-CH_2-CH_3), 0.88 (6 H, t, J 6.9 Hz, Ar-CH_2-CH_2-CH_2-CH_2-CH_2-CH_2-CH_2-CH_2-$\underline{CH_2}$-$\underline{CH_3}$)

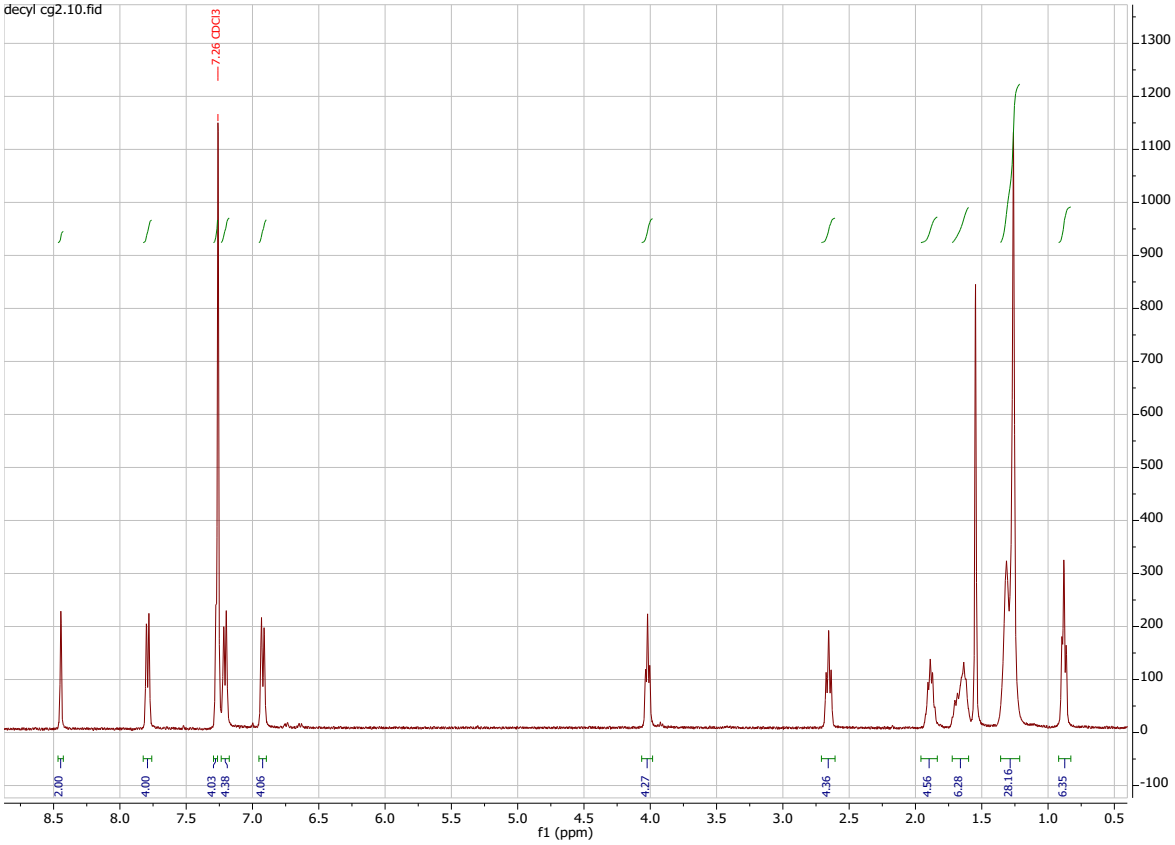

δ_C/ppm (100 MHz, $CDCl_3$): 158.44, 157.59, 146.50, 145.10, 134.10, 128.84, 128.58, 122.12, 114.98, 68.04, 36.01, 31.91, 31.29, 29.62, 29.60, 29.50, 29.34, 29.29, 29.09, 22.77, 22.70, 14.14

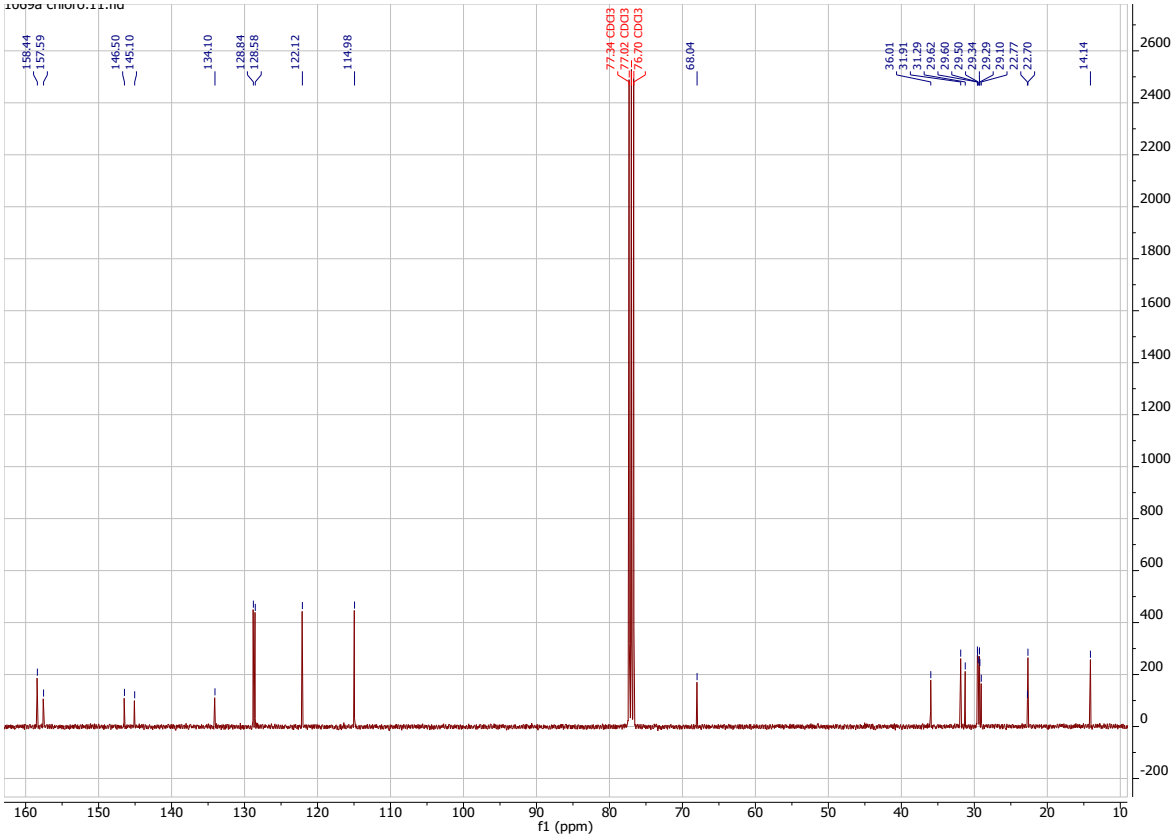

EA: Calculated for $C_{51}H_{70}N_2O_2$: C = 82.43 %, H = 9.49 %, N = 3.77 %; Found: C = 82.55 %, H = 9.60 %, N = 3.68 %

CBO5O-*m* Series

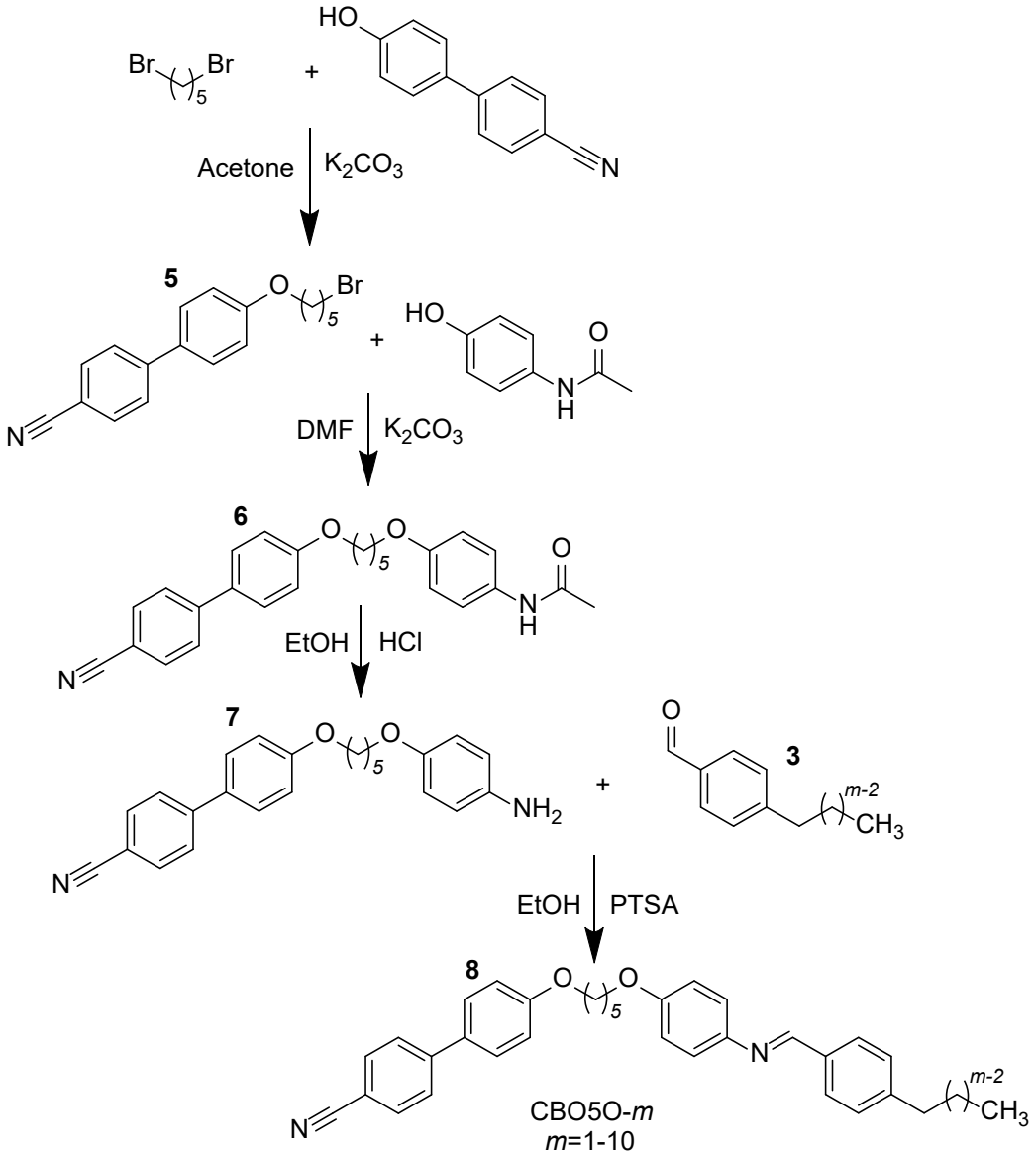

Scheme 2. Synthesis of the CBO5O-*m* series.

(5) 4'-[(5-Bromopentyl)oxy]-[1,1'-biphenyl]-4-carbonitrile

To a pre-dried flask, flushed with argon and fitted with a condenser, 4'-hydroxy-4-biphenylcarbonitrile (2.50 g, 1.28×10^{-2} mol) and potassium carbonate (3.60 g, 2.56×10^{-2} mol) were added. Acetone (50 mL) was added along with 1,5-dibromopentane (10.5 mL, 17.7 g, 7.68×10^{-2} mol). The reaction mixture was refluxed overnight, and the extent of the reaction monitored by TLC using dichloromethane as the solvent system (RF values quoted in the product data). The reaction mixture was cooled to room temperature, filtered and the residue washed with acetone (100 mL). The filtrate was concentrated under vacuum to give

a yellow solution which was added to 40:60 petroleum ether (100 mL). The resulting white precipitate was collected and recrystallised from hot ethanol (200 mL).

Yield: 3.52 g, 79.9 %. RF: 0.60

T_{CrI} 80°C T_{NI} (68 °C)

ν_{max}/cm^{-1}: 2945, 2869, 2222, 1603, 1494, 1474, 1396, 1292, 1245, 1202, 1178, 1038, 997, 822, 802, 734, 629, 564, 531

δ_H/ppm (400 MHz, $CDCl_3$): 7.72 (2 H, d, J 8.0 Hz, Ar-H), 7.66 (2 H, d, J 8.0 Hz, Ar-H), 7.56 (2 H, d, J 8.4 Hz, Ar-H), 7.02 (2 H, d, J 8.4 Hz, Ar-H), 4.05 (2 H, t, J 6.3 Hz, O-$\underline{CH_2}$-CH_2-), 3.48 (2 H, t, J 7.2 Hz, Br-$\underline{CH_2}$-CH_2-), 1.99 (2 H, quin, J 7.2 Hz, Br-CH_2-$\underline{CH_2}$-CH_2-), 1.89 (2 H, tt, J 7.2 Hz, 6.3 Hz, O-CH_2-$\underline{CH_2}$-CH_2-), 1.69 (2 H, quin, J 7.2 Hz, O-CH_2-CH_2-$\underline{CH_2}$-CH_2-)

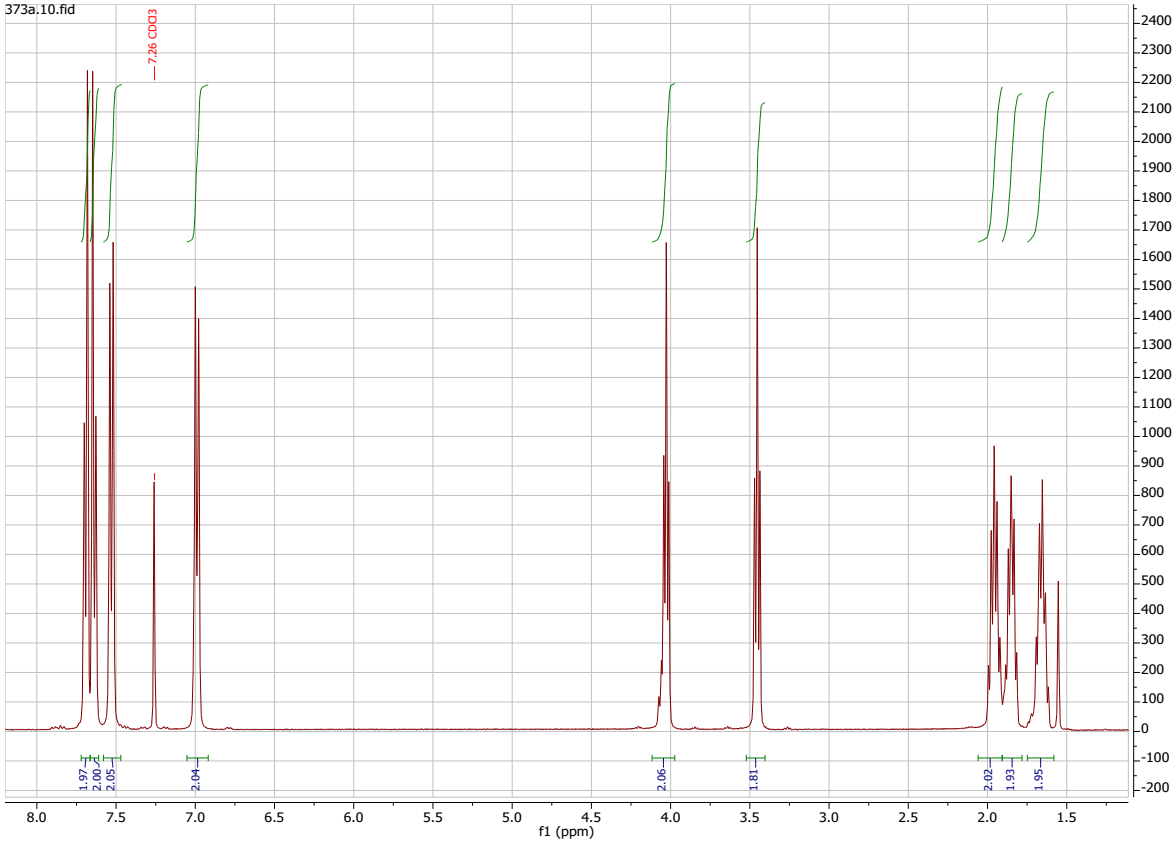

δ_C/ppm (100 MHz, $CDCl_3$): 159.62, 145.23, 132.58, 131.45, 128.36, 127.10, 119.11, 115.07, 110.10, 67.75, 33.57, 32.46, 28.41, 24.84

Data consistent with reported values.[6]

(6) *N*-[4-({5-[(4'-Cyano-[1,1'-biphenyl]-4-yl)oxy]pentyl}oxy)phenyl]acetamide

To a pre-dried flask flushed with argon and fitted with a condenser, 4-acetamidophenol (2.75 g, 0.0182 mol) and potassium carbonate (4.81 g, 0.0348 mol) were added.

Dimethylformamide (80 mL) was added with compound **5** (5.99 g, 0.0174 mol) and stirred. The reaction was heated to 90 °C, left overnight and the extent of the reaction monitored by TLC using dichloromethane as the solvent system (RF value quoted in the product data). The reaction mixture was cooled to room temperature and poured into water (250 mL). The resulting white precipitate was vacuum filtered and recrystallised from hot ethanol (250 mL). Yield: 4.85 g, 67.2 %. RF: 0.53.

T_{CrI} 144 °C T_{NI} (87 °C)

ν_{max}/cm^{-1}: 3268, 2930, 2226, 1654, 1602, 1508, 1493, 1469, 1393, 1373, 1318, 1287, 1242, 1220, 1182, 1107, 1064, 1032, 1001, 985, 946, 830, 819. 761, 658, 633, 590, 561, 533, 443

δ_H/ppm (400 MHz, DMSO-d_6): 9.75 (1 H, s, NH), 7.86 (2 H, d, J 8.6 Hz, Ar-H), 7.82 (2 H, d, J 8.6 Hz, Ar-H), 7.69 (2 H, d, J 8.7 Hz, Ar-H), 7.46 (2 H, d, J 8.8 Hz, Ar-H), 7.04 (2 H, d, J 8.7 Hz, Ar-H), 6.85 (2 H, d, J 8.8 Hz, Ar-H), 4.04 (2 H, t, J 6.4 Hz, O-$\underline{CH_2}$-CH_2-), 3.93 (2 H, t, J 6.4 Hz, O-$\underline{CH_2}$-CH_2-), 2.00 (3 H, s, (C=O)-$\underline{CH_3}$) 1.77 (4 H, m, O-CH_2-$\underline{CH_2}$-CH_2-$\underline{CH_2}$-CH_2-O), 1.56 (2 H, m, O-CH_2-CH_2-$\underline{CH_2}$-CH_2-CH_2-O)

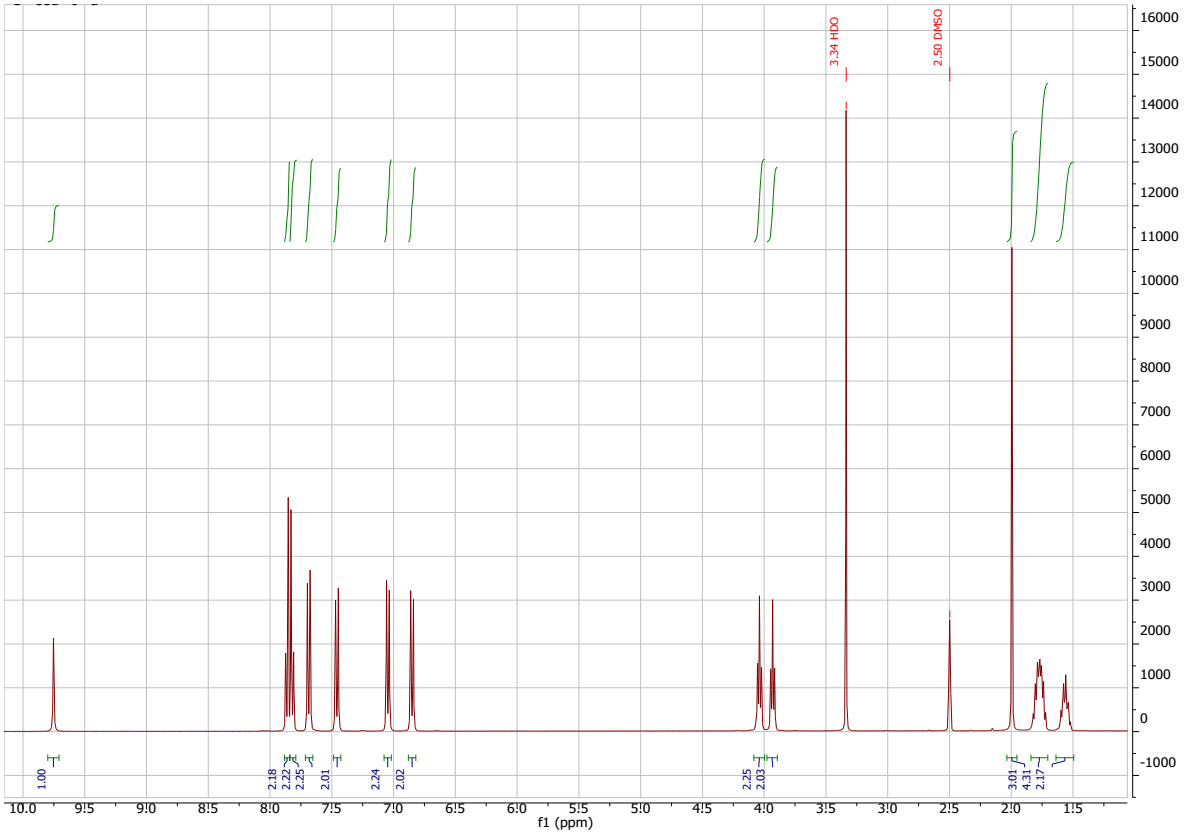

δ_C/ppm (100 MHz, $CDCl_3$): 168.28, 159.68, 155.87, 145.28, 132.56, 131.36, 130.94, 128.34, 127.09, 121.88, 119.12, 115.09, 114.77, 110.01, 68.00, 67.92, 29.01, 28.97, 24.32, 22.73

(7) 4'-{[5-(4-Aminophenoxy)pentyl]oxy}-[1,1'-biphenyl]-4-carbonitrile

To a pre-dried flask flushed with argon and fitted with a condenser, compound **6** (4.60 g, 0.0111 mol) was added. Ethanol (110 mL) was added along with 32 % hydrochloric acid (25 mL, 29.0 g, 0.795 mol) and stirred. The reaction was heated at reflux overnight and the extent of the reaction monitored by TLC using 50 % dichloromethane and 50 % ethyl acetate as the solvent system (RF value quoted in the product data). The reaction mixture was cooled to room temperature, poured into ice (150 g), and made alkaline using 15 M sodium hydroxide solution. The resulting brown solid was vacuum filtered and was recrystallised from hot ethanol (100 mL).

Yield: 3.92 g, 94.8 %. RF: 0.56

T_{CrI} 120 °C T_{NI} (85 °C)

ν_{max}/cm^{-1}: 3438, 3357, 2942, 2868, 2223, 1600, 1512, 1492, 1470, 1395, 1291, 1231, 1176, 1014, 835, 816, 771, 736, 659, 562, 517

δ_H/ppm (400 MHz, $CDCl_3$): 7.69 (2 H, d, J 8.4 Hz, Ar-H), 7.64 (2 H, d, J 8.4 Hz, Ar-H), 7.53 (2 H, d, J 8.7 Hz, Ar-H), 6.99 (2 H, d, J 8.7 Hz, Ar-H), 6.75 (2 H, d, J 8.8 Hz, Ar-H), 6.64 (2 H, d, J 8.8 Hz, Ar-H), 4.04 (2 H, t, J 6.4 Hz, O-$\underline{CH_2}$-CH_2-), 3.93 (2 H, t, J 6.4 Hz, O-$\underline{CH_2}$-CH_2-), 3.41 (2 H, br, NH_2), 1.86 (4 H, m, O-CH_2-$\underline{CH_2}$-CH_2-$\underline{CH_2}$-CH_2-O), 1.66 (2 H, m, O-CH_2-CH_2-$\underline{CH_2}$-CH_2-CH_2-O)

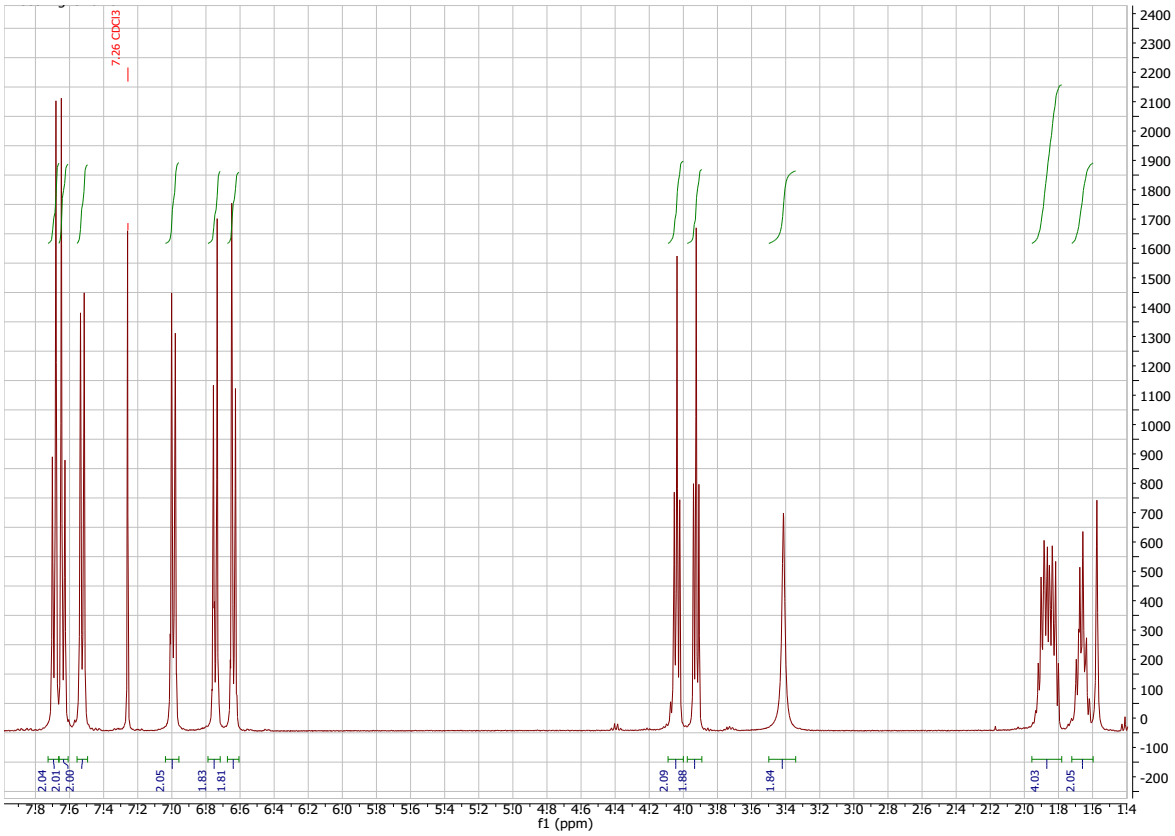

δ_C/ppm (100 MHz, $CDCl_3$): 159.72, 152.20, 145.28, 139.97, 132.57, 131.34, 128.34, 127.09, 119.13, 116.40, 115.69, 115.10, 110.06, 68.43, 67.97, 29.19, 29.01, 22.76

(8) 4'-{[5-(4-{(E)-[(4-Alkylphenyl)methylidene]amino}phenoxy)pentyl]oxy}-[1,1'-biphenyl]-4-carbonitriles (CBO5O-*m*)

To a pre-dried flask flushed with argon and fitted with a condenser, compound **7** (1 eq, 0.150 g, 4.03×10^{-4} mol) and compound **3** (2 eq) of the appropriate chain length were added along with ethanol (20 mL) and the mixture was stirred. The quantities of 4-alkylbenzaldehydes used in each reaction are listed in **Table SI3**. The reaction was heated to reflux, *p*-toluenesulfonic acid (catalytic amount) was added, and left overnight. The reaction mixture was cooled to room temperature and a purple precipitate formed which was collected by vacuum filtration. The purple solid was recrystallised from hot ethanol (15 mL).

Table SI3. Quantities of 4-alkylbenzaldehydes used in the syntheses of 4'-{[5-(4-{(E)-[(4-alkylphenyl)methylidene]amino}phenoxy)pentyl]oxy}-[1,1'-biphenyl]-4-carbonitriles (**8**).

m	4-Alkylbenzaldehyde
1	0.095 mL, 0.097 g, 8.06×10^{-4} mol
2	0.110 mL, 0.108 g, 8.06×10^{-4} mol
3	0.119 mL, 0.119 g, 8.06×10^{-4} mol
4	0.135 mL, 0.131 g, 8.06×10^{-4} mol
5	0.148 mL, 0.142 g, 8.06×10^{-4} mol
6	0.153 g, 8.06×10^{-4} mol
7	0.165 g, 8.06×10^{-4} mol
8	0.176 g, 8.06×10^{-4} mol
9	0.187 g, 8.06×10^{-4} mol
10	0.199 g, 8.06×10^{-4} mol

(8.1) 4'-{[5-(4-{(E)-[(4-Methylphenyl)methylidene]amino}phenoxy)pentyl]oxy}-[1,1'-biphenyl]-4-carbonitrile (CBO5O-1)

Yield: 0.101 g, 52.8 %

T_{CrN} 140 °C $T_{N_{TB}N}$ (85 °C) T_{NI} 166 °C

ν_{max}/cm^{-1}: 2928, 2865, 2228, 1622, 1601, 1573, 1494, 1467, 1390, 1284, 1244, 1213, 1184, 1111, 1065, 1034, 987, 946, 821, 772, 752, 724, 658, 610, 547, 533, 497

δ_H/ppm (400 MHz, $CDCl_3$): 8.44 (1 H, s, (C=N)-H), 7.77 (2 H, d, J 8.2 Hz, Ar-H), 7.69 (2 H, d, J 8.5 Hz, Ar-H), 7.64 (2 H, d, J 8.5 Hz, Ar-H), 7.53 (2 H, d, J 8.7 Hz, Ar-H), 7.28 (2 H, d, J 8.2 Hz, Ar-H), 7.21 (2 H, d, J 8.8 Hz, Ar-H), 7.00 (2 H, d, J 8.7 Hz, Ar-H), 6.93 (2 H, d, J 8.8 Hz, Ar-H), 4.04 (4 H, m, O-$\underline{CH_2}$-CH_2-CH_2-CH_2-$\underline{CH_2}$-O), 2.42 (3 H, s, Ar-$\underline{CH_3}$), 1.90 (4 H, m, O-CH_2-$\underline{CH_2}$-CH_2-$\underline{CH_2}$-CH_2-O), 1.70 (2 H, m, O-CH_2-CH_2-$\underline{CH_2}$-CH_2-)

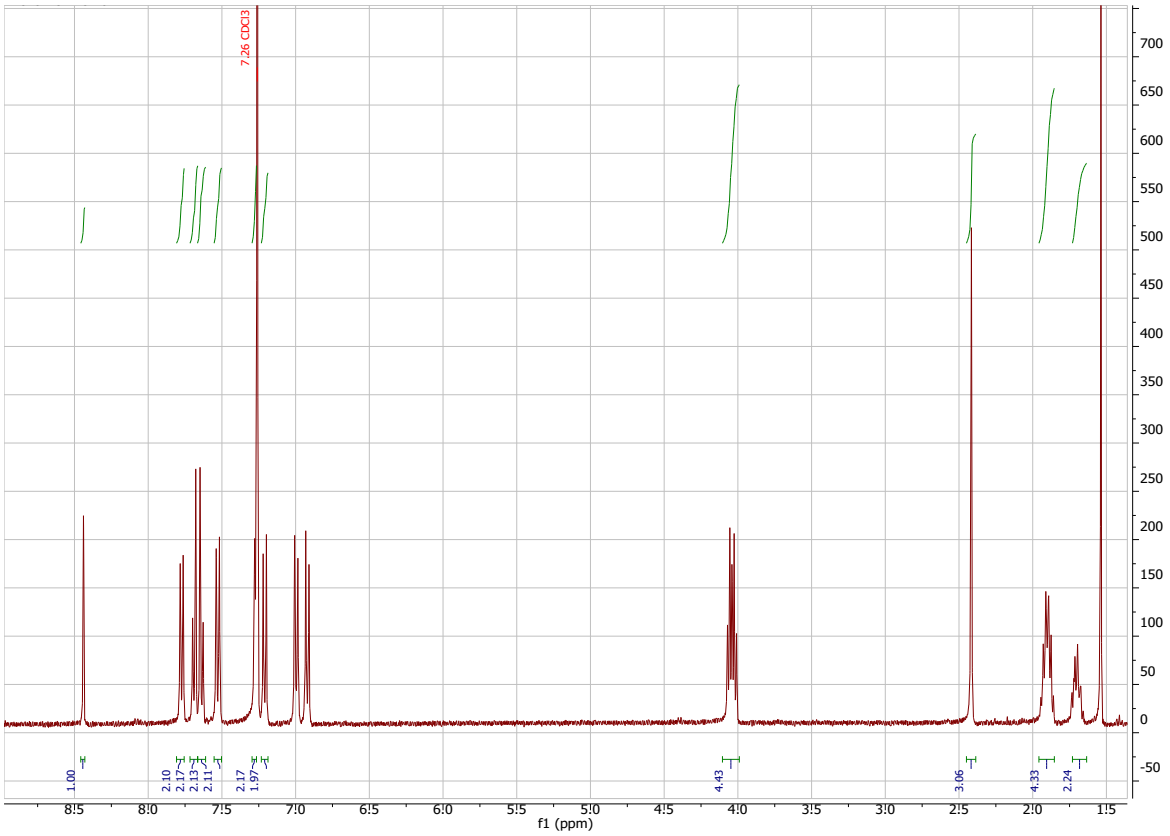

δ_C/ppm (100 MHz, $CDCl_3$): 159.71, 158.40, 157.57, 145.26, 145.06, 141.49, 133.89, 132.57, 131.37, 129.49, 128.57, 128.35, 127.09, 122.15, 119.12, 115.10, 114.97, 110.07, 67.99, 67.94, 29.06, 28.99, 22.76, 21.62

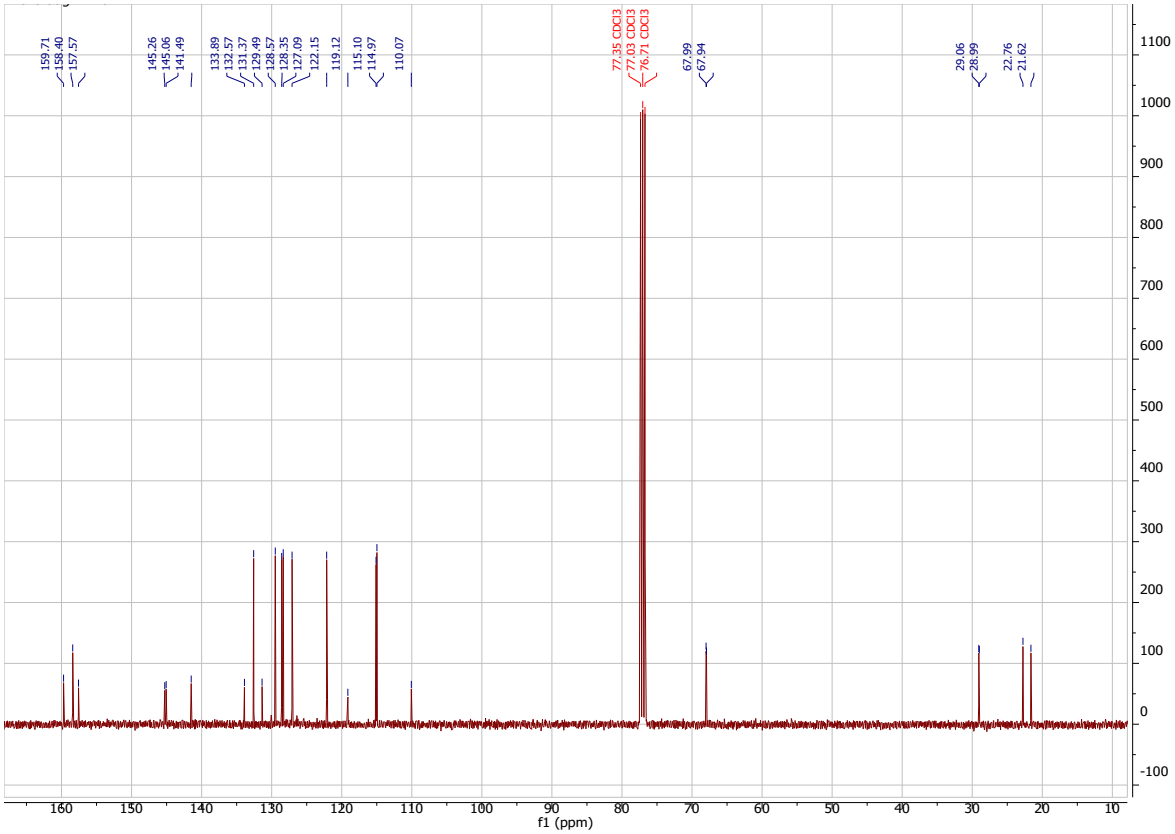

EA: Calculated for $C_{32}H_{30}N_2O_2$: C = 80.98 %, H = 6.37 %, N = 5.90 %; Found: C = 80.64 %, H = 6.35 %, N = 5.65 %

(8.2) 4'-{[5-(4-{(E)-[(4-Ethylphenyl)methylidene]amino}phenoxy)pentyl]oxy}-[1,1'-biphenyl]-4-carbonitrile (CBO5O-2)

Yield: 0.080 g, 40.6 %

T_{CrN} 143 °C T_{NI} 158 °C

ν_{max}/cm^{-1}: 2930, 2868, 2225, 1622, 1600, 1575, 1510, 1493, 1469, 1391, 1284, 1242, 1180, 1112, 1061, 1034, 1015, 986, 945, 819, 772, 724, 658, 610, 548, 532

δ_H/ppm (400 MHz, $CDCl_3$): 8.45 (1 H, s, (C=N)-H), 7.80 (2 H, d, J 8.0 Hz, Ar-H), 7.69 (2 H, d, J 8.5 Hz, Ar-H), 7.64 (2 H, d, J 8.5 Hz, Ar-H), 7.54 (2 H, d, J 8.7 Hz, Ar-H), 7.29 (2 H, d, J 8.0 Hz, Ar-H), 7.21 (2 H, d, J 8.7 Hz, Ar-H), 6.99 (2 H, d, J 8.7 Hz, Ar-H), 6.92 (2 H, d, J 8.7 Hz, Ar-H), 4.04 (4 H, m, O-$\underline{CH_2}$-CH_2-CH_2-CH_2-$\underline{CH_2}$-O), 2.71 (2 H, quart, J 7.6 Hz, Ar-$\underline{CH_2}$-CH_3), 1.89 (4 H, m, O-CH_2-$\underline{CH_2}$-CH_2-$\underline{CH_2}$-CH_2-O), 1.70 (2 H, m, O-CH_2-CH_2-$\underline{CH_2}$-CH_2-), 1.27 (3 H, t, J 7.6 Hz, Ar-CH_2-$\underline{CH_3}$)

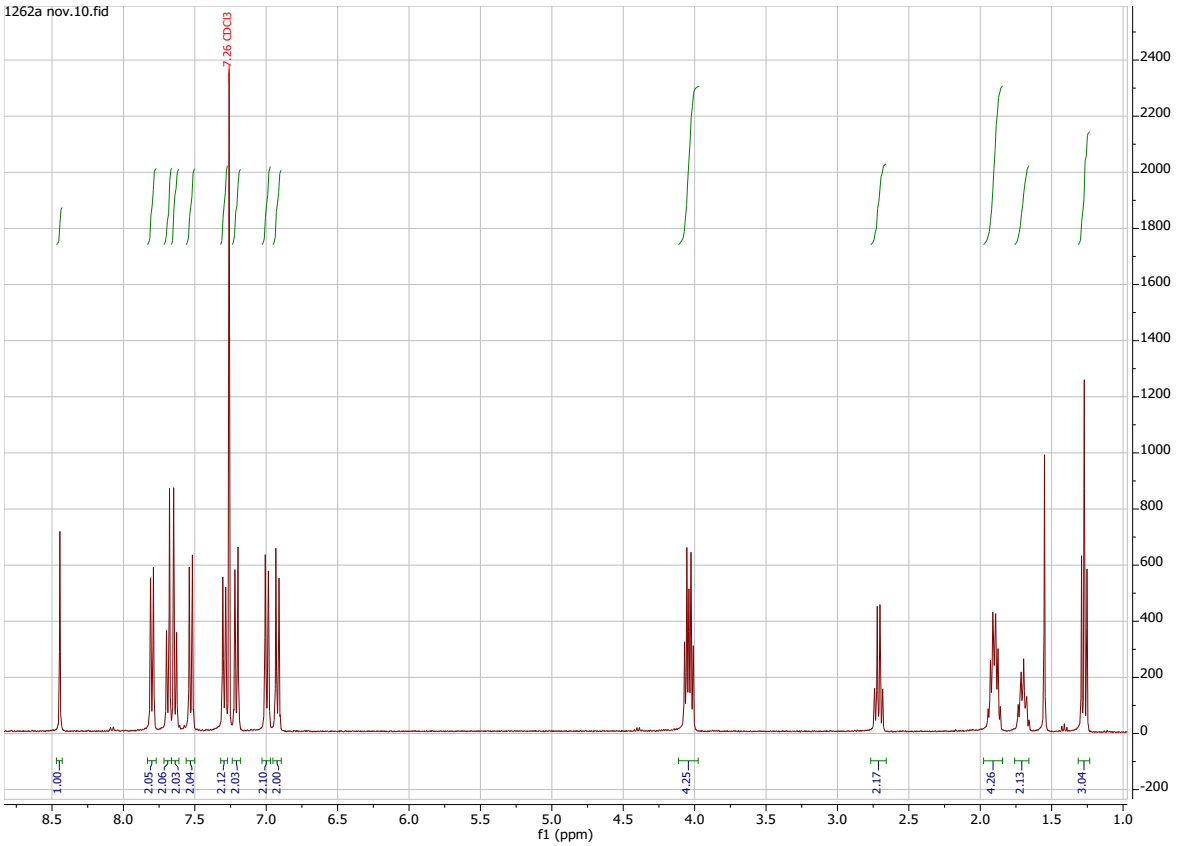

δ_C/ppm (100 MHz, $CDCl_3$): 159.70, 158.44, 157.56, 147.80, 145.26, 145.11, 134.11, 132.57, 131.37, 128.67, 128.35, 128.30, 127.09, 122.14, 119.12, 115.10, 114.97, 110.07, 68.00, 67.94, 29.06, 28.99, 28.95, 22.76, 15.40

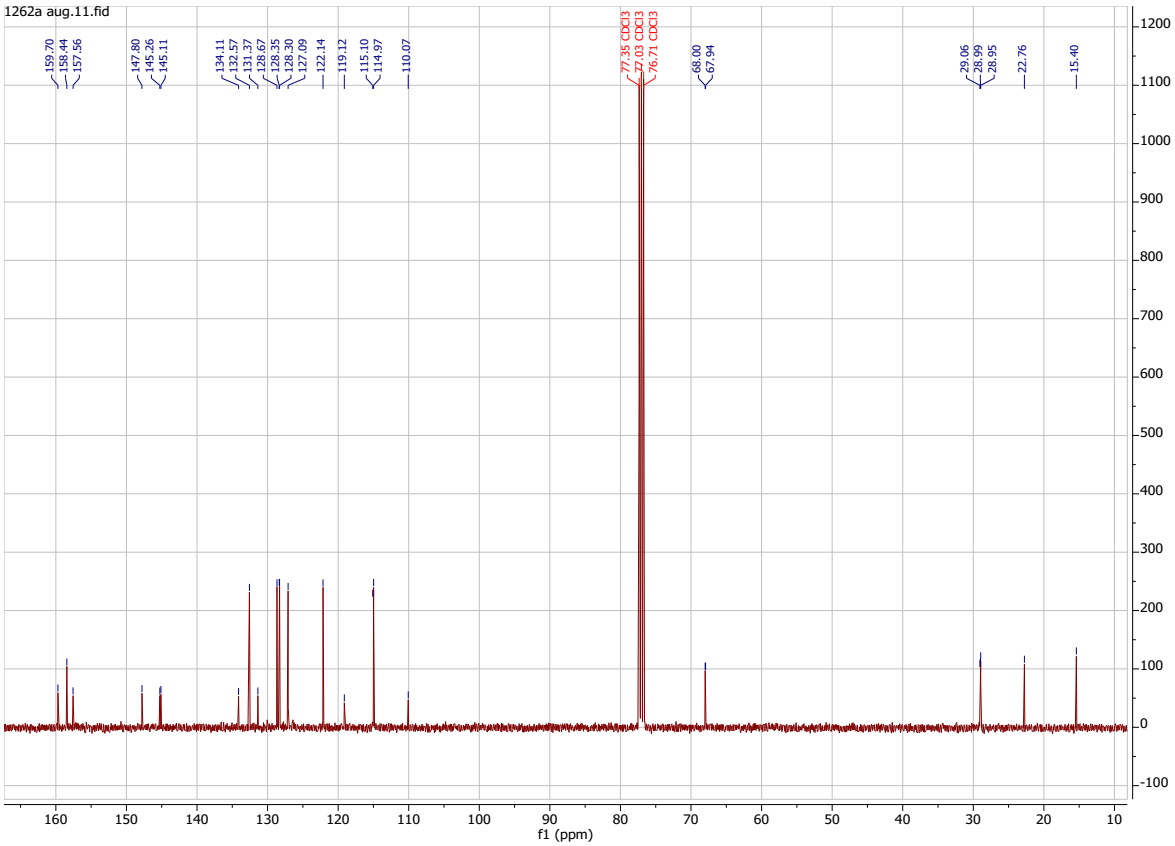

EA: Calculated for $C_{33}H_{32}N_2O_2$: C = 81.12 %, H = 6.60 %, N = 5.73 %; Found: C = 80.97 %, H = 6.59 %, N = 5.54 %

(8.3) 4'-{[5-(4-{(E)-[(4-Propylphenyl)methylidene]amino}phenoxy)pentyl]oxy}-[1,1'-biphenyl]-4-carbonitrile (CBO5O-3)

Yield: 0.127 g, 62.7 %

T_{CrN} 118 °C T_{NI} 160 °C

ν_{max}/cm^{-1}: 2929, 2871, 2228, 1622, 1602, 1575, 1494, 1469, 1390, 1284, 1243, 1184, 1171, 1113, 1062, 1033, 986, 945, 824, 757, 658, 547, 533

δ_H/ppm (400 MHz, $CDCl_3$): 8.44 (1 H, s, (C=N)-H), 7.79 (2 H, d, J 8.0 Hz, Ar-H), 7.69 (2 H, d, J 8.5 Hz, Ar-H), 7.63 (2 H, d, J 8.5 Hz, Ar-H), 7.54 (2 H, d, J 8.7 Hz, Ar-H), 7.28 (2 H, d, J 8.0 Hz, Ar-H), 7.21 (2 H, d, J 8.9 Hz, Ar-H), 7.00 (2 H, d, J 8.7 Hz, Ar-H), 6.92 (2 H, d, J 8.9 Hz, Ar-H), 4.04 (4 H, m, O-$\underline{CH_2}$-CH_2-CH_2-CH_2-$\underline{CH_2}$-O), 2.65 (2 H, t, J 7.4 Hz, Ar-$\underline{CH_2}$-CH_2-), 1.90 (4 H, m, O-CH_2-$\underline{CH_2}$-CH_2-$\underline{CH_2}$-CH_2-O), 1.69 (4 H, m, O-CH_2-CH_2-$\underline{CH_2}$-CH_2-, Ar-CH_2-$\underline{CH_2}$-CH_3), 0.96 (3 H, t, J 7.3 Hz, Ar-CH_2-CH_2-$\underline{CH_3}$)

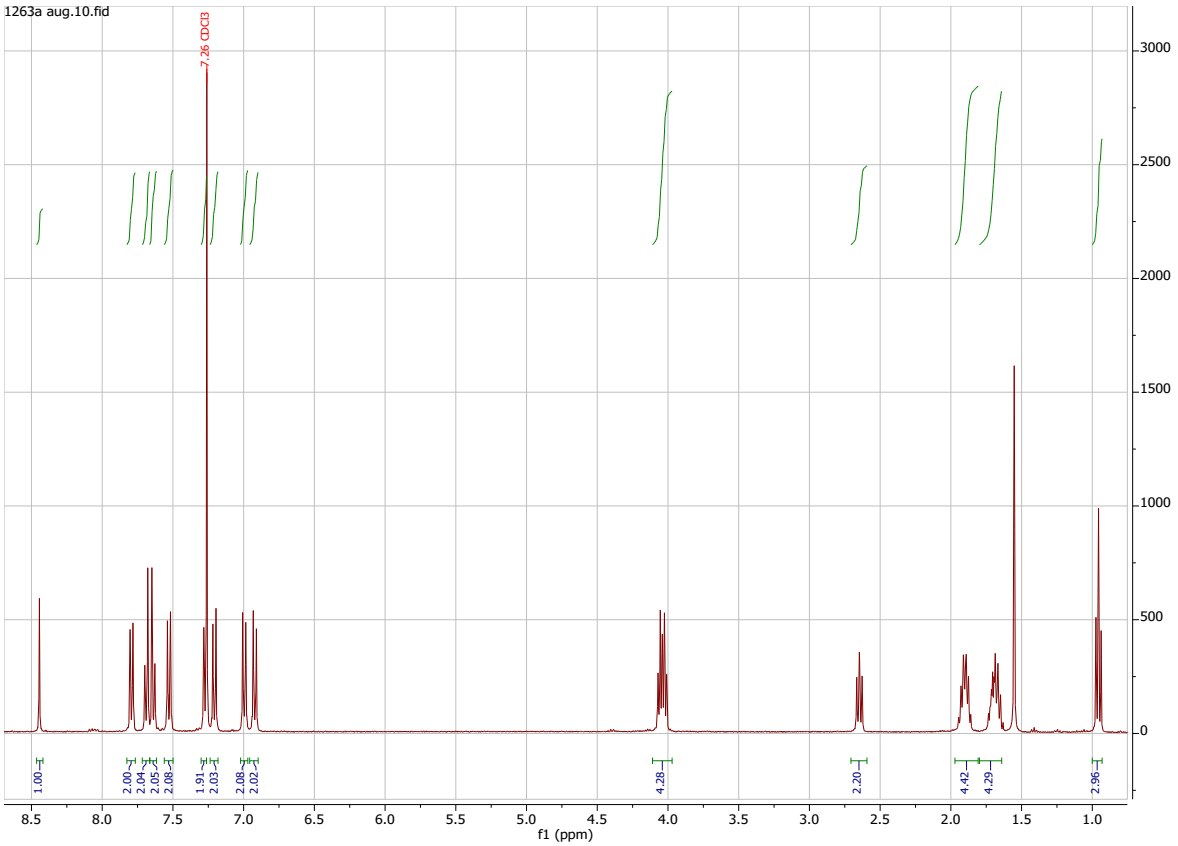

δ_C/ppm (100 MHz, $CDCl_3$): 159.70, 158.47, 157.56, 146.28, 145.27, 145.09, 134.16, 132.57, 131.38, 128.90, 128.57, 128.35, 127.09, 122.13, 119.12, 115.10, 114.97, 110.07, 67.99, 67.93, 38.06, 29.06, 28.99, 24.39, 22.76, 13.96

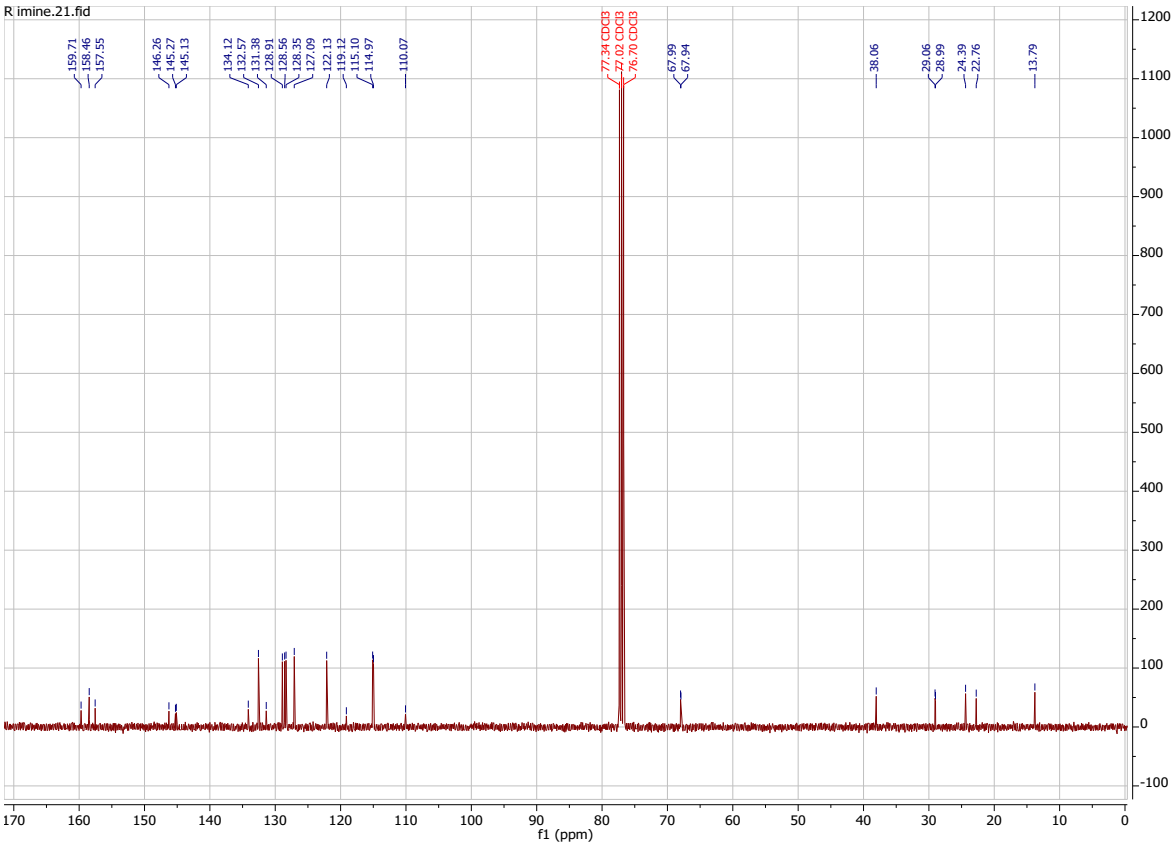

EA: Calculated for $C_{34}H_{34}N_2O_2$: C = 81.24 %, H = 6.82 %, N = 5.57 %; Found: C = 80.96 %, H = 6.78 %, N = 5.27 %

(8.4) 4'-{[5-(4-{(E)-[(4-Butylphenyl)methylidene]amino}phenoxy)pentyl]oxy}-[1,1'-biphenyl]-4-carbonitrile (CBO5O-4)

Yield: 0.104 g, 49.9 %

T_{CrN} 114 °C T_{NI} 151 °C

ν_{max}/cm^{-1}: 2929, 2860, 2229, 1622, 1602, 1575, 1494, 1469, 1391, 1284, 1242, 1185, 1171, 1137, 1113, 1062, 1033, 1016, 986, 945, 838, 824, 773, 757, 729, 657, 623, 549, 533

δ_H/ppm (400 MHz, $CDCl_3$): 8.44 (1 H, s, (C=N)-H), 7.79 (2 H, d, J 8.0 Hz, Ar-H), 7.69 (2 H, d, J 8.5 Hz, Ar-H), 7.63 (2 H, d, J 8.5 Hz, Ar-H), 7.54 (2 H, d, J 8.5 Hz, Ar-H), 7.28 (2 H, d, J 8.0 Hz, Ar-H), 7.21 (2 H, d, J 8.8 Hz, Ar-H), 7.00 (2 H, d, J 8.5 Hz, Ar-H), 6.92 (2 H, d, J 8.8 Hz, Ar-H), 4.04 (4 H, m, O-$\underline{CH_2}$-CH_2-CH_2-CH_2-$\underline{CH_2}$-O), 2.67 (2 H, t, J 7.6 Hz, Ar-$\underline{CH_2}$-CH_2-), 1.89 (4 H, m, O-CH_2-$\underline{CH_2}$-CH_2-$\underline{CH_2}$-CH_2-O), 1.65 (4 H, m, O-CH_2-CH_2-$\underline{CH_2}$-CH_2-, Ar-CH_2-$\underline{CH_2}$-CH_2-), 1.37 (2 H, sext, J 7.3 Hz, Ar-CH_2-CH_2-$\underline{CH_2}$-CH_3), 0.94 (3 H, t, J 7.3 Hz, Ar-CH_2-CH_2-CH_2-$\underline{CH_3}$)

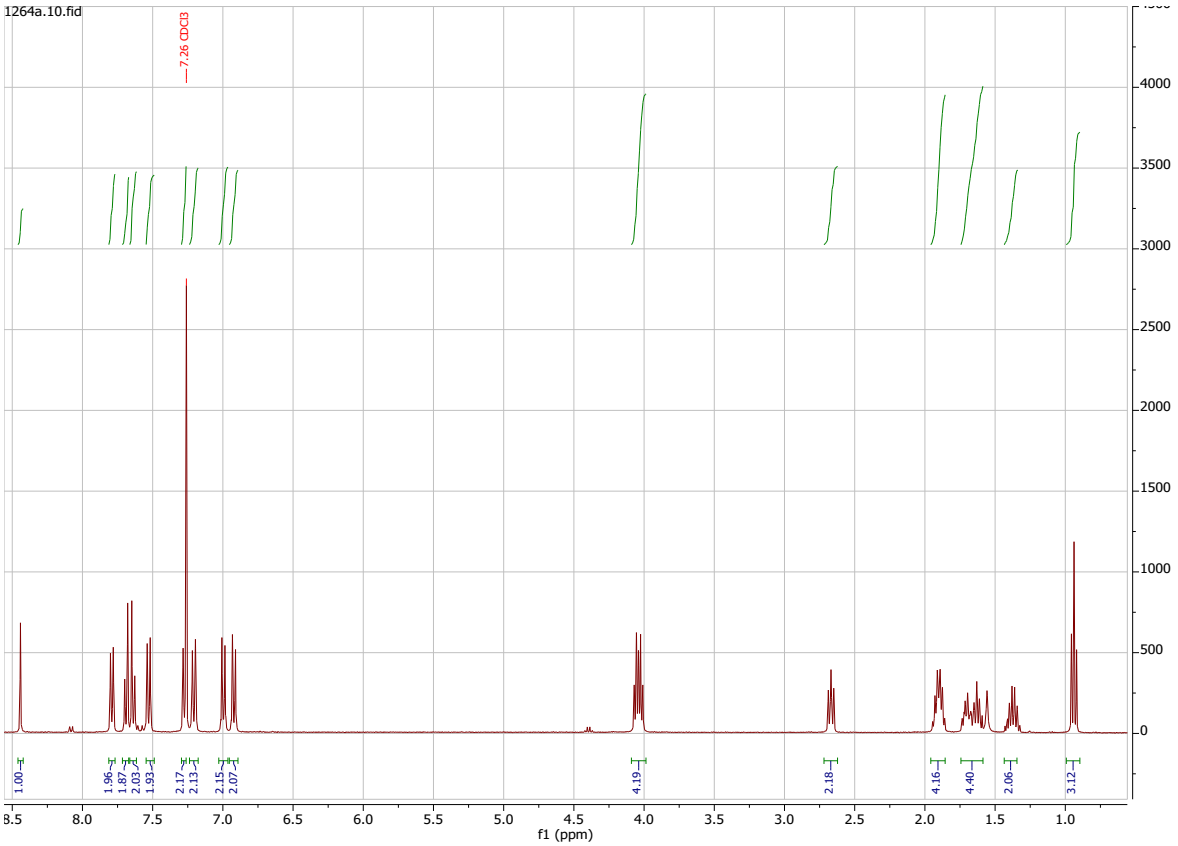

δ_C/ppm (100 MHz, $CDCl_3$): 159.71, 158.47, 157.56, 146.52, 145.26, 145.13, 134.08, 132.57, 131.37, 128.86, 128.59, 128.35, 127.09, 122.14, 119.13, 115.10, 114.98, 110.06, 68.00, 67.94, 35.70, 33.43, 29.07, 29.00, 22.76, 22.35, 13.96

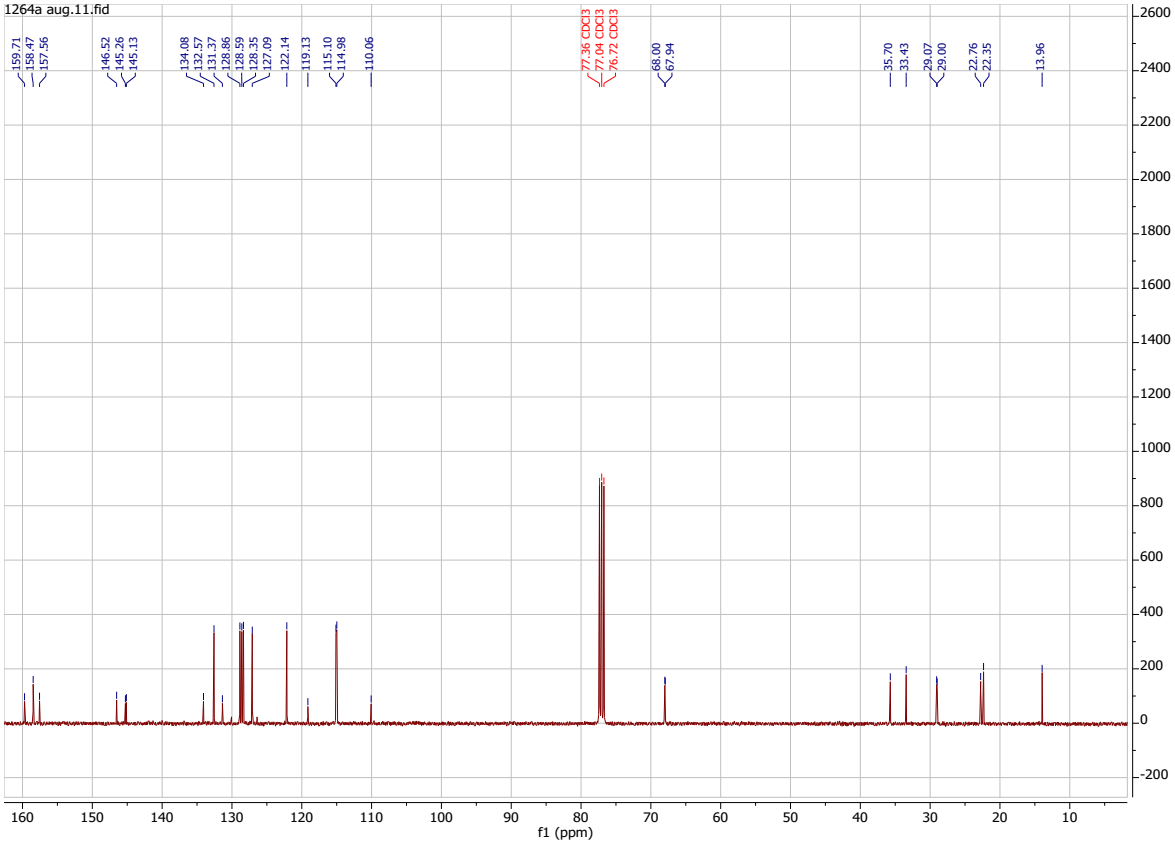

EA: Calculated for $C_{35}H_{36}N_2O_2$: C = 81.36 %, H = 7.02 %, N = 5.42 %; Found: C = 80.95 %, H = 6.98 %, N = 5.14 %

(8.5) 4'-{[5-(4-{(E)-[(4-Pentylphenyl)methylidene]amino}phenoxy)pentyl]oxy}-[1,1'-biphenyl]-4-carbonitrile (CBO5O-5)

Yield: 0.094 g, 44.0 %

T_{CrN} 107 °C T_{NI} 150 °C

ν_{max}/cm^{-1}: 2919, 2860, 2228, 1622, 1602, 1575, 1494, 1469, 1391, 1284, 1243, 1184, 1171, 1136, 1112, 1062, 1033, 986, 945, 824, 773, 757, 728, 658, 636, 548, 532

δ_H/ppm (400 MHz, $CDCl_3$): 8.44 (1 H, s, (C=N)-H), 7.79 (2 H, d, J 8.0 Hz, Ar-H), 7.69 (2 H, d, J 8.5 Hz, Ar-H), 7.64 (2 H, d, J 8.5 Hz, Ar-H), 7.54 (2 H, d, J 8.7 Hz, Ar-H), 7.27 (2 H, d, J 8.0 Hz, Ar-H), 7.21 (2 H, d, J 8.8 Hz, Ar-H), 7.00 (2 H, d, J 8.7 Hz, Ar-H), 6.92 (2 H, d, J 8.8 Hz, Ar-H), 4.04 (4 H, m, O-$\underline{CH_2}$-CH_2-CH_2-CH_2-$\underline{CH_2}$-O), 2.66 (2 H, t, J 7.4 Hz, Ar-$\underline{CH_2}$-CH_2-), 1.89 (4 H, m, O-CH_2-$\underline{CH_2}$-CH_2-$\underline{CH_2}$-CH_2-O), 1.68 (4 H, m, O-CH_2-CH_2-$\underline{CH_2}$-CH_2-, Ar-CH_2-$\underline{CH_2}$-CH_2-), 1.34 (4 H, m, Ar-CH_2-CH_2-$\underline{CH_2}$-$\underline{CH_2}$-CH_3), 0.90 (3 H, t, J 7.0 Hz, Ar-CH_2-CH_2-CH_2-CH_2-$\underline{CH_3}$)

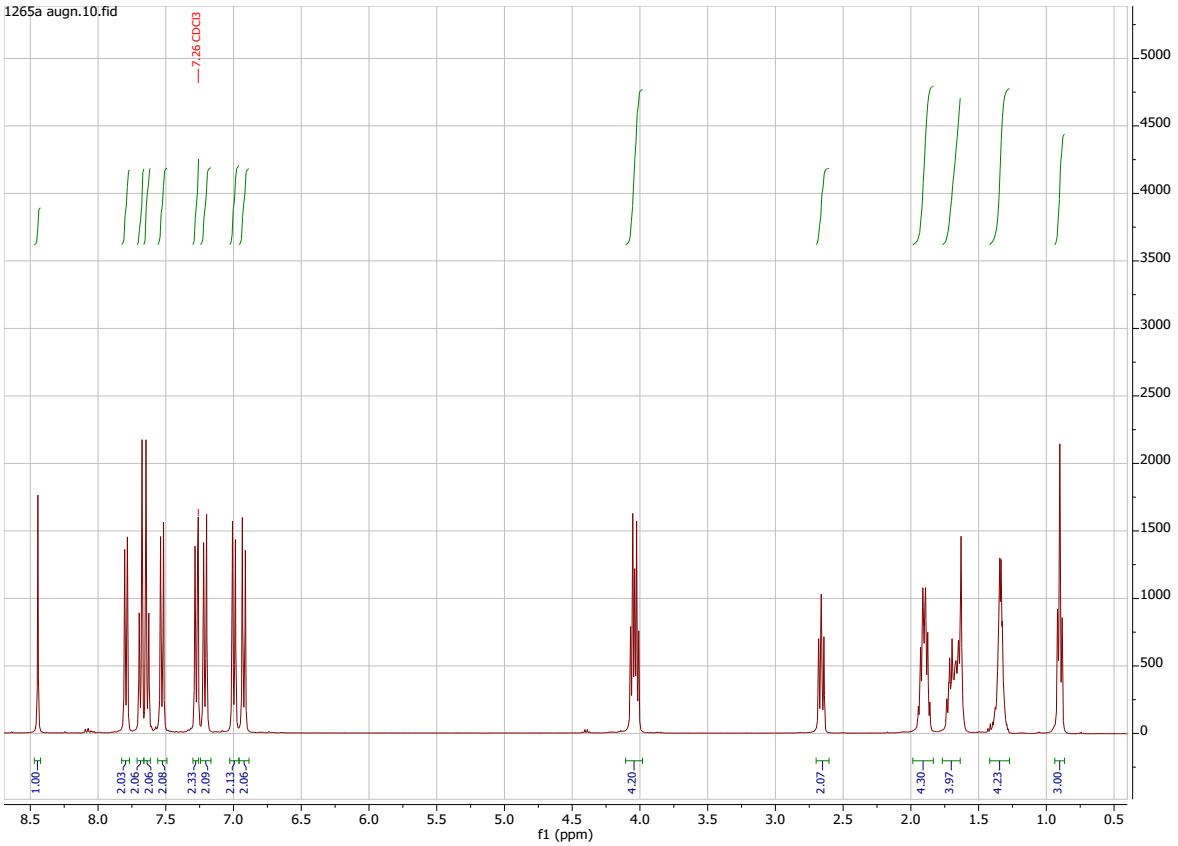

δ_C/ppm (100 MHz, $CDCl_3$): 159.71, 158.48, 157.56, 146.55, 145.26, 145.12, 134.07, 132.57, 131.37, 128.86, 128.59, 128.35, 127.09, 122.14, 119.13, 115.10, 114.98, 110.06, 68.00, 67.94, 35.98, 31.47, 30.97, 29.07, 29.00, 22.76, 22.54, 14.05

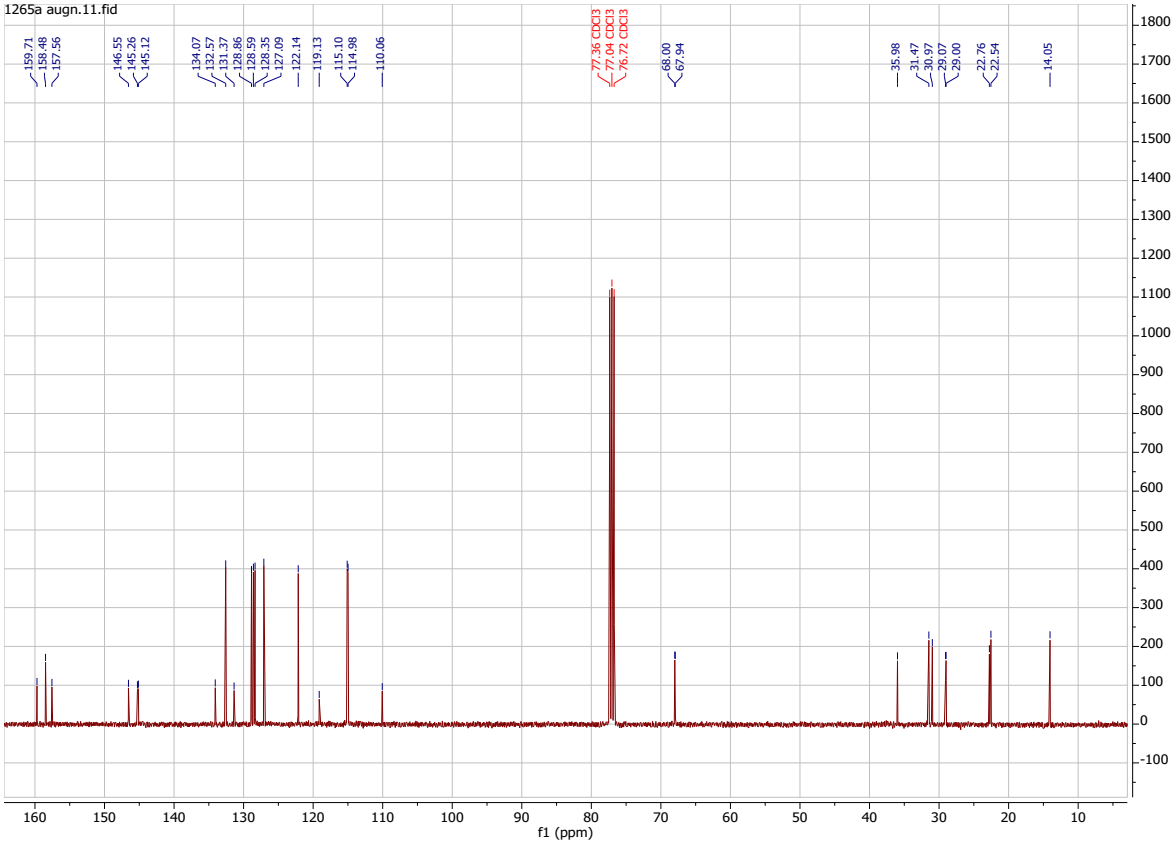

EA: Calculated for $C_{36}H_{38}N_2O_2$: C = 81.47 %, H = 7.22 %, N = 5.28 %; Found: C = 81.35 %, H = 7.18 %, N = 5.15 %

(8.6) 4'-{[5-(4-{(E)-[(4-Hexylphenyl)methylidene]amino}phenoxy)pentyl]oxy}-[1,1'-biphenyl]-4-carbonitrile (CBO5O-6)

Yield: 0.087 g, 39.6 %

T_{CrN} 108 °C T_{NI} 142 °C

ν_{max}/cm^{-1}: 2928, 2857, 2228, 1622, 1602, 1575, 1494, 1469, 1391, 1283, 1243, 1185, 1171, 1112, 1062, 1034, 986, 945, 824, 773, 758, 725, 657, 548, 532

δ_H/ppm (400 MHz, $CDCl_3$): 8.44 (1 H, s, (C=N)-H), 7.79 (2 H, d, J 8.1 Hz, Ar-H), 7.69 (2 H, d, J 8.4 Hz, Ar-H), 7.64 (2 H, d, J 8.4 Hz, Ar-H), 7.53 (2 H, d, J 8.7 Hz, Ar-H), 7.28 (2 H, d, J 8.1 Hz, Ar-H), 7.21 (2 H, d, J 8.8 Hz, Ar-H), 7.00 (2 H, d, J 8.7 Hz, Ar-H), 6.92 (2 H, d, J 8.8 Hz, Ar-H), 4.04 (4 H, m, O-$\underline{CH_2}$-CH_2-CH_2-CH_2-$\underline{CH_2}$-O), 2.66 (2 H, t, J 7.4 Hz, Ar-$\underline{CH_2}$-CH_2-), 1.90 (4 H, m, O-CH_2-$\underline{CH_2}$-CH_2-$\underline{CH_2}$-CH_2-O), 1.68 (4 H, m, O-CH_2-CH_2-$\underline{CH_2}$-CH_2-, Ar-CH_2-$\underline{CH_2}$-CH_2-), 1.34 (6 H, m, Ar-CH_2-CH_2-$\underline{CH_2}$-$\underline{CH_2}$-$\underline{CH_2}$-CH_3), 0.89 (3 H, t, J 7.0 Hz, Ar-CH_2-CH_2-CH_2-CH_2-CH_2-$\underline{CH_3}$)

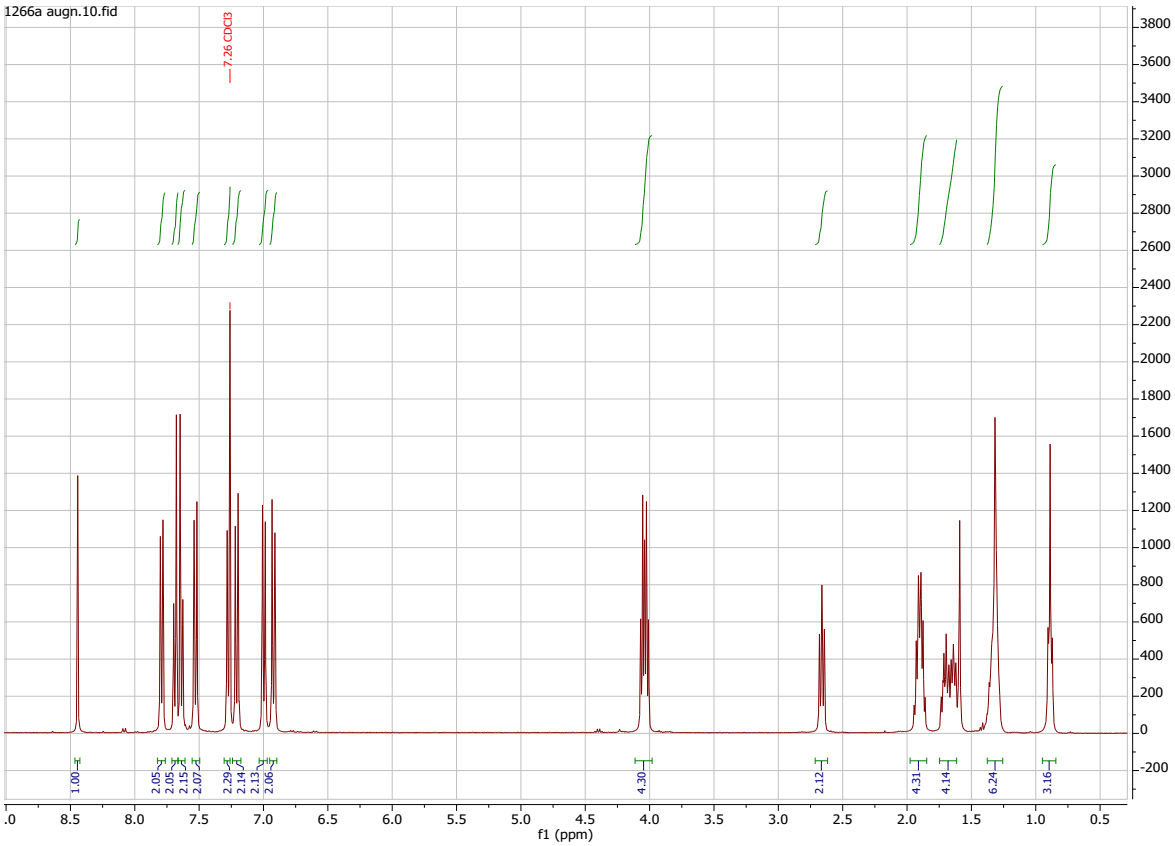

δ_C/ppm (100 MHz, $CDCl_3$): 159.71, 158.48, 157.55, 146.56, 145.26, 145.13, 134.07, 132.57, 131.37, 128.86, 128.58, 128.35, 127.09, 122.14, 119.12, 115.10, 114.97, 110.07, 68.00, 67.94, 36.01, 31.71, 31.25, 29.06, 28.99, 28.95, 22.76, 22.61, 14.11

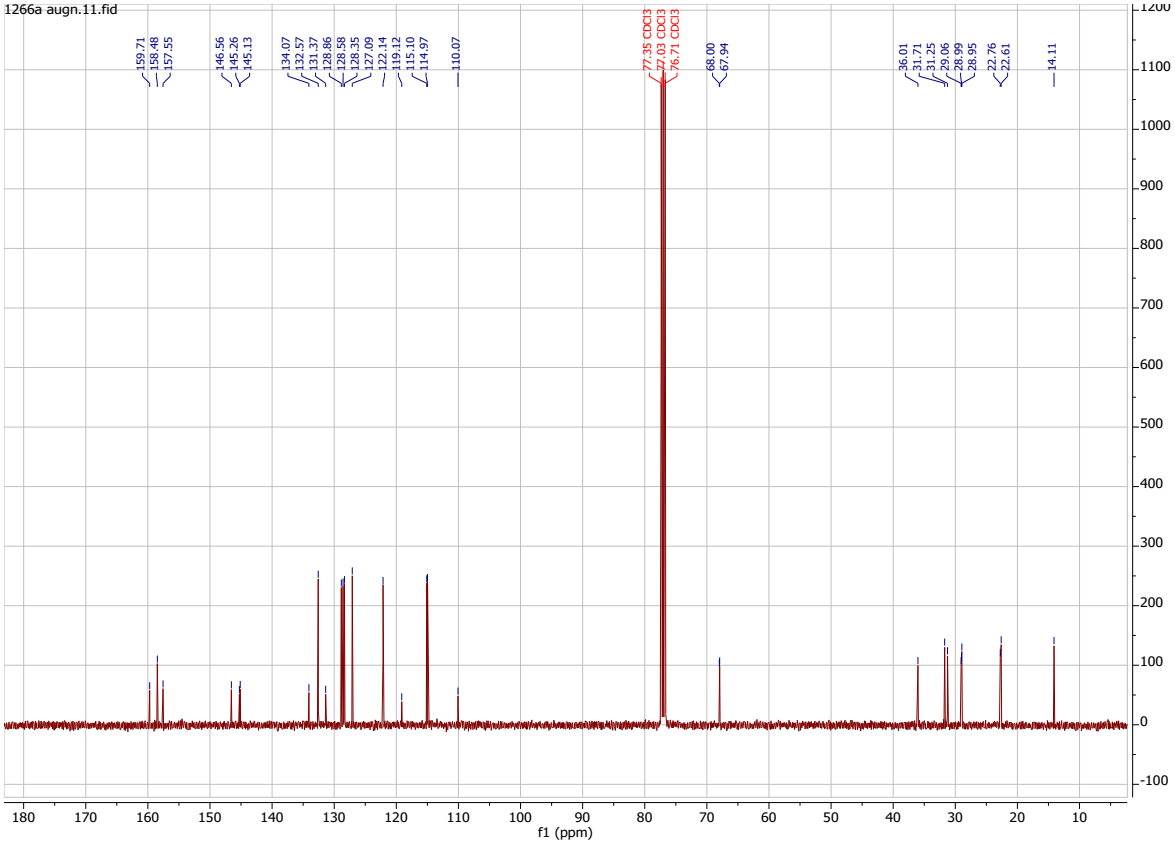

EA: Calculated for $C_{37}H_{40}N_2O_2$: C = 81.58 %, H = 7.40 %, N = 5.14 %; Found: C = 81.55 %, H = 7.44 %, N = 4.96 %

(8.7) 4'-{[5-(4-{(E)-[(4-Heptylphenyl)methylidene]amino}phenoxy)pentyl]oxy}-[1,1'-biphenyl]-4-carbonitrile (CBO5O-7)

Yield: 0.148 g, 65.7 %

T_{CrN} 109 °C T_{NI} 143 °C

ν_{max}/cm^{-1}: 2926, 2856, 2229, 1623, 1604, 1576, 1495, 1469, 1392, 1284, 1243, 1179, 1112, 1063, 1034, 1017, 986, 946, 825, 811, 757, 723, 658, 635, 563, 532

δ_H/ppm (400 MHz, $CDCl_3$): 8.44 (1 H, s, (C=N)-H), 7.79 (2 H, d, J 8.0 Hz, Ar-H), 7.69 (2 H, d, J 8.5 Hz, Ar-H), 7.64 (2 H, d, J 8.5 Hz, Ar-H), 7.53 (2 H, d, J 8.7 Hz, Ar-H), 7.28 (2 H, d, J 8.0 Hz, Ar-H), 7.21 (2 H, d, J 8.8 Hz, Ar-H), 6.99 (2 H, d, J 8.7 Hz, Ar-H), 6.92 (2 H, d, J 8.8 Hz, Ar-H), 4.04 (4 H, m, O-$\underline{CH_2}$-CH_2-CH_2-CH_2-$\underline{CH_2}$-O), 2.66 (2 H, t, J 7.6 Hz, Ar-$\underline{CH_2}$-CH_2-), 1.89 (4 H, m, O-CH_2-$\underline{CH_2}$-CH_2-$\underline{CH_2}$-CH_2-O), 1.69 (4 H, m, O-CH_2-CH_2-$\underline{CH_2}$-CH_2-, Ar-CH_2-$\underline{CH_2}$-CH_2-), 1.30 (8 H, m, Ar-CH_2-CH_2-$\underline{CH_2}$-$\underline{CH_2}$-$\underline{CH_2}$-$\underline{CH_2}$-CH_3), 0.88 (3 H, t, J 7.1 Hz, Ar-CH_2-CH_2-CH_2-CH_2-CH_2-CH_2-$\underline{CH_3}$)

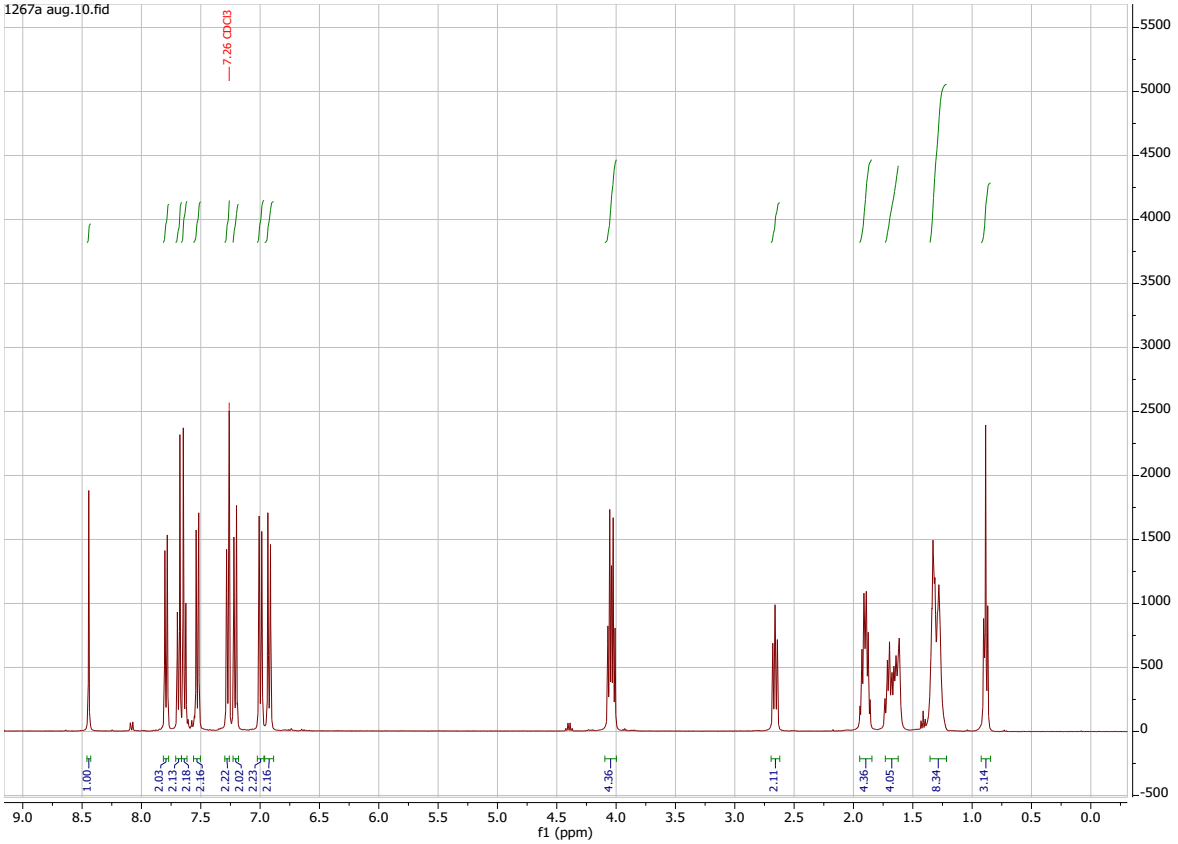

δ_C/ppm (100 MHz, $CDCl_3$): 159.71, 158.48, 157.56, 146.56, 145.26, 145.13, 134.07, 132.57, 131.37, 128.86, 128.58, 128.35, 127.09, 122.14, 119.12, 115.10, 114.97, 110.07, 68.00, 67.94, 36.01, 31.82, 31.30, 29.25, 29.17, 29.07, 29.00, 22.76, 22.67, 14.12

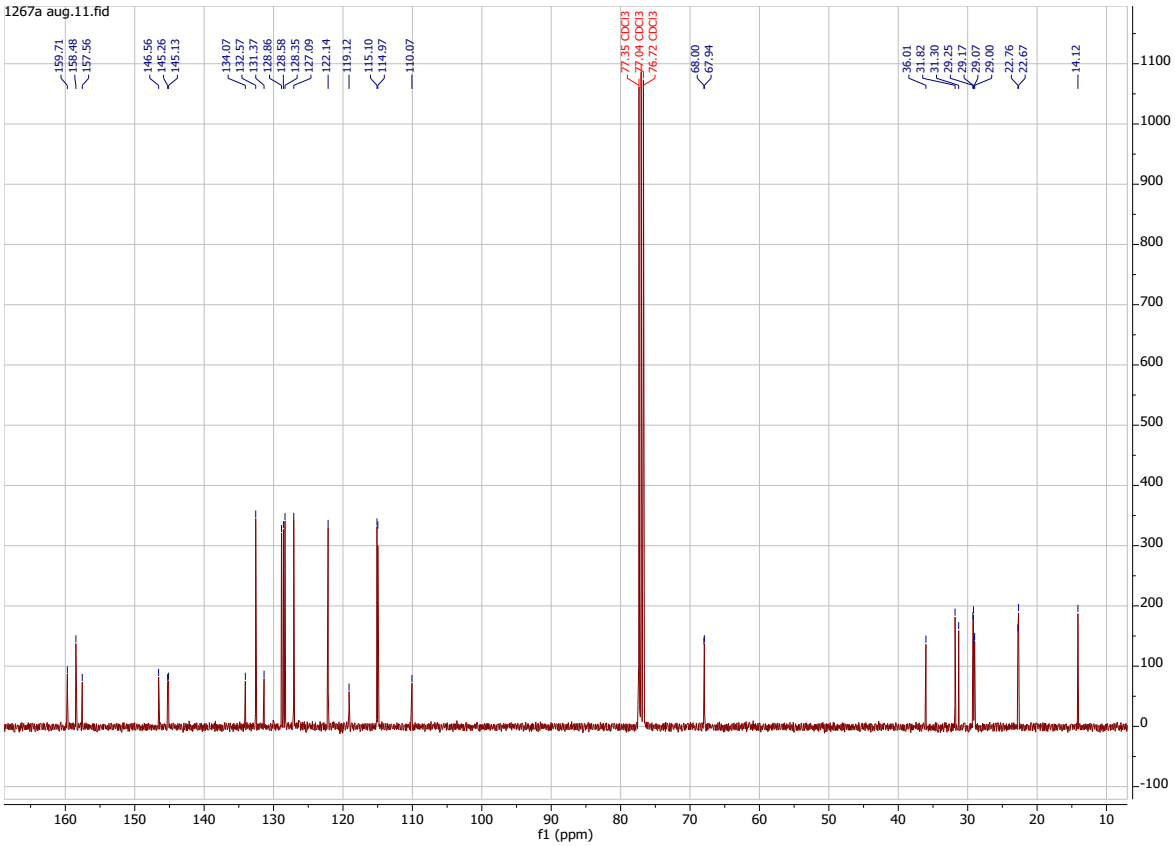

EA: Calculated for $C_{38}H_{42}N_2O_2$: C = 81.68 %, H = 7.58 %, N = 5.01 %; Found: C = 81.23 %, H = 7.51 %, N = 5.00 %

(8.8) 4'-{[5-(4-{(E)-[(4-Octylphenyl)methylidene]amino}phenoxy)pentyl]oxy}-[1,1'-biphenyl]-4-carbonitrile (CBO5O-8)

Yield: 0.134 g, 58.1 %

T_{CrN} 107 °C T_{NI} 137 °C

ν_{max}/cm^{-1}: 2924, 2856, 2234, 1623, 1606, 1576, 1495, 1468, 1391, 1286, 1243, 1177, 1111, 1063, 1036, 1016, 1001, 946, 825, 809, 737, 724, 661, 635, 563, 531

δ_H/ppm (400 MHz, $CDCl_3$): 8.44 (1 H, s, (C=N)-H), 7.79 (2 H, d, J 8.1 Hz, Ar-H), 7.69 (2 H, d, J 8.4 Hz, Ar-H), 7.64 (2 H, d, J 8.4 Hz, Ar-H), 7.53 (2 H, d, J 8.6 Hz, Ar-H), 7.27 (2 H, d, J 8.1 Hz, Ar-H), 7.21 (2 H, d, J 8.7 Hz, Ar-H), 6.99 (2 H, d, J 8.6 Hz, Ar-H), 6.92 (2 H, d, J 8.7 Hz, Ar-H), 4.04 (4 H, m, O-$\underline{CH_2}$-CH_2-CH_2-CH_2-$\underline{CH_2}$-O), 2.66 (2 H, t, J 7.7 Hz, Ar-$\underline{CH_2}$-CH_2-), 1.89 (4 H, m, O-CH_2-$\underline{CH_2}$-CH_2-$\underline{CH_2}$-CH_2-O), 1.68 (4 H, m, O-CH_2-CH_2-$\underline{CH_2}$-CH_2-, Ar-CH_2-$\underline{CH_2}$-CH_2-), 1.29 (10 H, m, Ar-CH_2-CH_2-$\underline{CH_2}$-$\underline{CH_2}$-$\underline{CH_2}$-$\underline{CH_2}$-$\underline{CH_2}$-CH_3), 0.88 (3 H, t, J 7.1 Hz, Ar-CH_2-CH_2-CH_2-CH_2-CH_2-CH_2-CH_2-$\underline{CH_3}$)

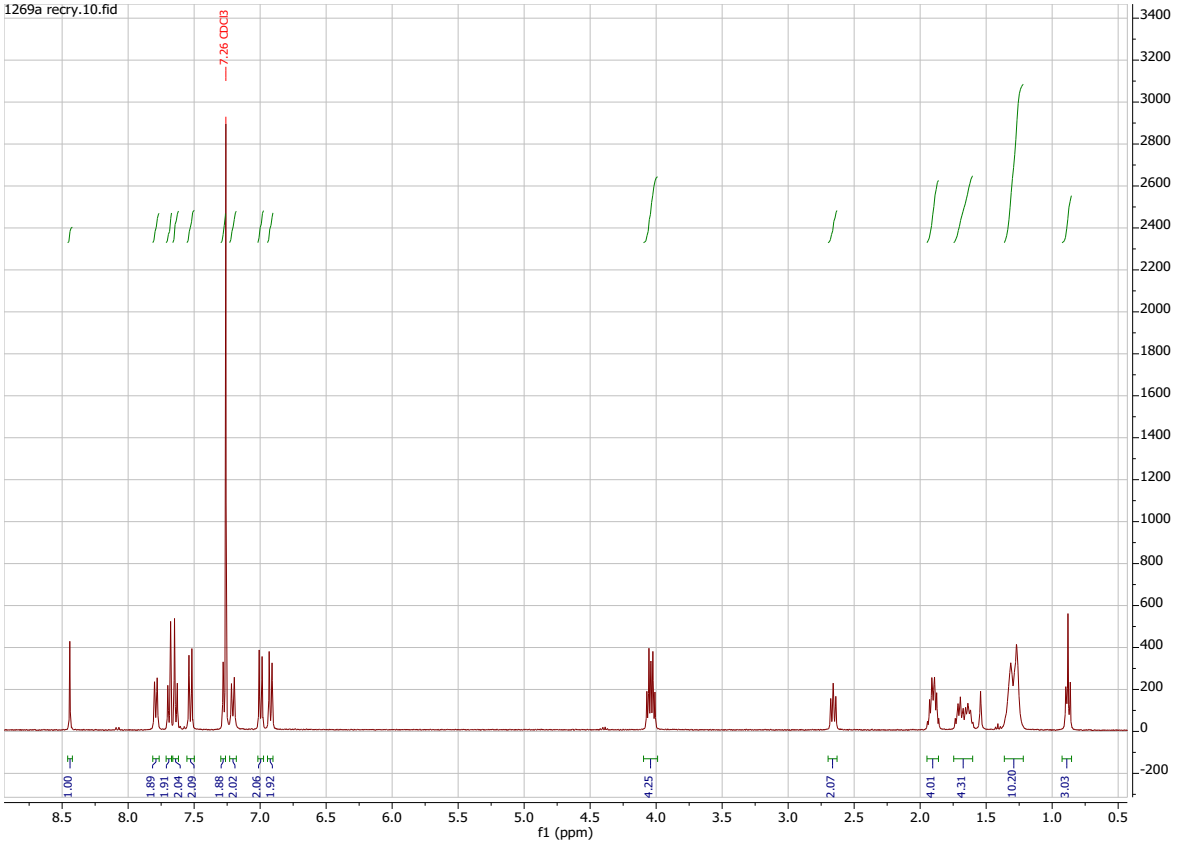

δ_C/ppm (100 MHz, $CDCl_3$): 159.71, 158.48, 157.56, 146.57, 145.26, 145.13, 134.07, 132.57, 131.37, 128.86, 128.58, 128.35, 127.09, 122.14, 119.12, 115.10, 114.97, 110.07, 68.00, 67.94, 36.02, 31.89, 31.30, 29.47, 29.30, 29.27, 29.07, 29.00, 22.76, 22.68, 14.13

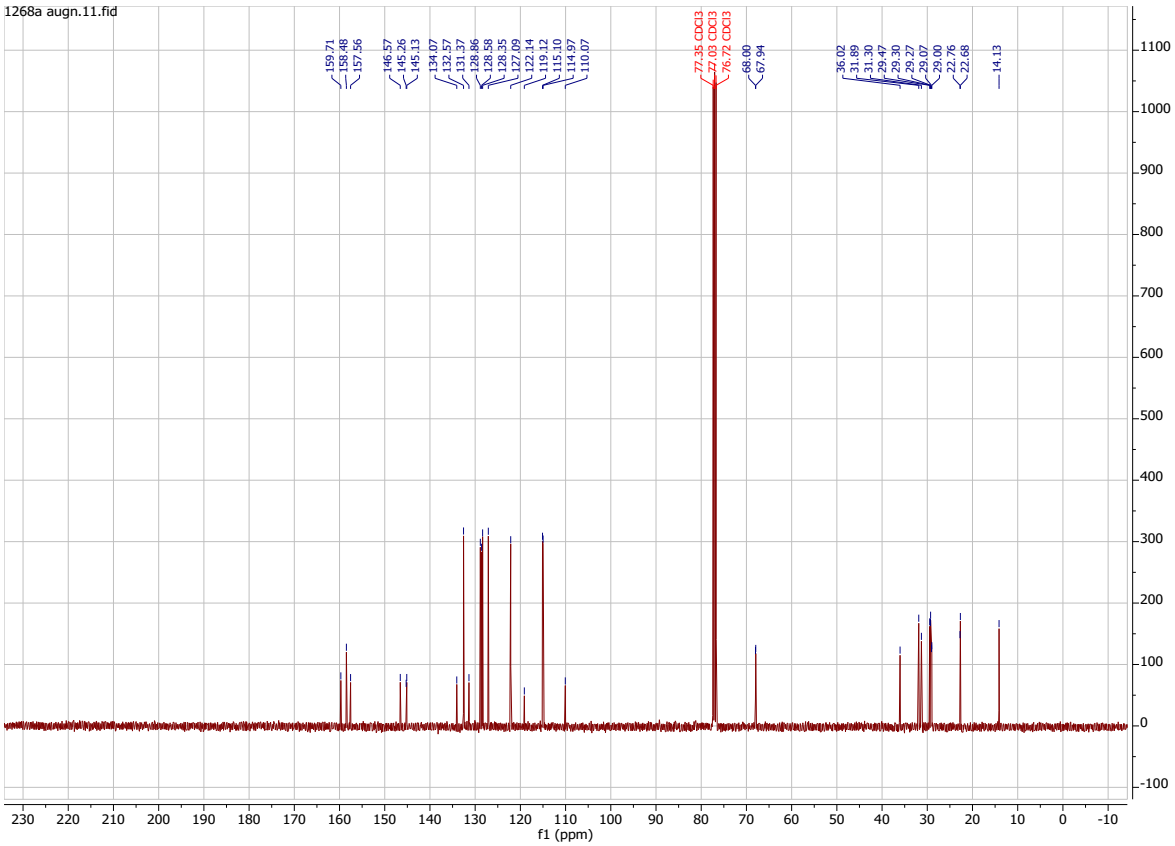

EA: Calculated for $C_{39}H_{44}N_2O_2$: C = 81.78 %, H = 7.74 %, N = 4.89 %; Found: C = 81.31 %, H = 7.71 %, N = 4.72 %

(8.9) 4'-{[5-(4-{(E)-[(4-Nonylphenyl)methylidene]amino}phenoxy)pentyl]oxy}-[1,1'-biphenyl]-4-carbonitrile (CBO5O-9)

Yield: 0.083 g, 35.1 %

T_{CrN} 110 °C T_{SmAN} (103 °C) T_{NI} 136 °C

ν_{max}/cm^{-1}: 2924, 2854, 2229, 1623, 1604, 1575, 1495, 1469, 1392, 1285, 1244, 1180, 1112, 1063, 1034, 1017, 1001, 986, 945, 825, 757, 722, 658, 563, 532

δ_H/ppm (400 MHz, $CDCl_3$): 8.44 (1 H, s, (C=N)-H), 7.79 (2 H, d, J 8.0 Hz, Ar-H), 7.69 (2 H, d, J 8.4 Hz, Ar-H), 7.64 (2 H, d, J 8.4 Hz, Ar-H), 7.53 (2 H, d, J 8.8 Hz, Ar-H), 7.28 (2 H, d, J 8.0 Hz, Ar-H), 7.21 (2 H, d, J 8.8 Hz, Ar-H), 7.00 (2 H, d, J 8.8 Hz, Ar-H), 6.92 (2 H, d, J 8.8 Hz, Ar-H), 4.04 (4 H, m, O-$\underline{CH_2}$-CH_2-CH_2-CH_2-$\underline{CH_2}$-O), 2.66 (2 H, t, J 7.7 Hz, Ar-$\underline{CH_2}$-CH_2-), 1.89 (4 H, m, O-CH_2-$\underline{CH_2}$-CH_2-$\underline{CH_2}$-CH_2-O), 1.68 (4 H, m, O-CH_2-CH_2-$\underline{CH_2}$-CH_2-, Ar-CH_2-$\underline{CH_2}$-CH_2-), 1.29 (12 H, m, Ar-CH_2-CH_2-$\underline{CH_2}$-$\underline{CH_2}$-$\underline{CH_2}$-$\underline{CH_2}$-$\underline{CH_2}$-$\underline{CH_2}$-CH_3), 0.88 (3 H, t, J 7.2 Hz, Ar-CH_2-CH_2-CH_2-CH_2-CH_2-CH_2-CH_2-CH_2-$\underline{CH_3}$)

δ_C/ppm (100 MHz, $CDCl_3$): 159.71, 158.48, 157.56, 146.57, 145.26, 145.13, 134.06, 132.57, 131.37, 128.86, 128.58, 128.35, 127.09, 122.14, 119.12, 115.10, 114.97, 110.07, 68.00, 67.94, 36.02, 31.90, 31.30, 29.56, 29.51, 29.33, 29.29, 29.07, 28.99, 22.76, 22.69, 14.14

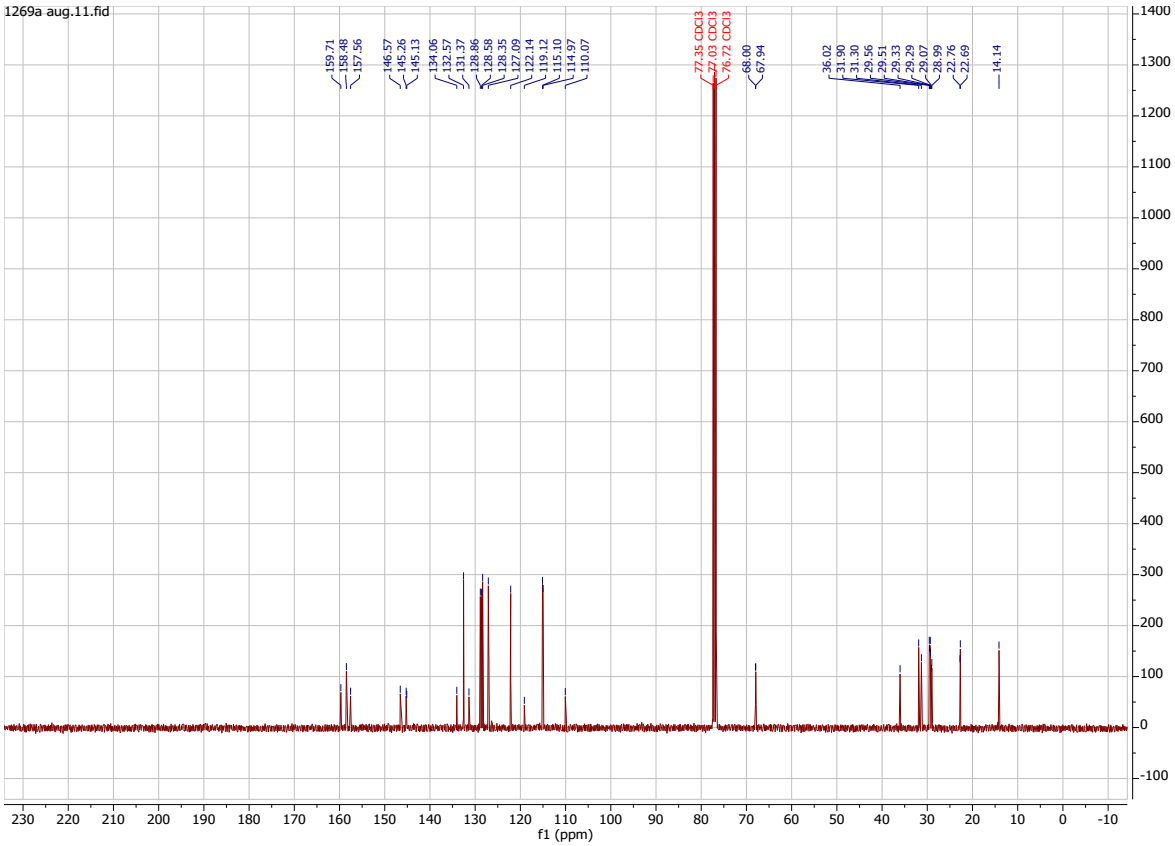

EA: Calculated for $C_{40}H_{46}N_2O_2$: C = 81.87 %, H = 7.90 %, N = 4.77 %; Found: C = 81.58 %, H = 7.83 %, N = 4.62 %

(8.10) 4'-{[5-(4-{(E)-[(4-Decylphenyl)methylidene]amino}phenoxy)pentyl]oxy}-[1,1'-biphenyl]-4-carbonitrile (CBO5O-10)

Yield: 0.121 g, 50.0 %

T_{CrSmA} 108 °C T_{SmXSmA} (92 °C) T_{SmAN} 123 °C T_{NI} 132 °C

ν_{max}/cm^{-1}: 2920, 2848, 2233, 1621, 1607, 1577, 1495, 1468, 1390, 1366, 1285, 1243, 1176, 1110, 1037, 1016, 1001, 964, 853, 826, 810, 736, 724, 662, 635, 564, 537, 531, 495

δ_H/ppm (400 MHz, $CDCl_3$): 8.44 (1 H, s, (C=N)-H), 7.79 (2 H, d, J 8.0 Hz, Ar-H), 7.69 (2 H, d, J 8.5 Hz, Ar-H), 7.64 (2 H, d, J 8.5 Hz, Ar-H), 7.53 (2 H, d, J 8.7 Hz, Ar-H), 7.28 (2 H, d, J 8.0 Hz, Ar-H), 7.21 (2 H, d, J 8.8 Hz, Ar-H), 7.00 (2 H, d, J 8.7 Hz, Ar-H), 6.92 (2 H, d, J 8.8 Hz, Ar-H), 4.04 (4 H, m, O-$\underline{CH_2}$-CH_2-CH_2-CH_2-$\underline{CH_2}$-O), 2.66 (2 H, t, J 7.4 Hz, Ar-$\underline{CH_2}$-CH_2-), 1.90 (4 H, m, O-CH_2-$\underline{CH_2}$-CH_2-$\underline{CH_2}$-CH_2-O), 1.68 (4 H, m, O-CH_2-CH_2-$\underline{CH_2}$-CH_2-, Ar-CH_2-$\underline{CH_2}$-CH_2-), 1.29 (14 H, m, Ar-CH_2-CH_2-$\underline{CH_2}$-$\underline{CH_2}$-$\underline{CH_2}$-$\underline{CH_2}$-$\underline{CH_2}$-$\underline{CH_2}$-$\underline{CH_2}$-CH_3), 0.88 (3 H, t, J 6.9 Hz, Ar-CH_2-CH_2-CH_2-CH_2-CH_2-CH_2-CH_2-CH_2-$\underline{CH_3}$)

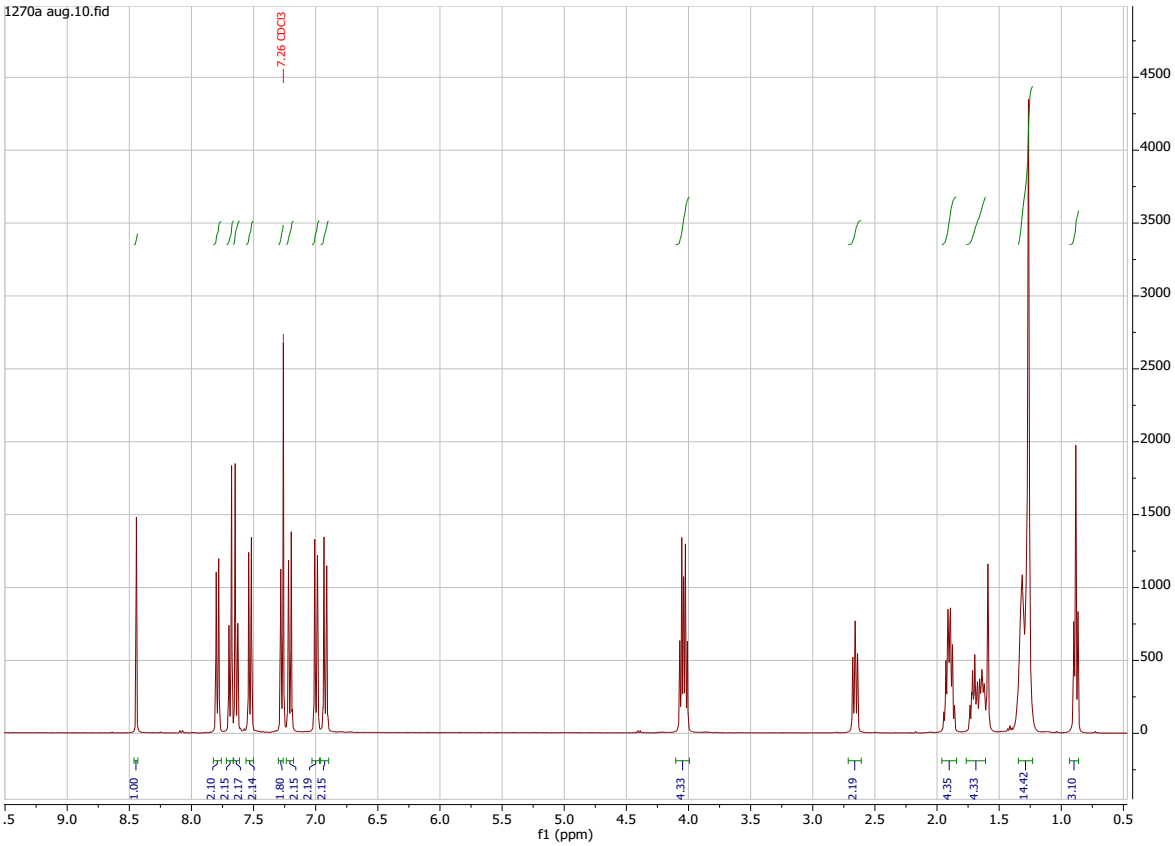

δ_C/ppm (100 MHz, $CDCl_3$): 159.71, 158.48, 157.55, 146.57, 145.26, 145.13, 134.07, 132.57, 131.37, 128.86, 128.58, 128.35, 127.09, 122.13, 119.12, 115.10, 114.97, 110.07, 67.99, 67.94, 36.02, 31.92, 31.30, 29.62, 29.60, 29.50, 29.34, 29.29, 29.06, 28.99, 22.76, 22.70, 14.14

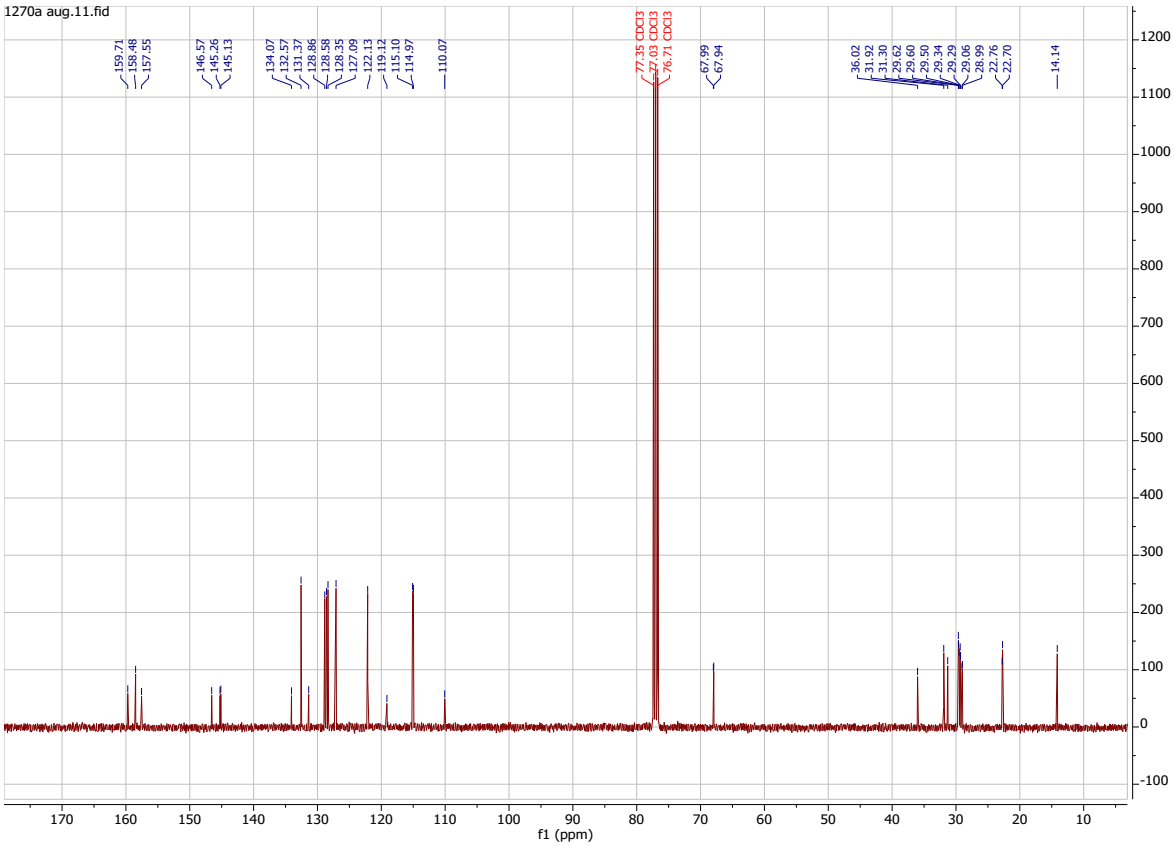

EA: Calculated for $C_{41}H_{48}N_2O_2$: C = 81.96 %, H = 8.05 %, N = 4.66 %; Found: C = 81.77 %, H = 7.89 %, N = 4.51 %

Additional Experimental Results

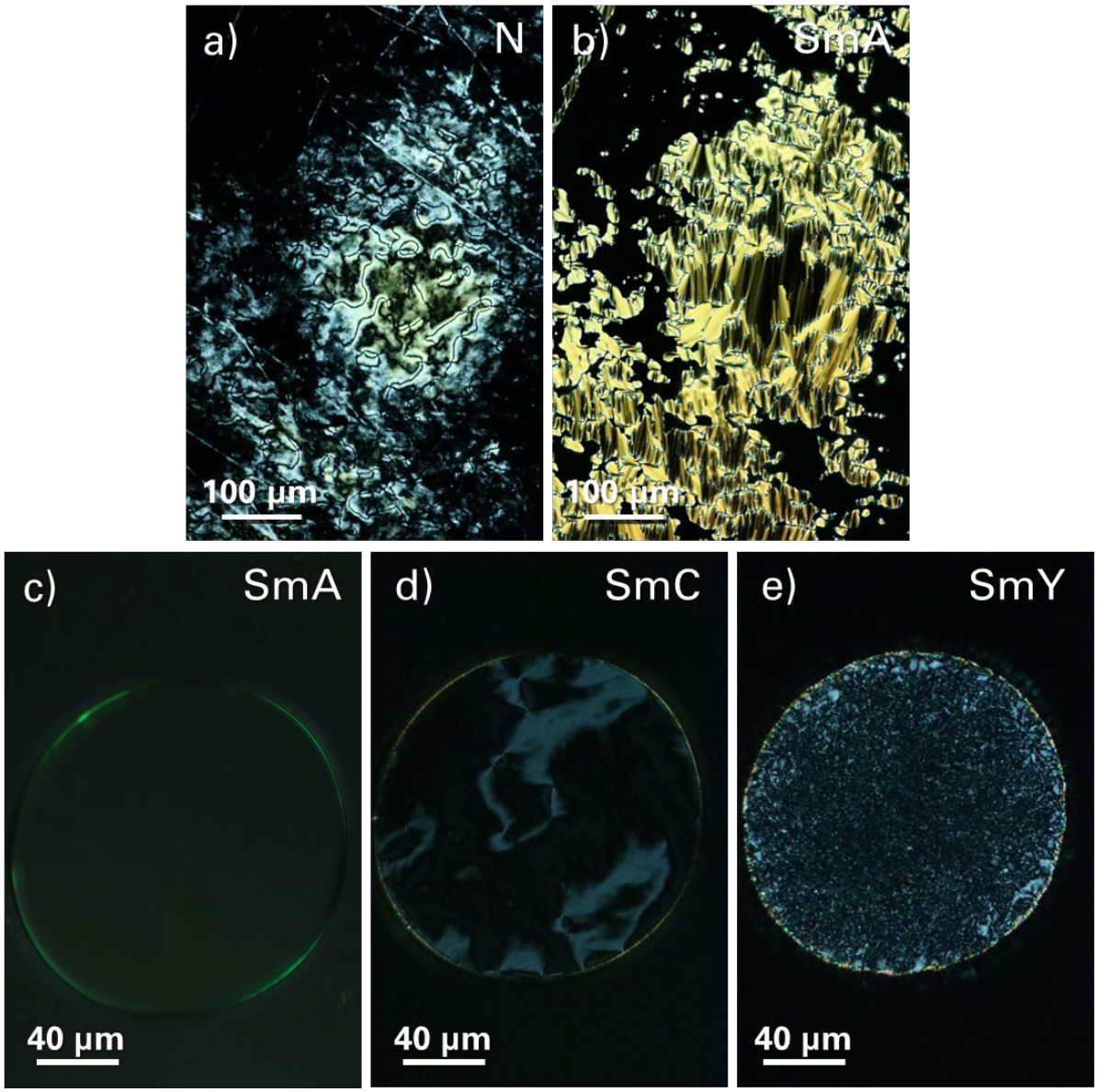

Figure S1. Additional Textures observed for 7-O5O-7: (a) schlieren texture of the nematic phase (T = 127 °C); (b) focal conic fan texture with homeotropic regions of the smectic A phase (T = 126 °C); (c) homeotropic texture of the smectic A phase in isolated droplets (124 °C); (d) schlieren texture of the smectic C phase in isolated droplets (T = 115 °C); (d) representative texture of the smectic Y phase in isolated droplets (T = 112 °C).

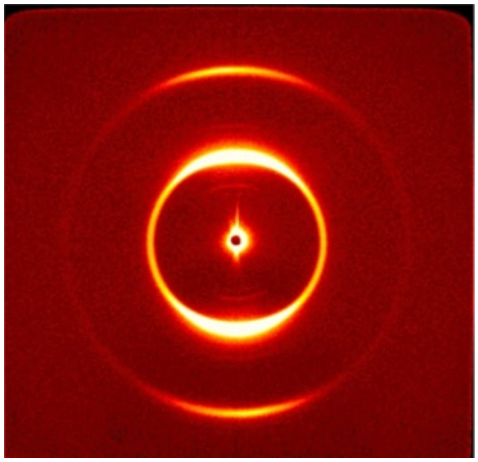

Figure S2. Small angle X-ray diffraction patterns for (a) 9-O5O-9 in the smectic Y phase (T = 114 °C)

Table SI5. Transition temperatures for the CBO5O.*m* series with the scaled entropy changes associated with the transitions, ΔS/R, in brackets.[7,8]

m	T_{Cr-}/ °C (ΔS/R)	$T_{SmC_{TB-SH}N}$/ °C (ΔS/R) *$T_{SmC_{TB-SH}SmA}$/ °C (ΔS/R)	T_{SmAN}/ °C (ΔS/R)	$T_{N_{TB}N}$/ °C (ΔS/R)	T_{NI}/ °C (ΔS/R)
1	116 (10.0)	-	-	[a]86 (≈ 0)	168 (0.46)
2	107 (10.9)	-	-	[a]83 (≈ 0)	165 (0.47)
3	107 (10.9)	-	-	[a]80 (≈ 0)	164 (0.53)
4	99 (9.96)	-	-	[a]73 (≈ 0)	155 (0.44)
5	102 (10.1)	-	-	[a]74 (≈ 0)	155 (0.53)
6	100 (10.6)	-	-	[a]67 (≈ 0)	149 (0.47)
7	107 (9.16)	-	-	[a]71 (≈ 0)	143 (0.38)
8	105 (12.8)	[a]71 (0.068)	-	-	137 (0.31)
9	107 (12.1)	*[a]84 (0.024)	92 (≈ 0)	-	137 (0.34)
10	105 (13.9)	*[a]90 (0.018)	116 (0.022)	-	134 (0.40)

[a]Values extracted from DSC cooling traces.

References

1. Henderson, P. A., Inkster, R. T., Seddon, J. M. & Imrie, C. T. Highly non-linear liquid crystal tetramers. *J. Mater. Chem.* **11**, 2722–2731 (2001).
2. Kim, Y., Kim, J., Oh, K., Lee, D. S. & Park, S. B. Heteroaromatic moieties in the sphingosine backbone of α-Galactosylceramides for noncovalent interactions with CD1d. *ACS Med. Chem. Lett.* **3**, 151–154 (2012).
3. Koide, Y., Hasegawa, T., Takahashi, A., Endo, A., Mochizuki, N., Nakagawa, M. & Nishida, A. Development of novel EDG3 antagonists using a 3D database search and their structure-activity relationships. *J. Med. Chem.* **45**, 4629–4638 (2002).
4. Ezoe, M., Yagi, S., Nakazumi, H., Itou, M., Araki, Y. & Ito, O. Molecular recognition of viologen by zinc porphyrinic receptors with diarylurea sidearms. Toward construction of a supramolecular electron transfer system. *Tetrahedron*. **62**, 2501–2510 (2006).
5. Hilbold, B., Perrault, M., Ehret, C., Niu, S. L., Frisch, B., Pécheur, E. I. & Bourel-Bonnet, L. Benzophenone-containing fatty acids and their related photosensitive fluorescent new probes: Design, physico-chemical properties and preliminary functional investigations. *Bioorganic Med. Chem.* **19**, 7464–7473 (2011).
6. Attard, G. S., Imrie, C. T. & Karasz, F. E. Low Molar Mass Liquid-Crystalline Glasses: Preparation and Properties of the α-(4-Cyanobiphenyl-4’-oxy)-ω-(l-pyreniminebenzylidene-4’-oxy)alkanes. *Chem. Mater.* **4**, 1246–1253 (1992).
7. Walker, R., Pociecha, D., Strachan, G. J., Storey, J. M. D., Gorecka, E. & Imrie, C. T. Molecular curvature, specific intermolecular interactions and the twist-bend nematic phase: the synthesis and characterisation of the 1-(4-cyanobiphenyl-4’-yl)-6-(4-alkylanilinebenzylidene-4’-oxy)hexanes (CB6O.*m*). *Soft Matter*. **15**, 3188–3197 (2019).
8. Attard, G. S., Date, R. W., Imrie, C. T., Luckhurst, G. R., Roskilly, S. J., Seddon, J. M. & Taylor, L. Non-symmetric dimeric liquid crystals The preparation and properties of the α-(4-cyanobiphenyl-4’-yloxy)-ω-(4-n-alkylanilinebenzylidene-4’-oxy)alkanes. *Liq. Cryst.* **16**, 529–581 (1994).